Chapter 4

Heterocyclic Fused Aromatic Dithienopyrrolobenzothiadiazole (DTPBT)-Based Conjugated Polymers

Table of Contents

Introduction

An enormous number of conjugated polymers have been developed as the active materials for organic electronic devices, such as organic light emitting diodes (OLEDs), organic field effect transistors (OFETs) and organic photovoltaics (OPVs) during the past two decades.[1–3] For improvement in the efficiencies of these devices, development of novel conjugated polymers plays the most important role which can afford low cost, light weight and flexible electronic devices.[4] Many recent research studies have exhibited that the development of conjugated polymers require alternating sequence of aromatic and quinoidal units as well as the combination of the electron-releasing and electron-withdrawing units along the polymer chain, which in turn will lead to the donor-acceptor (D-A) polymer having a low bandgap.[5–7]

In contrast to the traditional linear conjugated polymers, which are having continuous aromatic rings interconnected by carbon-carbon single bonds, ladder type polymers are the conjugated frame-works, that are comprised of linearly fused aromatic or heterocyclic subunits connected *via* sharing the endo-cyclic carbon-carbon double bonds.[8–18] Covalently forced planarization within the ladder structure enhances the parallel *p*-orbital interactions and increases the effective conjugation length by facilitating the π electron delocalization. Moreover, the rigidified coplanar structure suppresses the rotational disorder around the inter-annular single bonds and lowers the reorganization energy, which in turn enhances the intrinsic charge mobility.[19] Such double stranded conjugated structures exhibit high thermal, chemical and mechanical stabilities. Though, the physical and electronic properties of the ladder-type polymers have attained considerable interest in the area of non-linear optics, light emitting diodes and organic field effect transistors, the highly rigid ladder-type polymers suffer from the disadvantages like poor solubility and solution processability due to the strong π-π interactions, which greatly limits their optoelectronic applications. It is envisaged that the well-defined ladder type small molecules which up on polymerization leads to a new class of donor-acceptor-type semi-ladder polymers, can circumvent the problems associated with highly rigid ladder-type polymers.

Thus, incorporation of electron-rich and electron-poor subunits into the mutually ring-fused structures has acquired much attention of researchers. A large variety of electron-rich aromatic and heterocyclic building blocks such as benzene,

thiophene, furan, selenophene, pyrrole, silole, germole, cyclopentadiene, etc., and electron-poor aromatic and heterocyclic building blocks such as benzothiadiazole, thieno-pyrrolodione, bithiopheneimide, quinoxaline, naphthobisthiadiazole, lactam, diketopyrrolopyrrole, thiazolothiazole, etc., can be chemically assembled to afford a range of fascinating ladder-type conjugated skeletons with tunable properties and functions.[20–23] Till date, a wide range of D-A conjugated polymers have been reported having electron-rich and/or electron-deficient multi-fused aromatic and heterocyclic building blocks, arrayed into the polymer backbone.[24] Amongst all the reported heteroatom containing multi-fused polycyclic aromatic systems, most of the systems are electron-rich and acts as a donor unit, while some of the systems are electron-poor and acts as an acceptor unit. Some of the very few reported fused D-A systems are proficient of exhibiting ambipolar behaviour, one of such D-A integrated structure, dithienopyrrolobenzothiadiazole (**DTPBT**) is reported for the first time by Cheng *et al*. (Figure 4.1), in which an electron-deficient 2,1,3-benzothiadiazole (BT) unit is covalently fused with two outer electron-rich thiophene units *via* two embedded pyrrole rings.[4]

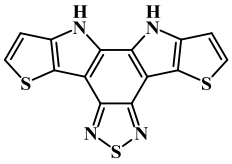

Figure 4.1 Structure of D-A intergrated dithienopyrrolobenzothiadiazole (**DTPBT**)

Compared to the traditional D-A linkage, where the donor and acceptor units are fastened together by a single carbon-carbon bond, the directly fused D-A structures are expected to have efficient intramolecular charge transfer (ICT) interactions owing to the coplanar structure.[7,25] Since 2011, DTPBT-based conjugated polymers have attracted attention of the researchers because of the superior properties of DTPBT building block like rigid and coplanar structure, better intramolecular charge transfer (ICT) properties leading to the enhanced light absorption properties, ambipolar behaviour, extended π- conjugation, ability to form π-stacked structures in the solid state *via* strong π-π interactions, etc.. Cheng *et al*. reported DTPBT-based D-A polymers utilizing 9,9-dioctyl-9*H*-fluorene (F), 9-heptadecanyl-9*H*-carbazole (C) and 4,4-bis(2-ethylhexyl)-4*H*-cyclopenta[2,1-*b*:3,4-*b*′]dithiophene (CPDT) *via* Suzuki and Stille polymerization (Figure 4.2). The space-charge limit current (SCLC) hole

mobilities of these DTPBT-based polymers; **poly(DTPBT-*alt*-F)**, **poly(DTPBT-*alt*-C)** and **poly(DTPBT-*alt*-CPDT)** were measured to be 4.7 X 10^{-5}, 1.8 X 10^{-5} and 1.3 X 10^{-5} cm^2 V^{-1} s^{-1}, respectively.[26]

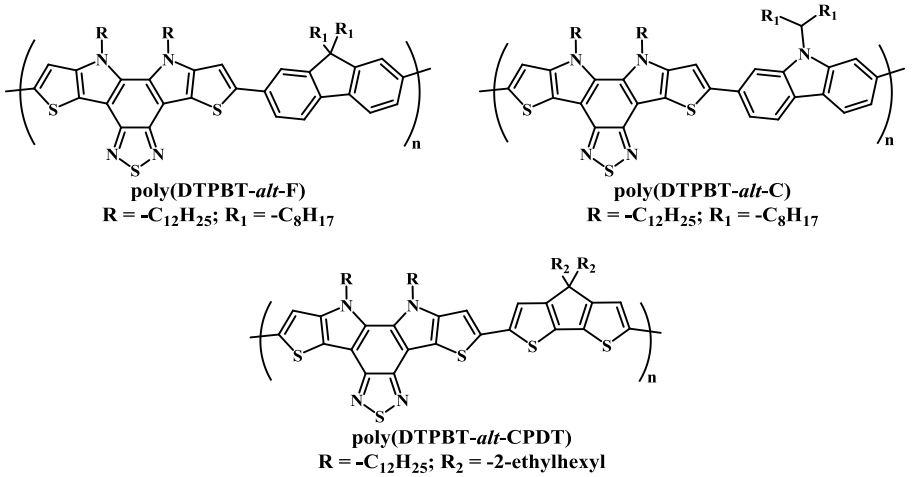

Figure 4.2 Structures of reported DTPBT-based D-A polymers[26]

Carsten *et al*. reported two novel DTPBT-based copolymers (Figure 4.3) with 4,8-bis(2-butyloctyloxy)benzo[1,2-*b*:4,5-*b*′]dithiophene (BDT) and 3-fluorothieno[3,4-*b*]thiophene-2-(2-ethylhexyl)carboxylate (fTT) *via* Stille polymerization. These DTPBT-based D-A polymers, **poly(DTPBT-*alt*-BDT)** and **poly(DTPBT-*alt*-fTT)** exhibited relatively higher SCLC hole mobilities of 3.43 X 10^{-4} and 2.95 X 10^{-4} cm^2 V^{-1} s^{-1}, respectively.[27]

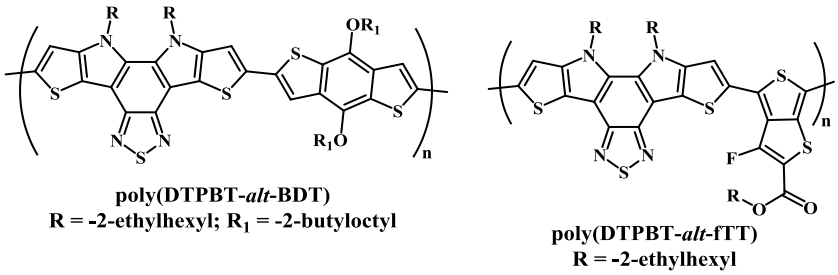

Figure 4.3 Structures of reported DTPBT-based D-A polymers[27]

Recently, Liu *et al*. reported DTPBT-based D-A polymers using 4,8-bis(5-(2-ethylhexyl)thiophenyl)benzo[1,2-*b*:4,5-*b*′]dithiophene (BT-BDT) as electron-rich donor unit and 2,5-bis(2-ethylhexyl)-3,6-bisthiophenylpyrrolo[3,4-*c*]pyrrole-1,4-dione (DPP) as electron-poor acceptor unit *via* Stille polymerization (Figure 4.4). The D-A copolymer **poly(DTPBT-*alt*-BT-BDT)** showed SCLC hole mobility of 2.1 X 10^{-5} cm^2 V^{-1} s^{-1}, while ternary D-A copolymer **poly{(DTPBT-*alt*-BT-BDT)$_{0.7}$-*alt*-(BT-BDT-**

***alt*-DPP)$_{0.3}$}** exhibited slightly improved SCLC hole mobility of 2.9 X 10^{-5} cm^2 V^{-1} s^{-1}.[1]

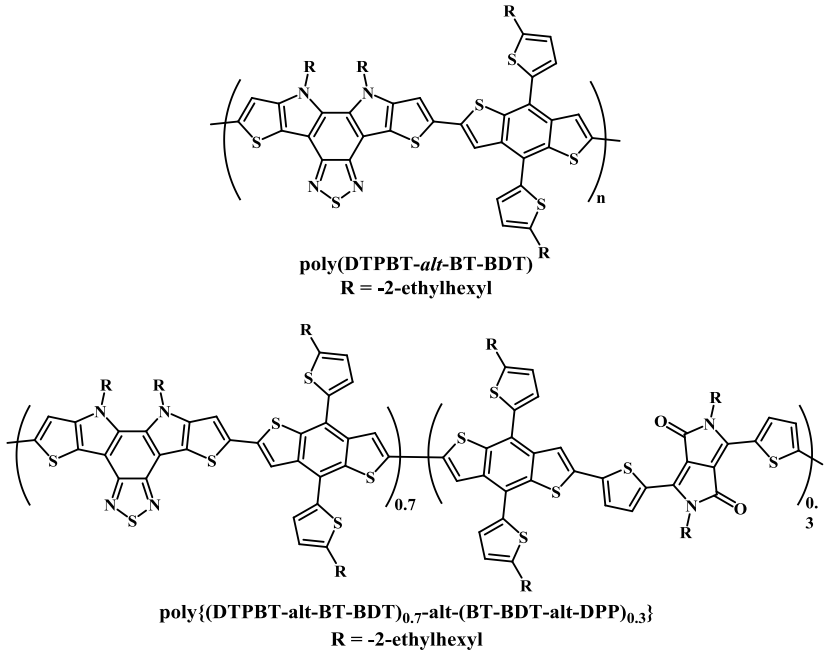

Figure 4.4 Structures of reported DTPBT-based D-A polymers[1]

Thus, focusing the superior properties of DTPBT-scaffold, like coplanar structure, enhanced absorption properties, ambipolar behaviour, strong intermolecular π-π interaction, etc., we have synthesized 10,11-dioctyl-2,8-bis(tri-*n*-butylstannyl)-10,11-dihydro-[2,1,3]thiadiazolo[4,5-*e*]thieno[2',3':4,5]pyrrolo[3,2-*g*]thieno[3,2-*b*]indole (**TP-M1**), which can be easily incorporated into a D-A polymer *via* Stille polymerization with three different co-monomers.

2,1,3-Benzothiadiazole (BT) is one of the most widely explored electron-withdrawing unit in the field of organic electronics.[28–30] Various electron-rich and some electron-poor units have been attached or inserted into the BT unit to further tune the opto-electronic properties of BT-based scaffolds.[31–39] Particularly, introducing the strongly electron-withdrawing fluorine atoms to the BT-unit has been found to stabilize both LUMO and HOMO energy levels and this modification has led to the many new high performing organic electronic materials.[31,40–44] Tamilavan *et al*. have reported BT-based acceptor-acceptor-acceptor-type monomer by introducing the two weak electron-accepting *N*-alkylbenzimidazole scaffolds into the central strong electron-accepting BT-unit, and utilized this novel acceptor to form a D-A polymer with 2,6-bis(trimethylstannyl)-4,8-bis(2-ethylhexyloxy)benzo[1,2-*b*:4,5-*b*′]dithiophene *via* Stille

polymerization. Synthesized D-A polymer exhibited optical bandgap of 2.34 eV, though the novel acceptor unit utilized in D-A polymer was proven to be a strongly electron-withdrawing, that could lower the HOMO energy level of D-A polymer.[45] This intrigued us to explore this strong acceptor unit and we have synthesized a similar acceptor unit, **BTD-IMD-M5**, having solubilising *n*-octyl chains at nitrogen atoms of imidazole rings. Accounting the strong electron-withdrawing behaviour of **BTD-IMD-M5**, we have developed a ternary D-A polymer **TP-TP-IMD** by Stille polymerization of DTPBT-based monomer **TP-M1** with DTPBT-based monomer **TP-M2** and a strong acceptor **BTD-IMD-M5** in 1:1 stoichiometric ratio, thereby increasing the percentage of donor DTPBT-units to 75% and reducing the percentage of acceptor BTD-IMD units to 25%.

Recently, quinoxaline-based D-A polymers have garnered attention of researchers for organic electronic devices, due to the strong electron withdrawing properties of quinoxaline ring system.[46–52] 6*H*-indolo[2,3-*b*]quinoxaline (Figure 4.5) has emerged as a novel D-A molecule, having fused electron-rich indole and electron-deficient quinoxaline.[53] Due to this unique dipolar structure, indoloquinoxaline exhibits better intramolecular charge transfer (ICT). Moreover, coplanar structure with extended π-conjugation endows indoloquinoxaline to form π-stacked aggregates, both in solution as well as in solid state, *via* strong π-π interaction.[53,54]

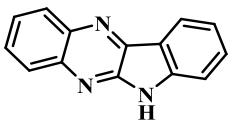

Figure 4.5 Structure of D-A integrated 6*H*-indolo[2,3-*b*]quinoxaline

Tyagi *et al*. have reported a series of indoloquinoxaline derivatives and utilized them as electron transporting and emitting layer in OLEDs.[55] Qian *et al*. and Payne *et al*. have reported 6*H*-indolo[2,3-b]quinoxaline-based organic sensitizers for dye-sensitized solar cells (DSSCs).[53,56,57] Recently Dong *et al*. reported indoloquinoxaline-based hole-injection materials for multi-layered OLEDs.[58] To the best of our knowledge, a D-A-type coplanar tetracyclic fused system, 6*H*-indolo[2,3-*b*]quinoxaline has not been incorporated yet into the conjugated polymers. Thus, focusing the advantages offered by 6*H*-indolo[2,3-*b*]quinoxaline scaffold, like tetracyclic fused coplanar structure, better intramolecular charge transfer (ICT) owing to the unique

dipolar structure, ability to form π-stacked aggregates due to the strong intermolecular π-π interactions, ambipolar behaviour, etc., we have developed a novel 2,9-dibromo-6-dodecyl-6*H*-indolo[2,3-*b*]quinoxaline (**INQx-M3**), which can be easily subjected to the Stille polymerization with synthesized DTPBT-based monomer, **TP-M1**, to give a novel D-A polymer **TP-INQx**.

In the past few years, new electron deficient units have been identified such as the double B ← N bridged bipyridyl (BNBP) as well as several lactam-based electron-deficient units, including diketopyrrolopyrrole (DPP) and isoindigo (IIG).[59–62] Recently, DPP unit containing small molecules and polymers have exhibited high charge carrier mobilities for both holes and electrons, owing to the strongly polar pyrrole functionality and electron-withdrawing carbonyl carbons, which facilitates intermolecular associations.[63] Similar to DPP, IIG is identified as one of the most efficient electron-withdrawing units, due to the polar bicyclic lactam units.[63,64] IIG-based D-A polymers show good charge carrier mobilities and excellent stabilities in ambient conditions due to the lowering of the HOMO-LUMO energy levels. Furthermore, strongly electron-withdrawing fluorine atoms have also been introduced to the IIG-scaffold, to improve the charge mobilities and ambient stability by lowering the LUMO levels.[65–69]

Recently, Li *et al*. reported a novel pyrazine-fused isoindigo (PzIIG), having a more planar structure and extended π-conjugation compared to the IIG unit. The two PzIIG-based D-A polymers, having two BDT-derivatives, namely 4,8-bis(4,5-dioctylthiophenyl)benzo[1,2-*b*:4,5-*b*′]dithiophene ($BDT2TC_8$) and 4,8-bis(4,5-didecylthiophenyl)dithieno[2,3-*d*:2′,3′-*d*]benzo[1,2-b:4,5-b′]dithiophene ($DTBDT2TC_{10}$), were reported to exhibit deeper HOMO-LUMO levels; −5.48 eV and −3.64 eV, respectively for poly(PzIIG-*alt*-$BDT2TC_8$) and −5.40 eV and −3.58 eV for poly(PzIIG-*alt*-$DTBDT2TC_{10}$). Both polymers showed moderate SCLC hole mobilities of 6.57 X 10^{-5} cm^2 $V^{-1}s^{-1}$ and 5.92 X 10^{-5} cm^2 $V^{-1}s^{-1}$ for poly(PzIIG-*alt*-$BDT2TC_8$) and poly(PzIIG-*alt*-$DTBDT2TC_{10}$), respectively.[64] Inspired form this, we have developed a novel benzene-fused isoindigo scaffold, namely (3*E*,3′*E*)-3,3′-(1,4-phenylenebis(methanylylidene))bis(5-bromo-*N*-dodecylindolin-2-one) (**BIIG-M4**), which is subjected to the Stille polymerization with **TP-M1** to yield a novel D-A polymer **TP-BIIG**.

Results and discussion

Synthesis of monomers and polymers

A nitrogen-bridged pentacyclic donor-acceptor type dithienopyrrolobenzothiadiazole (**DTPBT**) was synthesized from 5,6-dinitro-4,7-dithienyl-2,1,3-benzothiadiazole (compound **4**) by intramolecular cadogan annulation (Scheme 4.1) according to the literature procedure reported by Kato *et al.*[70] In **DTPBT**, two outer electron rich thiophene moieties are covalently fastened with central electron-deficient benzothiadiazole core with an aid of two nitrogen bridges. Synthesized **DTPBT** was subjected to the *N*-alkylation using *n*-octylbromide and sodium hydroxide powder in DMF under nitrogen atmosphere, to yield **DTPBT-C8**.

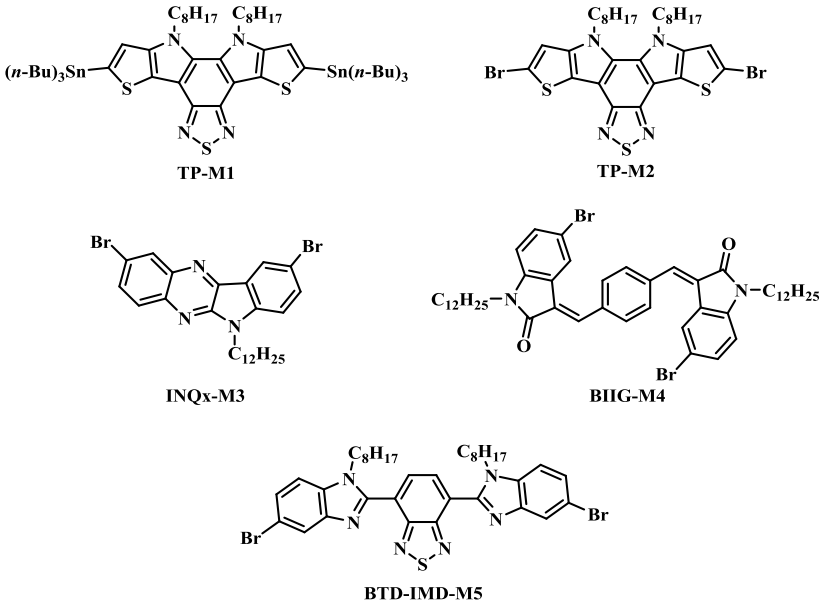

Figure 4.6 Structures of the synthesized monomers

DTPBT-based monomers **TP-M1** and **M2** were synthesized according to the modified literature procedure reported by Carsten *et al.* (Scheme 4.2).[71] **TP-M1** was synthesized by lithiation of **DTPBT-C8** using *in-situ* prepared lithium diisopropylamide (LDA) at −78 °C in dry THF, followed by quenching the lithiated salt with dropwise addition of tri-*n*-butyltin chloride solution in dry THF. Obtained crude product after reaction, was directly utilized for polymerization without further purification, the percentage conversion and yield of the reaction was determined by ^{1}H NMR spectroscopy of the crude reaction mass. The second DTPBT-based monomer **TP-M2** was synthesized by reacting **DTPBT-C8** with *N*-bromosuccinamide in anhydrous DMF under dark conditions at room temperature.

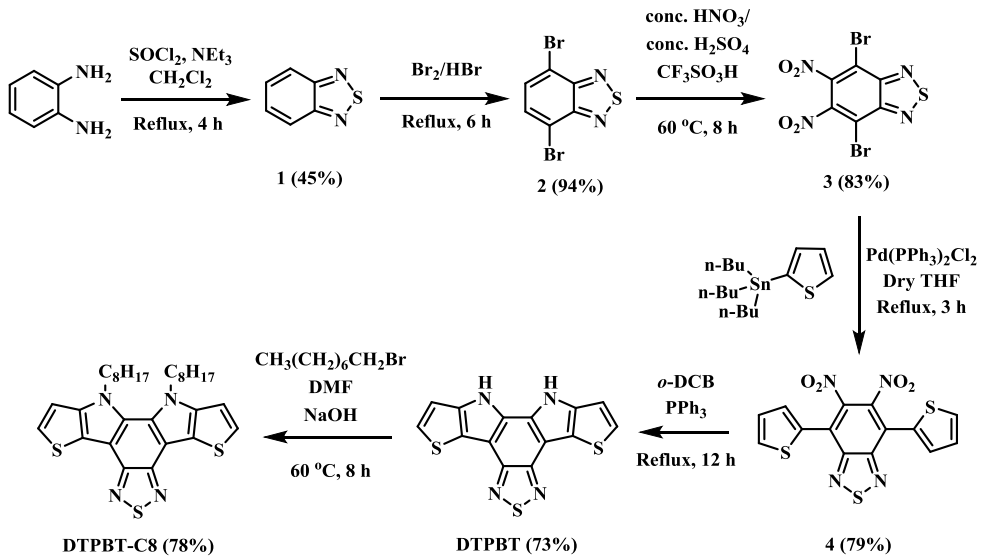

Scheme 4.1 Synthesis of **DTPBT** and **DTPBT-C8**

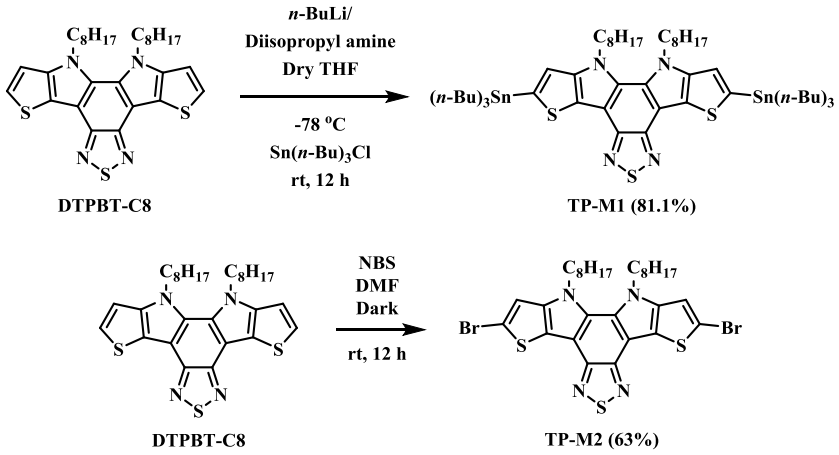

Scheme 4.2 Synthesis of **TP-M1** and **TP-M2** from **DTPBT-C8**

The indoloquinoxaline-based **INQx-M3** was synthesized by acetic acid catalyzed condensation reaction between 5-bromoisatin and compound **6** under nitrogen atmosphere, followed by the *N*-alkylation reaction using *n*-dodecylbromide and K_2CO_3 in DMF (Scheme 4.3). In accordance with the two equally possible approaches of 4-bromo-1,2-diaminobenzene (compound **6**) towards condensation with 5-bromoisatin, two condensation products, namely 2,9-dibromo-6-dodecyl-6*H*-indolo[2,3-*b*]quinoxaline (**INQx-M3**) and 3,9-dibromo-6-dodecyl-6*H*-indolo[2,3-*b*]quinoxaline (compound **7**) are being formed in 1:1 ratio (confirmed by ^{1}H NMR spectroscopy).

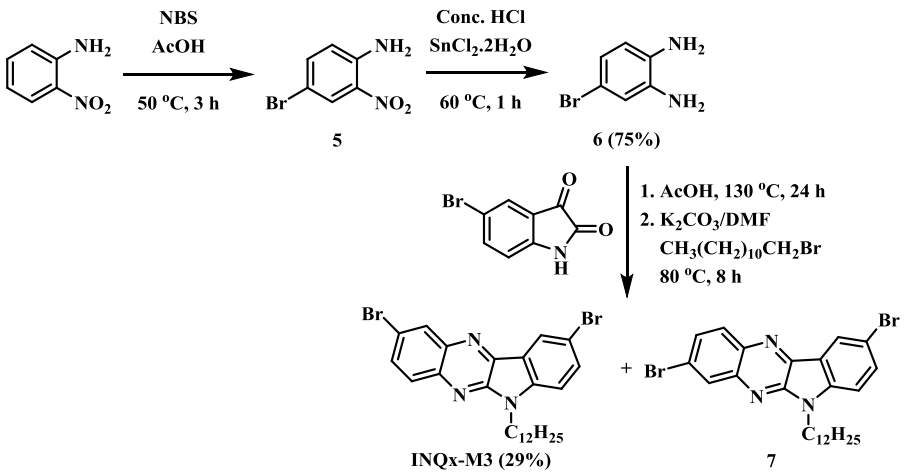

Scheme 4.3 Synthesis of **INQx-M3** from 5-bromoisatin and 4-bromo-1,2-diaminobenzene

A mixture of both the products (**INQx-M3** and **7**) were isolated as a bright yellow band from the column chromatography. The isolated mixture was further purified by extensive column chromatography over silica gel using 5% ethyl acetate-petroleum ether as an eluent, yielding relatively pure slowly moving **INQx-M3** from the later fractions of the column. Isolated pure product was further purified by re-crystallization from ethanol-chloroform solution, yielding pure **INQx-M3** as bright yellow needles. Moreover, positions of bromine atoms were confirmed by single crystal X-ray diffraction study of **INQx-M3**. It is noteworthy that out of the two possible structural isomers, **INQx-M3** and **7**, the isomer having both bromine atoms on the same side of the molecule (**INQx-M3**) crystallizes as bright yellow needle shaped crystals under ambient conditions, while the second isomer comes out from the solution as bright yellow beads.

The benzene-fused iso-indigo **BIIG-M4** was synthesized by Knoevenagel-type condensation reaction between 5-bromo-*N*-dodecylindolin-2-one (compound **9**) and terephthalaldehyde using piperidine as a base in refluxing ethanol under nitrogen atmosphere (Scheme 4.4). 5-bromo-*N*-dodecylindolin-2-one (compound **9**) was synthesized from 5-bromo-1-dodecylisatin (compound **8**) by Wolff-Kishner type reduction reaction using refluxing hydrazine hydrate (99%).

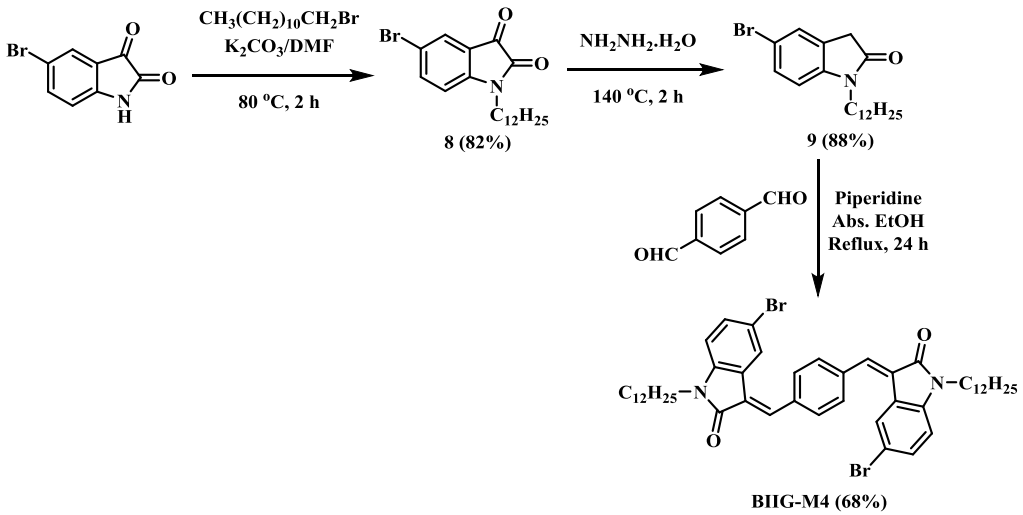

Scheme 4.4 Synthesis of **BIIG-M4** from compound **9** (5-bromo-*N*-dodecylindolin-2-one) and terphthalaldehyde

An acceptor-acceptor-acceptor type benzothiadiazole-imidazole based monomer **BTD-IMD-M5** was synthesized by reacting 2,1,3-benzothiadiazole-4,7-dicarbaldehyde (compound **12**) with 4-bromo-1,2-diaminobenzene (compound **6**) in DMF using OXONE as an oxidizing agent (Scheme 4.5). The reaction proceeds through the condensation reaction followed by the OXONE-mediated oxidative cyclisation reaction.

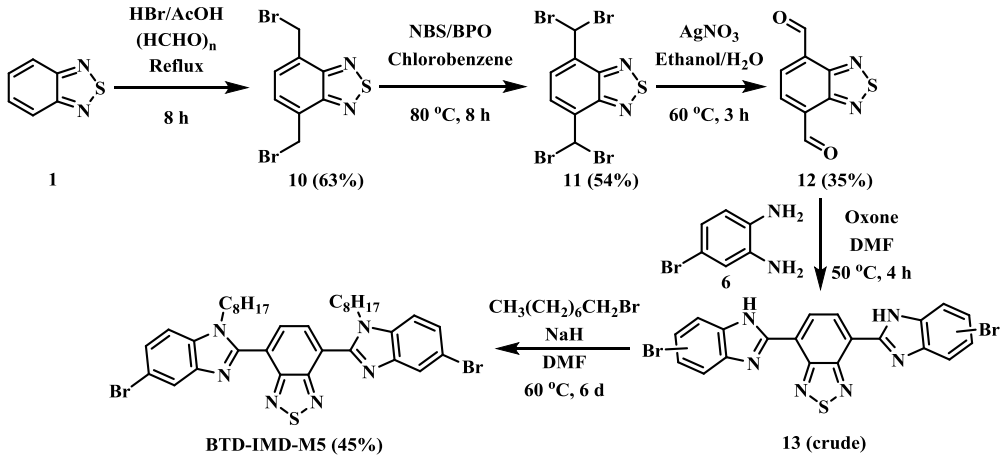

Scheme 4.5 Synthesis of **BTD-IMD-M5** from compound **12** (2,1,3-benzothiadiazole-4,7-dicarbaldehyde) and compound **6** (4-bromo-1,2-diaminobenzene)

The crude product **13** obtained from the reaction was isolated and subjected to the *N*-alkylation reaction using sodium hydride (60% mineral oil suspension) in anhydrous DMF. 2,1,3-benzothiadiazole-4,7-dicarbaldehyde (compound **12**) was synthesized from 4,7-bis(dibromomethy)-2,1,3-benzothiadiazole (compound **11**) in refluxing ethanol using silver nitrate as an oxidizing agent.

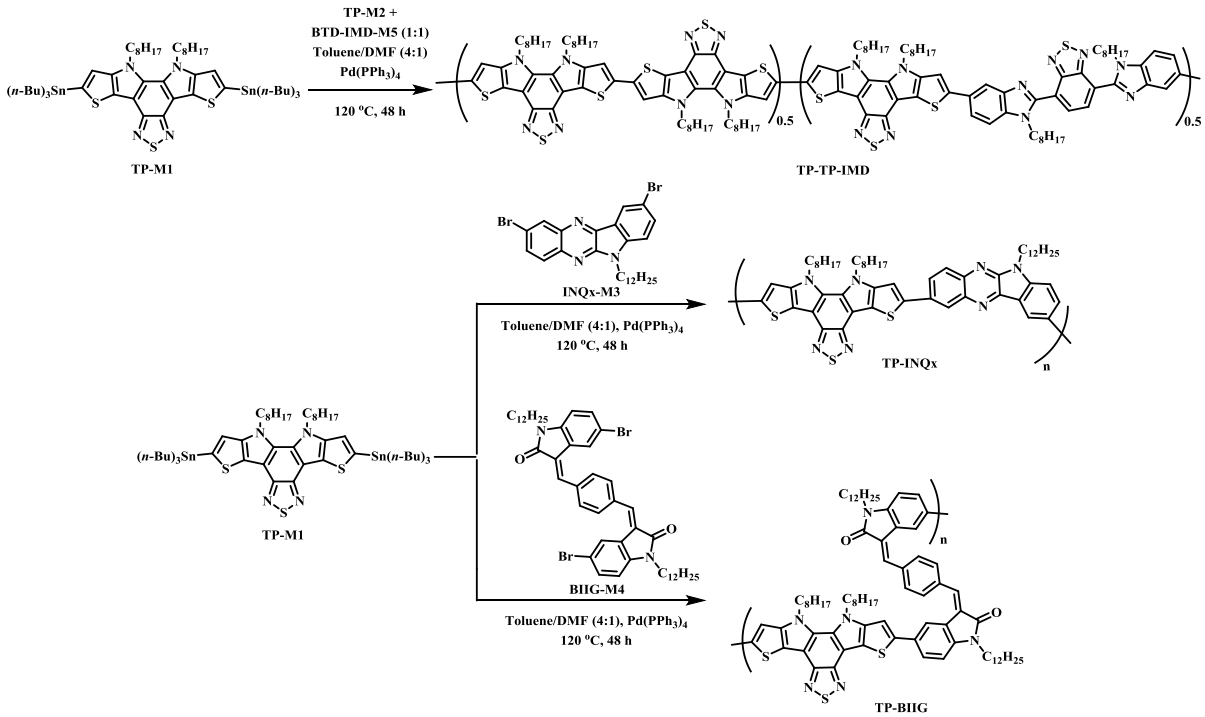

Scheme 4.6 Synthesis of DTPBT-based co-polymers **TP-TP-IMD**, **TP-INQx** and **TP-BIIG** by Stille polymerization

The dithienopyrrolobenzothiadiazole (DTPBT)-based conjugated polymers, namely **TP-TP-IMD**, **TP-INQx** and **TP-BIIG**, were synthesized by stille coupling reaction between distannyl derivative of DTPBT, **TP-M1** and corresponding dibromo derivatives (**TP-M2+BTD-IMD-M5** (1:1), **INQx-M3** and **BIIG-M4**) using $Pd(PPh_3)_4$ as catalyst in toluene/DMF (4:1) under nitrogen atmosphere (Scheme 4.6). The obtained polymers were further purified by sequential soxhlet extraction using different solvents like methanol, acetone, petroleum ether and the pure polymer fraction was finally eluted using chloroform. The solvent was evaporated under reduced pressure and solids were further dried under vacuum at 50 °C.

Structural aspects of monomers

The molecular structures of two nitrogen-bridged donor-acceptor type molecules DTPBT and its *N*-alkylated derivative have been studied extensively using single crystal X-ray diffraction studies by Kato *et al.*[70] X-ray analysis has confirmed that these π-extended thiadiazoles have highly planar frameworks with good π–π stacking ability. Moreover, *N*-alkylated DTBPT showed head-to-tail packing, forming 1D columns in a parallel and slanted arrangement. These columns are held together by weak S···H interactions.

Structural aspects of the indoloquinoxaline-based monomer **INQx-M3** were studied by single crystal X-ray diffraction technique. A single crystal of **INQx-M3** was obtained by re-crystallization from ethanol-chloroform. Data were collected using Mo Kα (λ = 0.71073) radiation on an Xcalibur-Eos-Gemini diffractometer. The crystal was kept at 293 K during data collection. The structure was solved and refined using Olex2[72] computer program, using ShelXL structure solution program[73] and refined with ShelXL refinement package[74] using least squares minimization. X-ray analysis confirmed that **INQx-M3** has highly planar framework (Figure 4.7a and b).

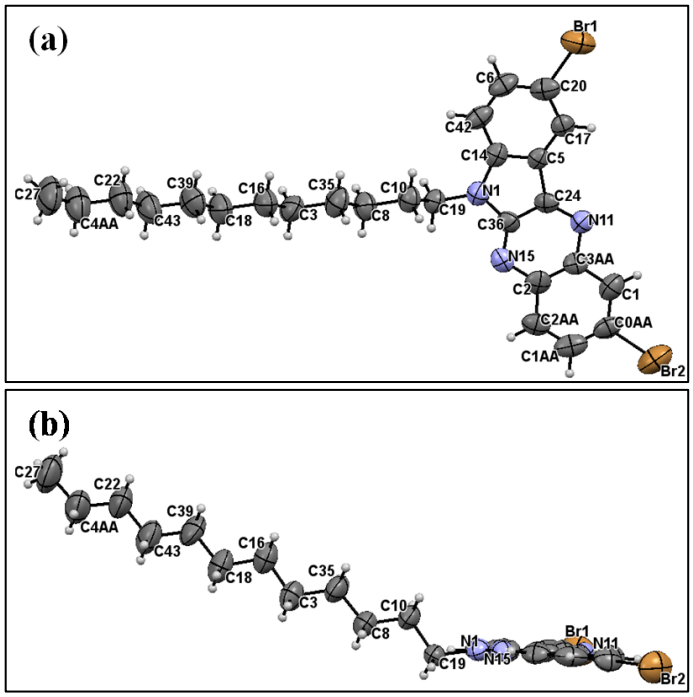

Figure 4.7 ORTEP drawing of **INQx-M3**; (a) top view and (b) side view

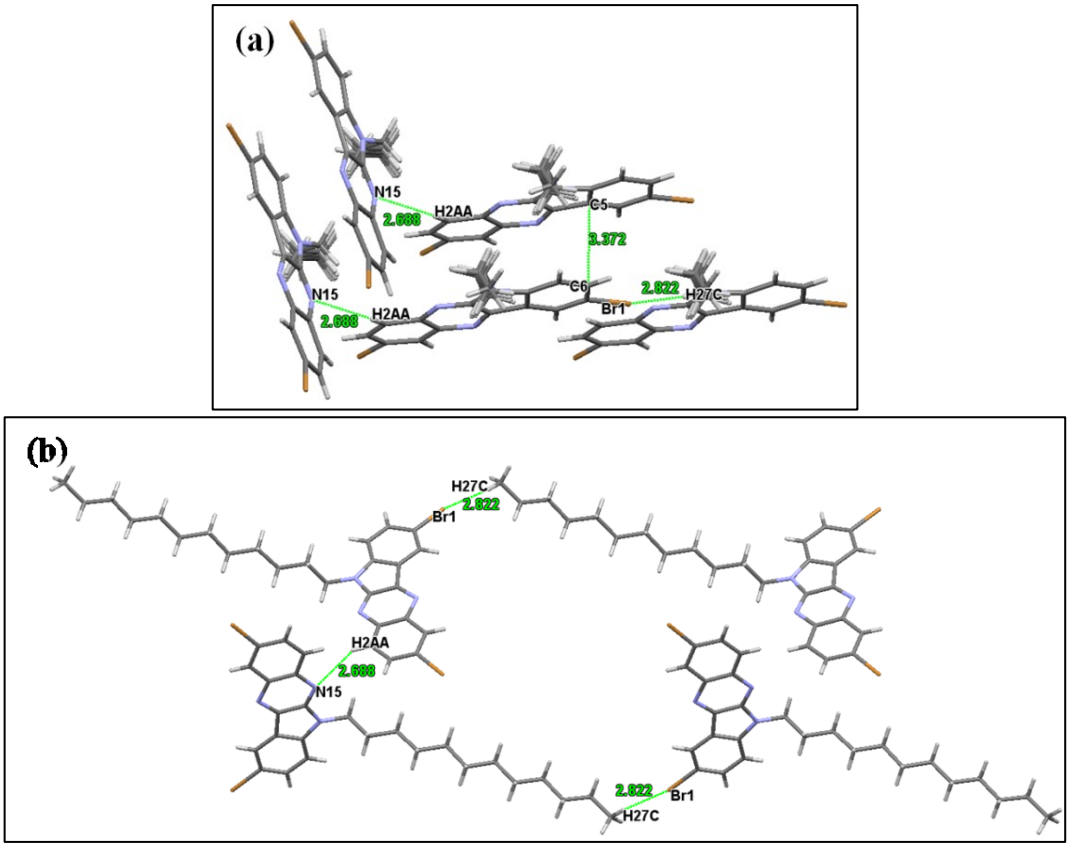

Figure 4.8 (a) Arrangement of neighbouring molecules in the crystal packing of **INQx-M3** and (b) Crystal packing of **INQx-M3** along *b*-axis.

The dihedral angle between both of the terminal phenylene rings is 5.4°. In solid state, the molecular structure showed no noticeable bond length alteration and bond angles are inconspicuous. In the crystal structure, no intramolecular hydrogen bonding was observed. Moreover, **INQx-M3** exhibited good π-π stacking with a distance of about 3.36−3.38 Å as shown in Figure 4.8a and Figure 4.9a. The molecules are arranged in a sheet like structure with head-to-tail packing, influenced by weak Br···H interactions (Br1···H27C) with a distance of 2.82 Å.

Additionally, the molecules are packed in head-to-head manner to form a 1D column in a parallel and slanted arrangement (Figure 4.9), governed by strong π-π interaction between quinoxaline ring and phenyl ring adjacent to the quinoxaline ring. These columns are held together by weak N···H interactions (N15···H2AA) with a distance of 2.69 Å at an angel of 84.3°. The crystal packing of **INQx-M3** showed large solvent accessible voids along the *b*-axis (Figure 4.9b).

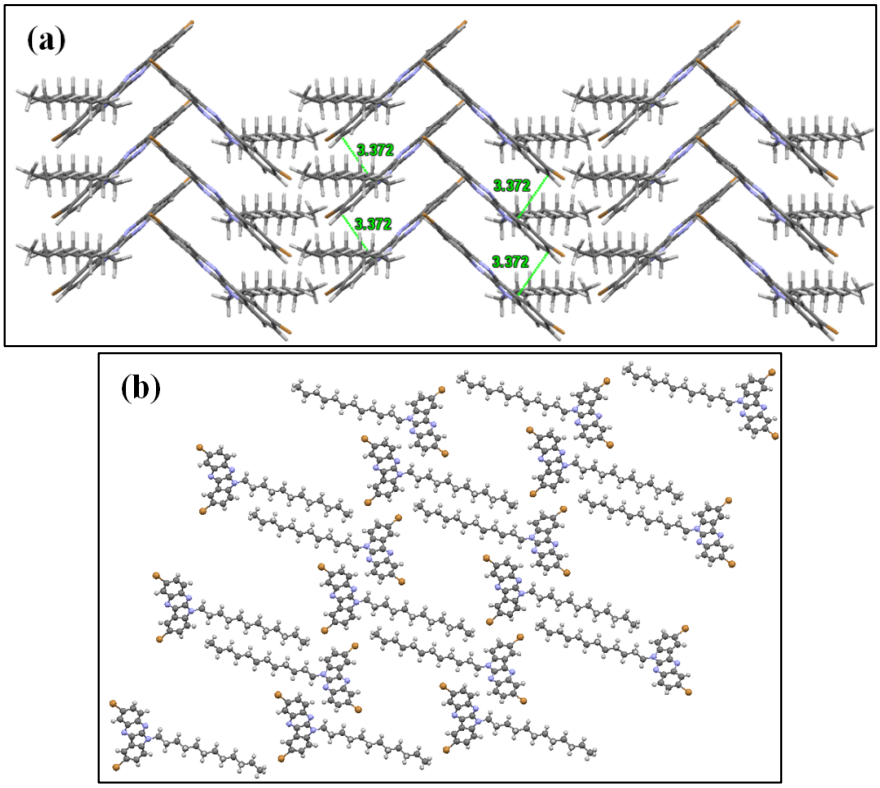

Figure 4.9 (a) Formation of 1D columns in parallel and slanted arrangement in the crystal packing of **INQx-M3** along *c*-axis; (b) Formation of large solvent accessible voids in the crystal packing of **INQx-M3** along *b*-axis

The benzene fused iso-indigo **BIIG-M4** contains one phenyl ring inserted in the middle of isoindigo. This inserted phenyl ring is providing a longer effective conjugation length compared to the isatin-derived isoindigo. Moreover, the inserted phenyl ring preferably remains *trans*- to the carbonyl group of the oxindole ring, making **BIIG-M4** structurally rigid. The benzothiadiazole-imidazole based compound **13** is having central strong electron withdrawing benzothiadiazole ring, which is connected to the weak electron accepting benzimidazole rings at 4- and 7- positions. Though, only one structure is presented for compound **13** in Scheme 4.5, compound **13** can exist as three isomers due to the N−H hydrogen exchange between 1,3-positions of the imidazole ring.[45] However, after *N*-alkylation of compound **13**, resulting monomer **BTD-IMD-M5** showed symmetrical structure as deduced from the ^{1}H and ^{13}C NMR spectra. The two *n*-octyl chains attached to the benzimidazole units, should be on the same side of the molecule and in order to avoid steric hinderance with the thiadiazole ring, the *n*-octyl chains might be positioned to the opposite side of the thiadiazole ring.[45] However, the bromine atoms can be present at either 5- or 6- position of the benzimidazole ring, and to have a better look at the position of bromine atoms, single

crystal of the monomer **BTD-IMD-M5** was developed from its saturated chloroform solution. The suitable single crystal of **BTD-IMD-M5** was picked and was studied by the single crystal X-ray diffraction technique. Data were collected using Mo Kα (λ = 0.71073) radiation on an Xcalibur-Eos-Gemini diffractometer. The crystal was kept at 298 K during data collection. The structure was solved and refined using Olex2[72] computer program, using SUPERFLIP structure solution program[75–77] and refined with ShelXL refinement package[74] using least squares minimization.

To our surprise, the crystal structure of **BTD-IMD-M5** is non-symmetrical, contradictory to our previous deductions from the ^{1}H and ^{13}C NMR spectra of **BTD-IMD-M5**. Moreover, both of the *n*-octyl chains, attached to the benzimidazole units are on the opposite sides of each-other. Also, the bromine atoms are oriented on the opposite sides of the **BTD-IMD-M5** molecule.

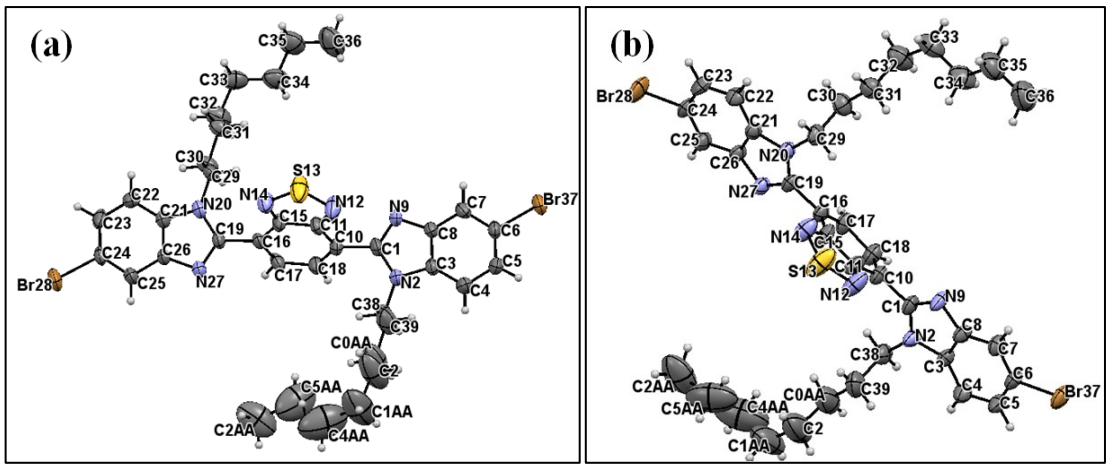

Figure 4.10 ORTEP drawing of **BTD-IMD-M5**; (a) view along *ab* axis and (b) view along *b** axis

As suggested from the crystal structure, **BTD-IMD-M5** is not completely planar molecule. The central benzothiadiazole (BTD) unit is twisted and the dihedral angle between the BTD unit and the coplanar terminal 5-bromo-1-octylbenzimidazole (IMD) units is 61.8°. In solid state, the molecular structure showed no noticeable bond length alteration and bond angles are inconspicuous. In the crystal structure, intramolecular hydrogen bonding between N14···H29A (2.69 Å) was observed.

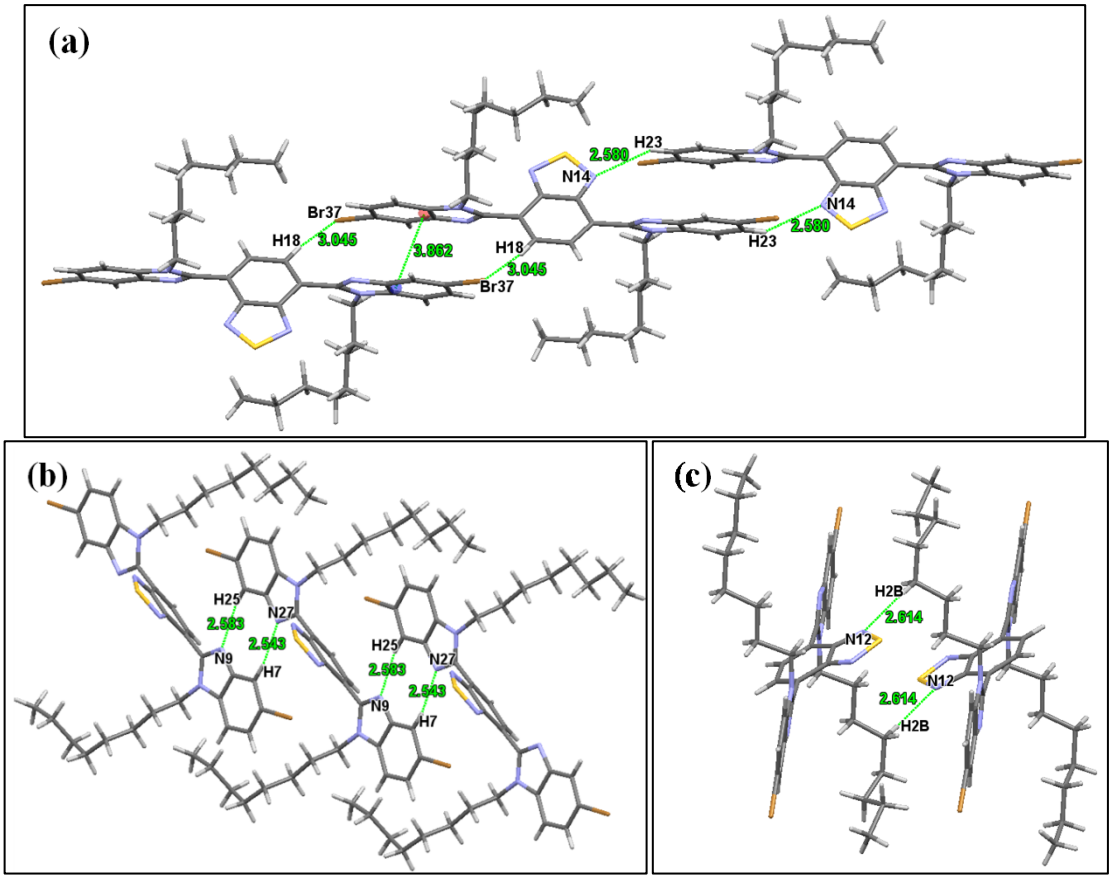

Figure 4.11 (a), (b) and (c) Arrangement of neighbouring molecules in the crystal packing of **BTD-IMD-M5**.

The IMD units within **BTD-IMD-M5** exhibit oppositely aligned stacked arrangement with a distance of 3.86 Å as shown in Figure 4.11a. These stacked IMD units are held together by the weak N···H interactions (N14···H23) with a distance of 2.58 Å and weaker Br···H interactions (Br37···H18) with a distance of 3.04 Å. Moreover, the IMD

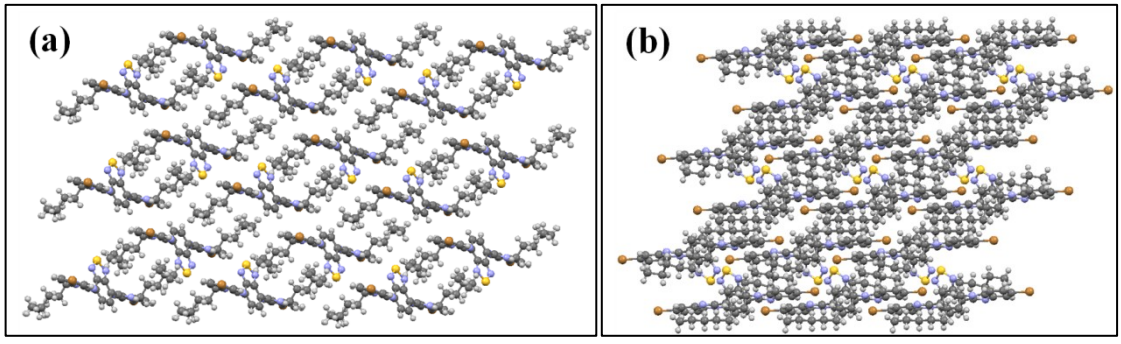

Figure 4.12 (a) *Zig-zag* type arrangement of **BTD-IMD-M5** molecules with up and down alignment of BTD-units along *a*-axis; (b) arrangement of **BTD-IMD-M5** molecules along *c*-axis

units form two dimensional sheet like structure along the direction of *a* axis, governed by the weak N···H interactions between N9···H25 and N27···H7, with a distance of

2.58 Å and 2.54 Å, respectively (Figure 4.11b). The distance between these two dimensional sheets of IMD units is controlled by the weak N···H interactions (N12···H2B) with a distance of 2.61 Å (Figure 4.11c), and the overall distance between two successive sheets is 6.71 Å. The crystal packing of **BTD-IMD-M5** showed *zig-zag* type packing of molecules with up and down alignment of BTD-units along the *a*-axis (Figure 4.12a).

Table 4.1 Crystallographic data and structures refinement parameters

Parameters	Values	Values
Identification code	**INQx-M3**	**BTD-IMD-M5**
Empirical formula	$C_{26}H_{31}N_3Br_2$	$C_{36}H_{42}Br_2N_6S$
Formula weight	544.28	748.62
Temperature/K	293	298
Crystal system	Monoclinic	Triclinic
Space group	$P2_1$	P-1
a/Å	17.493(4)	11.0330(6)
b/Å	4.6336(6)	11.1291(7)
c/Å	21.536(6)	15.7037(7)
α/°	90.00	94.670(4)
β/°	111.82(3)	96.188(4)
γ/°	90.00	110.510(5)
Volume/Å^3	1620.5(7)	1780.70(18)
Z	31	2
ρ_{calc}g/cm^3	1.110	1.396
Crystal size/mm^3	0.5×0.6×1.0	0.1×0.3×0.6
Radiation	Mo Kα (λ = 0.71073)	Mo Kα (λ = 0.71073)
Reflections collected	19557	19937
Independent reflections	6298 [R_{int} = 0.1205, R_{sigma} = 0.1871]	7144 [R_{int} = 0.0589, R_{sigma} = 0.1004]
Data/restraints/parameters	6298/312/281	7144/28/408
Goodness-of-fit on F^2	0.860	1.001
Final R indexes [I>=2σ (I)]	R_1 = 0.0755, wR_2 = 0.1629	R_1 = 0.0655, wR_2 = 0.1603
Final R indexes [all data]	R_1 = 0.2185, wR_2 = 0.2280	R_1 = 0.1399, wR_2 = 0.2023
Largest diff. peak/hole/eÅ^{-3}	0.9/-0.28	1.35/-0.42
CCDC Number	1882341	1882340

From the ^{1}H, ^{13}C NMR studies and SCXRD studies of **BTD-IMD-M5**, it can be concluded that within the solution, the IMD-units are free to rotate and hence exhibits an averaged symmetrical structure, while in the solid state, it exhibits non-symmetrical structure, with *n*-octyl chains on the opposite side of each-other.

Molecular weight and thermal properties of polymers

The DTPBT-based conjugated polymers **TP-TP-IMD**, **TP-INQx** and **TP-BIIG**, synthesized by stille coupling reaction showed weight average molecular weights (M_w) in the range of 9 kDa to 13.5 kDa, measured by GPC analysis. Introduction of alkyl chains in the monomers promoted the solubility of the resulting conjugated polymers. All the synthesized polymers showed moderate to good solubility properties in the common organic solvents, like dichloromethane, chloroform, dichlorobenzene and tetrahydrofuran. Thermal properties of all the synthesized conjugated polymers were analyzed by thermogravimetric analysis (TGA) at a heating rate of 10 ^{o}C/min under nitrogen atmosphere (Figure 4.13). The decomposition temperature (T_d) of the polymer is defined as the temperature at which, the polymer loses 5% of its weight. All the synthesized polymers showed decomposition temperatures above 300 ^{o}C, which demonstrates their sufficiently high thermal stabilities for applications of PSCs. Weight average molecular weight (M_w), poly-dispersity index (PDI) and decomposition temperatures (T_d) of the DTPBT-based conjugated polymers are summarized in Table 4.2.

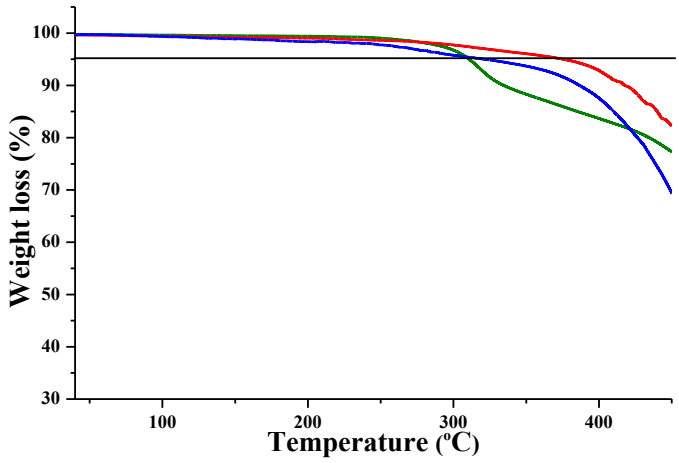

Figure 4.13 Thermogravimetric analysis (TGA) of DTPBT-based conjugated polymers; **TP-TP-IMD** (olive green line), **TP-INQx** (red line) and **TP-BIIG** (blue line)

Photo-physical properties of polymers

The photo-physical properties of all the polymers were studied by UV-visible spectroscopy of dilute chloroform solutions of the polymers as well as thin films on quartz glass casted from chloroform solution. All the polymers showed multiple band absorption spectra with complex band splitting patterns, both in the solution as well as in the film state. As shown in Figure 4.14a, **TP-TP-IMD** showed first absorption band ranging from 320 nm to 390 nm, having an absorption maxima (λ_{max}) at 374 nm with complex band splitting, which can be ascribed to the π–π^* transitions of both DTPBT and BTD-IMD scaffolds and an internal charge transfer transition from a short D–π–A diaminobenzothiadiazole chromophore present in DTPBT scaffold.

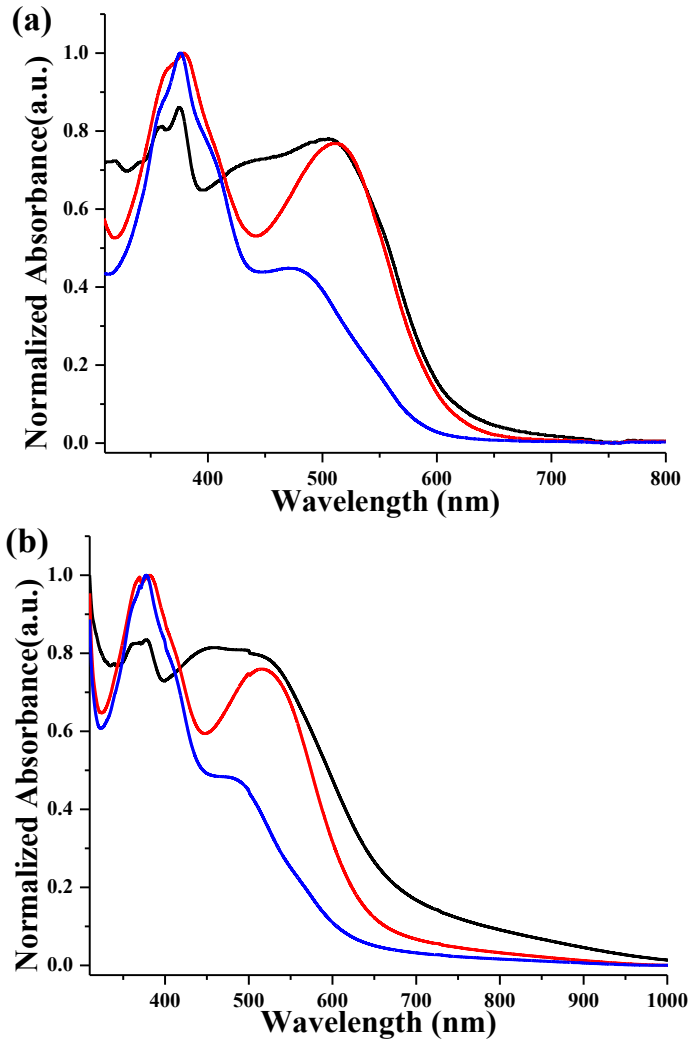

Figure 4.14 Absorption spectra of DTPBT-based conjugated polymers; (a) in chloroform and (b) in the film state. The black solid line corresponds to the absorption spectra of **TP-TP-IMD**, red solid line corresponds to the **TP-INQx** and blue solid line corresponds to the **TP-BIIG**

The second broad absorption band ranging from 395 nm to 650 nm; having absorption maxima at 507 nm with a shoulder peak at 442 nm, can be correlated to the charge transfer between donor and acceptor along the polymer chain. However, the solution spectra of **TP-INQx** and **TP-BIIG** exhibited relatively broader first absorption band starting from 315 nm and extending up to 440 nm, having λ_{max} at 377 nm and 378 nm, respectively. The first absorption band of **TP-INQx** is having a shoulder peak at 364 nm, while that of **TP-BIIG** exhibited two shoulder peaks at 358 nm and 400 nm, respectively. The second band in the absorption spectrum of **TP-INQx**, ranging from 441 nm to 650 nm, with λ_{max} at 513 nm can be related to the intramolecular charge transfer. The CT band in **TP-BIIG** appeared at relatively higher energy side, peaking at 474 nm and intensity of absorption is much lower compared to the rest of the DTPBT-based conjugated polymers. This can be related to the possible chain folding and twisting in **TP-BIIG** due to the loss of linearity. Even more, the possible steric repulsion forces between the central phenyl ring proton and terminal oxindole ring proton can cause the loss of planarity within **BIIG-M4**, which in turn, will lead to the poor CT along the polymer chain.[64]

Table 4.2 Photo-physical properties, decomposition temperature T_d (obtained from TGA), Molecular weight M_w and poly-dispersity index (obtained from GPC analysis) of synthesized DTPBT-based polymers; [a] from UV-visible spectroscopy of chloroform solution of polymers; [b] from UV-visible spectroscopy of polymer films casted on quartz plate; [c] calculated using equation $E_g^{opt} = 1240/\lambda_{edge}$.

Polymer	λ_{max} [a] (nm)	λ_{edge} [b] (nm)	E_g^{opt} [c] (eV)	T_d (^oC)	M_w (Dalton)	PDI
TP-TP-IMD	374, 507	742	1.67	310	9352	3.24
TP-INQx	377, 513	699	1.77	375	13186	3.48
TP-BIIG	378, 474	649	1.91	321	12227	3.24

In the film state, the absorption spectra of all the polymers exhibited broadening of the CT bands compared to the absorption spectra in the solution state (Figure 4.14b). Also, the absorption edges are shifted bathochromically, however, the absorption behaviour exhibits the same trend as the absorption in solution. The bathochromic shift observed in the absorption edge of **TP-TP-IMD** is ~85 nm while that in case of **TP-**

INQx is ~40 nm and for **TP-BIIG**, bathochromic shift observed in the absorption edge is ~45 nm. The optical band-gaps of all the polymers were calculated from the absorption edges of the polymer films and were found to be in following order: **TP-TP-IMD** (1.67 eV) < **TP-INQx** (1.77 eV) < **TP-BIIG** (1.91 eV). Obviously, **TP-TP-IMD** exhibited bathochromically shifted absorption edge and lowest optical band-gap owing to the more numbers of the coplanar DTPBT scaffolds present along the backbone chain, which in turn, leads to the better π–π stacking between the polymer chains and the extended effective π-conjugation along the polymer chain. Moreover, **TP-INQx** showed lower optical band-gap compared to the **TP-BIIG**, owing to the presence of highly coplanar INQx scaffolds within the polymer which extends the effective π-conjugation length. The photo-physical properties of the synthesized polymers are summarized in Table 4.2.

Electrochemical properties of polymers

The frontier orbital energy levels of the synthesized DTPBT-based conjugated polymers were measured using cyclic voltammetry (CV). CV experiments were performed in the dry acetonitrile using TBAPC as a supporting electrolyte (~50 mM) using a three electrode system: a glassy carbon electrode as the working electrode, a Pt wire electrode as the counter electrode and Ag/Ag^{+} as the reference electrode. Polymer films were casted on the glassy carbon working electrode from its chloroform solution (~10 mg/mL), the films were dried under nitrogen gas flow and were subjected to the CV measurement.

All the polymers showed irreversible oxidation and reduction waves in the cyclic-voltammogram (Figure 4.15a). The onset oxidation potentials of **TP-TP-IMD**, **TP-INQx** and **TP-BIIG** were measured from the oxidation wave (Figure 4.15b) and found to be at +0.83 V, +1.01 V and +1.25 V, respectively. The corresponding HOMO energy levels were calculated from the onset oxidation potentials. The HOMO energy level of **TP-BIIG** was found to be at −5.60 eV and it is the lowest lying HOMO energy level amongst all the synthesized DTPBT-based conjugated polymers. The lowering of the HOMO energy level can be ascribed to the superior electron withdrawing properties of BIIG scaffold, emerging from the two oxindoles, fused with a phenyl ring. BIIG scaffold resembles isoindigo in electron withdrawing properties.[64] The **TP-INQx** showed elevated HOMO energy level at −5.36 eV compared to the **TP-BIIG**, owing to

the indoloquinoxaline scaffold incorporated within the polymer. The electron affinity of quinoxaline moiety is somewhat diluted due to the fused indole, which is electron donating in nature. **TP-TP-IMD** has the highest lying HOMO energy level at −5.18 eV amongst all the polymers.

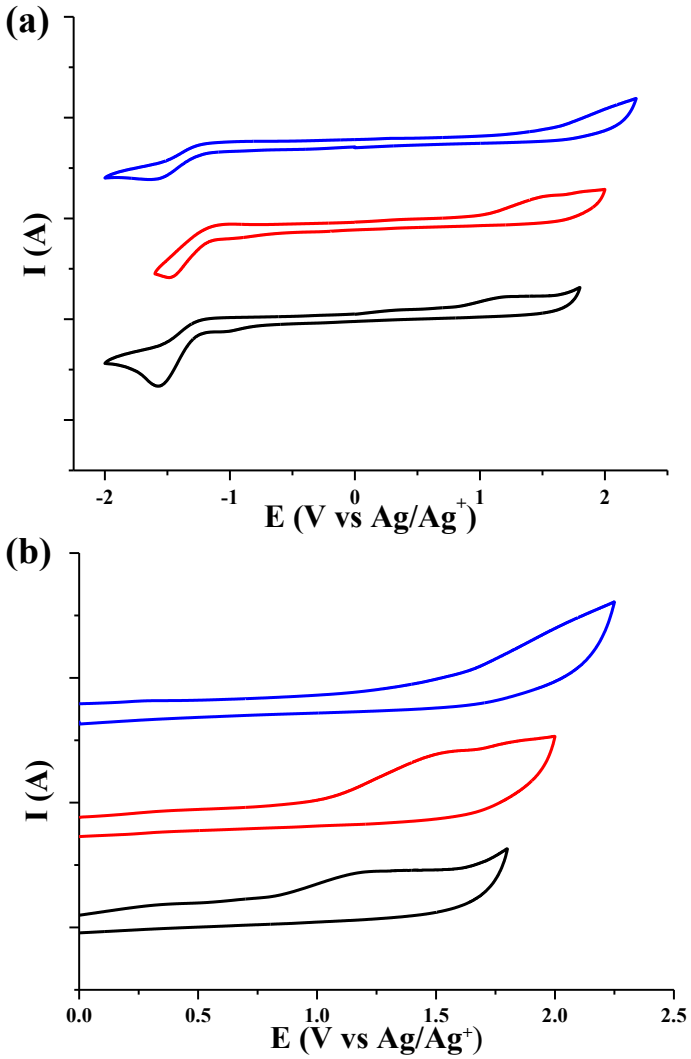

Figure 4.15 Cyclic voltammogram of DTPBT-based conjugated polymers **TP-TP-IMD** (black line), **TP-INQx** (red line) and **TP-BIIG** (blue line); (a) full scan and (b) oxidation wave; polymer films were casted from its chloroform solution (~10 mg/mL) on the glassy carbon working electrode and were scanned at 30 mV/s in dry acetonitrile using TBAPC as a supporting electrolyte. $E_{onset\ (Fc/Fc+)}$ = 0.45 V

The reason behind the elevated HOMO level of **TP-TP-IMD** is the increased percentage of donor DTPBT-units to 75% and reducing the percentage of acceptor BTD-IMD units to 25% within the polymer chain. Though, BTD-IMD has one central strong electron acceptor benzothiadiazole unit and two terminal weak electron acceptor benzimidazole units, the increased number of DTPBT scaffolds along the polymer

chain have elevated the HOMO energy level of the resulting polymer. On the other hand, LUMO energy levels of **TP-TP-IMD**, **TP-INQx** and **TP-BIIG** were calculated using the equation: $E_{LUMO} = E_{HOMO} + E_g^{opt}$, and were found to be −3.51 eV, −3.59 eV and −3.69 eV. The electrochemical properties of the synthesized DTPBT-based conjugated polymers are summarized in Table 4.3.

Table 4.3 Electrochemical properties of synthesized polymers; [a] potential v/s Ag/Ag^+; [b] calculated from equation $E_{HOMO} = -(E_{oxi,onset} + 4.8 - E_{Fc/Fc+})$; [c] calculated from equation $E_{LUMO} = E_{HOMO} + E_g^{opt}$; [d] unresolved peak.

Polymer	E_{oxi} [a] (V)	$E_{oxi,onset}$ [a] (V)	E_{HOMO} [b] (eV)	E_{LUMO} [c] (eV)
TP-TP-IMD	+1.17	+0.83	−5.18	−3.51
TP-INQx	+1.51	+1.01	−5.36	−3.59
TP-BIIG	--[d]	+1.25	−5.60	−3.69

Space charge limited current (SCLC) hole mobilities of polymers

The hole mobility of polymers was measured according to a similar method described in the literature,[71] using a diode configuration of ITO/poly(ethylenedioxythiophene) doped with poly(styrenesulfonate) (PEDOT:PSS)/polymer/Al by taking current-voltage current in the range of 0~6 V and fitting the results to a space charge limited form; the SCLS is described by,

$$J = {}^{9\varepsilon_0\varepsilon_r\mu V^2}/_{8L^3}$$

In the equation, ε_0 is the permittivity of free space, ε_r is the dielectric constant of the polymer, μ is the hole mobility, V is the voltage drop across the device, and L is the polymer thickness, $V = V_{appl} - V_r - V_{bi}$, where V_{appl} is the applied voltage to the device, V_r is the voltage drop due to constant resistance series resistance across the electrodes, and V_{bi} is the built-in voltage due to the difference in work function of the two electrodes. The resistance of the device was measured using a blank configuration ITO/PEDOT/Al. The dielectric constants of the polymers in our analysis were determined by using the equation of $\varepsilon_r = {}^{Cd}/_{A\varepsilon_0}$, where C, d, A and ε_0 are the

capacitance of the device, the thickness of the polymer film, the area of the device and permittivity of the free space, respectively.

The measured SCLC hole mobilities for synthesized DTPBT-based conjugated polymers are 9.26 X 10^{-4}, 5.58 X 10^{-4} and 12.47 X 10^{-4} $cm^2V^{-1}s^{-1}$, respectively for **TP-TP-IMD**, **TP-INQx** and **TP-BIIG**, which are found to be much higher than that of other DTPBT-based polymers reported in the literature. These high hole mobilities allow these polymers to be used as hole transporting materials (HTMs) for organic photovoltaic devices.

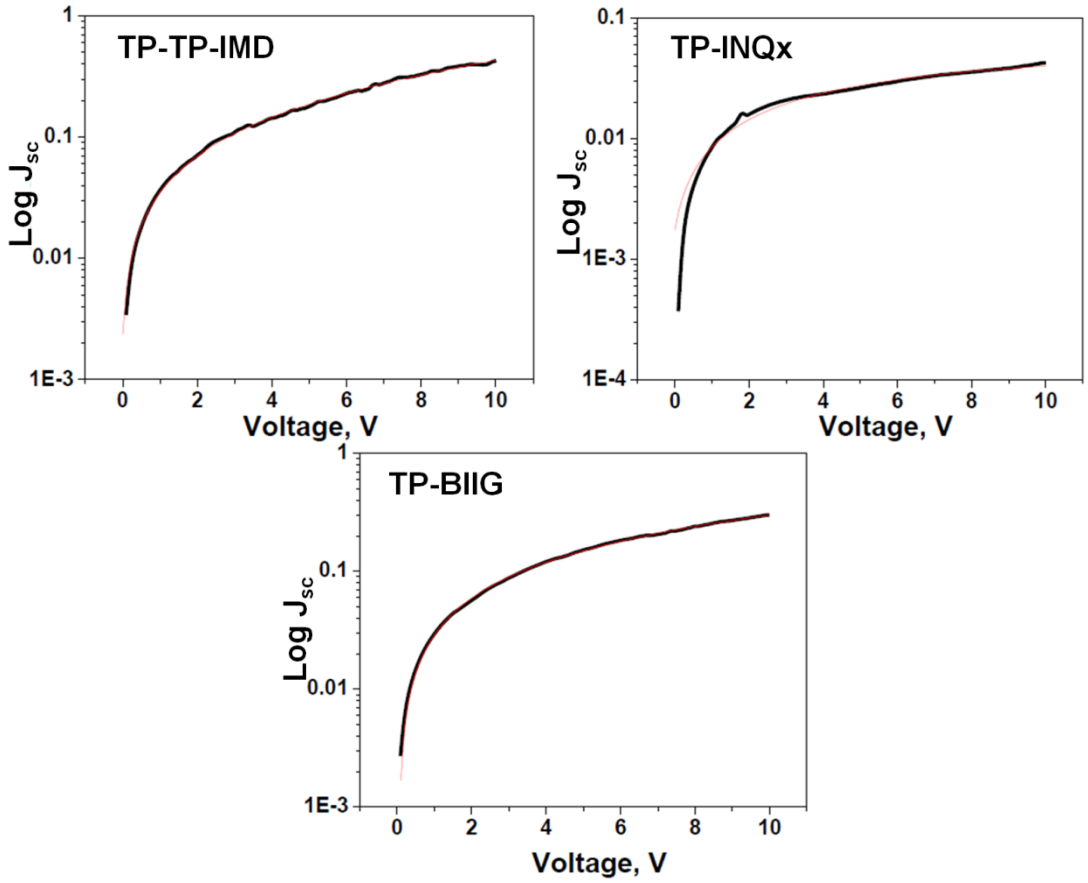

Figure 4.16 SCLC hole mobility of synthesized DTPBT-based conjugated polymers

Conclusion

The donor-acceptor integrated heterocyclic fused aromatic core dithienopyrrolobenzothiadiazole (DTPBT) has been synthesized and successfully incorporated as a fused planar building block into the conjugated polymers. Three different conjugated building blocks are synthesized, characterized and have been co-polymerized with 10,11-dioctyl-2,8-bis(tri-*n*-butylstannyl)-10,11-dihydro-[2,1,3]thiadiazolo[4,5-*e*]thieno[2',3':4,5]pyrrolo[3,2-*g*]thieno[3,2-*b*]indole (**TP-M1**), resulting into the three conjugated low band-gap D-A polymers. All the synthesized

polymers showed moderate to good solubility properties in the common organic solvents and sufficiently high thermal stabilities. All the DTPBT-based conjugated polymers exhibited moderate to good absorptivities in the UV and visible region of the solar spectrum. Moreover, in the solid state, all the polymers showed bathochromically shifted absorption edges due to the better π-π stacking between the polymer chains. Also, the synthesized DTPBT-based polymers exhibited low-lying HOMO energy levels (below −5.0 eV) whereas LUMO energy levels are ranging between −3.5 to −3.7 eV. The synthesized DTPBT-based conjugated polymers exhibited good SCLC hole mobilities of 9.26 X 10^{-4}, 5.58 X 10^{-4} and 12.47 X 10^{-4} $cm^2V^{-1}s^{-1}$, respectively for **TP-TP-IMD**, **TP-INQx** and **TP-BIIG**, in consequence of the coplanar fused D-A type building blocks, incorporated within the polymer chain. Synthesized DTPBT-based conjugated polymers can work as an efficient hole transporting materials (HTMs) for organic photovoltaic devices.

Experimental procedures

General procedures

All the chemicals were reagent grade and used as purchased. Moisture-sensitive reactions were performed under an inert atmosphere of dry nitrogen with dried solvents. Reactions were monitored by thin-layer chromatography (TLC) using Merck 60 F_{254} aluminium-coated plates and the spots were visualized under ultraviolet (UV) light. Column chromatography was carried out on silica gel (60–120 mesh). NMR spectra were recorded on a Bruker Avance-III 400 spectrometer in $CDCl_3$ and DMSO-D_6. The high resolution mass spectra were recorded on Xevo G2-XS QTOF Mass Spectrometer. Diffraction data were collected using Mo Kα (λ = 0.71073) radiation on an Xcalibur, Eos, Gemini diffractometer. UV-Visible absorption spectra were recorded on Jasco V-630 spectrophotometer using quartz cuvette. CV data were obtained with CH Instruments model of CHI 600E with three electrode (Glassy carbon as the working electrode, platinum as the counter electrode, and nonaqueous $Ag/AgNO_3$ as the reference electrode) cells in anhydrous acetonitrile solution containing 50 mM tetra-*n*-butylammoniumperchlorate (TBAPC) at a scan rate of 100 mV/s. Molecular weights of the polymer samples were measured with Agilent 1260 Infinity GPC instrument, equipped with RI detector. Polystyrene was used as a calibration standard. Polymer samples (~5 mg) were dissolved in THF (~5 mL) and were filtered through a 0.2 μ

filter. The analysis was done using THF as an eluent at a flow rate of 1-2 mL/min. Thermo-Gravimmetric Analysis (TGA) of the polymer was done on Exstar SII TG/DTA 6300 using N_2 as inert gas.

Synthesis of monomers

Compounds **1** and **2** were synthesized according to the literature procedures[78] and detailed synthetic procedures are given in Chapter 2. Compound **3** was prepared from compound **2** using nitronium trifluoromethanesulfonate (NTMS) as a nitrating agent according to the literature procedure reported by Wang *et al.*[79] Compound **4** was synthesized by Stille coupling reaction between compound **3** and 2-(tri-*n*-butylstannyl)thiophene in dry THF using $Pd(PPh_3)_2Cl_2$ as a catalyst under nitrogen atmosphere using literature procedure.[80] **DTPBT** was synthesized by Cadogan intramolecular annulation according to the literature procedure reported by Kato *et al.*[70]

Compound **1**[78]: White solid; ^{1}H NMR (400 MHz, $CDCl_3$): 8.00−8.05 (dd, J_1 = 6.8 Hz, J_2 = 3.2 Hz, 1H), 7.59−7.63 (dd, J_1 = 6.8 Hz, J_2 = 3.2 Hz, 1H).

Compound **2**[78]: Off-white solid; ^{1}H NMR (400 MHz, $CDCl_3$): 7.75 (s, 1H).

Synthesis of 4,7-dibromo-5,6-dinitro-2,1,3-benzothiadiazole, **3**: Compound **3** was prepared by following the literature procedure.[79] In a 150 mL two-necked round bottom flask, fuming nitric acid (1.50 g; 23.8 mmol) was added dropwise to trifluoromethanesulfonic acid (15.00 g; 100 mmol) at 0 °C. Up on complete addition of fuming nitric acid, an insoluble nitrating mixture $2CF_3SO_3H/HNO_3$ appeared as white solids immediately. To this, compound **2** (2.50 g; 8.5 mmol) was added in portion-wise over a period of 20 min to avoid exothermicity. After addition, the reaction mixture was kept stirring at 50 °C for 8 h, during which evolution of brisk red coloured gas was noted. After completion, the mixture was poured into ice water slowly, and then sodium hydroxide solution was added to neutralize the excess acid. The precipitates were filtered and washed with water. The pure product was obtained by recrystallization of crude product from ethanol.

Compound **3**[79]: Yellow beige solid (2.71 g, 83%); ^{1}H NMR (400 MHz, $CDCl_3$): No proton signals observed. ^{13}C NMR (100 MHz, $CDCl_3$): 151.3, 144.9, 110.3.

Synthesis of 5,6-dinitro-4,7-di(thiophene-2-yl)-2,1,3-benzothiadiazole, **4**: Compound **4** was synthesized following the literature procedure.[80] In a 100 mL two-necked round bottom flask, compound **3** (3.80 g; 9.90 mmol), $PdCl_2(PPh_3)_2$ (0.14 g; 0.2 mmol) and 30 mL of dried THF were degassed by purging nitrogen gas through the reaction mixture for 15 min. To the degassed reaction mixture, tri-*n*-butyl(thiophen-2-yl)stannane (8.51 g; 22.8 mmol) was added and the mixture was refluxed for 3 h under nitrogen atmosphere. After cooling the reaction mixture, an orange solid appeared which was filtered off, washed with acetonitrile and dried under vacuum to give pure product as an orange solid.

Compound **4**[80]: Orange solid (3.05 g, 79%); ^{1}H NMR (400 MHz, $CDCl_3$): 7.76−7.77 (dd, J_1 = 4.8 Hz, J_2 = 1.2 Hz, 1H), 7.53−7.54 (dd, J_1 = 4.0 Hz, J_2 = 1.2 Hz, 1H), 7.25−7.27 (m, 1H).

Synthesis of **DTPBT**: **DTPBT** was synthesized by following the literature procedure reported by Kato *et al.*[70] A 250 mL two-necked round bottom flask was charged with compound **4** (1.50 g; 3.85 mmol), PPh_3 (10.08 g; 38.5 mmol) and 192 mL of 1,2-dichlorobenzene (*o*-DCB) under nitrogen atmosphere. The reaction mixture was degassed by purging nitrogen gas through the reaction mixture for 15 min. The degassed reaction mixture was refluxed under nitrogen atmosphere for 12 h. The reaction mixture was cooled to room temperature and was subjected to the column chromatography. The 1,2-dichlorobenzene along with excessive PPh_3 was eluted using petroleum ether. The pure product was eluted using 50% ethyl acetate-petroleum ether as eluent and dried under vacuum to give bright yellow air-sensitive solid.

DTPBT[70]: Bright yellow solid (0.91 g, 73%); ^{1}H NMR (400 MHz, DMSO-D_6): 11.90 (s, 1H), 7.61−7.63 (d, J = 5.2 Hz, 1H), 7.43−7.44 (d, J = 5.2 Hz, 1H).

Synthesis of **DTPBT-C8**: *N*-Alkylation of DTPBT was carried out by dissolving **DTPBT** (0.77 g; 2.37 mmol) in anhydrous DMF (120 mL; ~ 20 mM solution). To this stirred solution was added NaOH powder (0.95 g; 23.7 mmol) and *n*-octyl bromide (2.6 mL; 15.4 mmol) and the resulting mixture was allowed to stir under nitrogen atmosphere at 60 ^{o}C for 8 h. After the completion of reaction, the reaction mixture was poured into the water, the resulting suspension was extracted with ethyl acetate. The combined organic phase was washed with water, and evaporated in vacuo after drying

over anhydrous sodium sulphate. The residue was purified by column chromatography over silica gel using 10% ethyl acetate-petroleum ether as eluent.

DTPBT-C8: Yellowish orange solid (1.01 g, 78%); ^{1}H NMR (400 MHz, $CDCl_3$): 7.45−7.46 (d, J = 4.8 Hz, 1H), 7.20−7.21 (d, J = 5.2 Hz, 1H), 4.50−4.54 (t, J = 7.6 Hz, 2H), 1.81−1.88 (m, 2H), 1.07−1.27 (m, 10H), 0.80−0.84 (t, J = 7.2 Hz, 3H). ^{13}C NMR (100 MHz, $CDCl_3$): 147.5, 145.5, 132.1, 126.8, 121.2, 111.8, 110.8, 50.3, 31.6, 30.0, 29.0, 28.9, 26.5, 22.5, 14.0. HRMS (ES+): $C_{30}H_{39}N_4S_3$ requires 551.2337, found 551.2333. IR (KBr, cm^{-1}): 2923.6, 2850.7, 1556.4, 1499.7, 1465.5, 1395.1, 1353.3, 1294.9, 1185.7, 1154.7, 1093.8, 1038.4, 968.2, 808.0, 719.4, 652.0.

Synthesis of **TP-M1**: **TP-M1** was prepared according to the modified synthetic procedure reported by Carsten *et al.*[71] A solution of LDA was first prepared by adding of 1.6 M *n*-butyllithium solution in hexane (1.94 mL; 3.0 mmol) dropwise to a dry THF solution (2 mL) of diisopropylamine (0.42 mL, 2.95 mmol) in a single neck round bottom flask at 0 ^{o}C under nitrogen atmosphere. This solution was stirred at the same temperature for 30 minutes. This solution of LDA was then added dropwise *via* syringe to a stirred solution of **DTPBT-C8** (0.55 g; 1 mmol) in 3 mL of dry THF, kept at −78 ^{o}C under nitrogen atmosphere. The reaction mixture was stirred for 1 hour at this temperature, then quenched by dropwise addition of Sn(*n*-Bu)$_3$Cl (0.7 mL; 2.5 mmol) *via* syringe. The mixture was allowed to warm gradually to room temperature and stirred overnight, and then quenched with saturated aqueous sodium bicarbonate solution. The mixture was extracted with diethyl ether and combined organic phase was washed with water and brine. The crude solid obtained by evaporation of solvent under vacuum after treatment of anhydrous sodium sulphate and the residue obtained was used for next step without purification. The percentage conversion of the reaction and purity of the product was determined by subjecting the crude product to NMR spectroscopy.

TP-M1: Orange-red liquid (0.9 g, 81.1% NMR conversion); ^{1}H NMR (400 MHz, $CDCl_3$) δ: 7.17 (s, 1H), 4.50−4.54 (t, J = 7.6 Hz, 2H), 1.10−1.87 (bulk of signals, m, 30H), 0.90−0.96 (m, 9H), 0.80−0.84 (t, J = 7.2 Hz, 3H).

Synthesis of **TP-M2**: **TP-M2** was prepared according to the modified synthetic procedure reported by Carsten *et al.*[71] **DTPBT-C8** (0.200 g; 0.36 mmol) was dissolved in 5 mL of DMF in single neck round bottom flask and placed under nitrogen in the

dark. To this, a solution of *N*-bromosuccinamide (0.14 g; 0.80 mmol) in 4 mL of DMF was added drop wise *via* addition funnel and the reaction mixture was allowed to stir in the dark at room temperature overnight. The mixture was then quenched with water and extracted with ethyl acetate. The combined organic phase was washed with water and brine, finally dried over anhydrous sodium sulphate and evaporated to dryness under vacuum. The residue was subjected column chromatography over silica gel and the pure product was eluted using 10% ethyl acetate-petroleum ether as eluent.

TP-M2: Orange-red solid (0.162 g, 63%); ^{1}H NMR (400 MHz, $CDCl_3$) δ: 7.20 (s, 1H), 4.40−4.44 (m, 2H), 1.77−1.84 (m, 2H), 1.27−1.37 (m, 13H), 1.18−1.22 (t, J = 7.6 Hz, 3H). ^{13}C NMR (100 MHz, $CDCl_3$): 147.0, 143.1, 130.8, 121.2, 115.0, 113.6, 110.7, 50.3, 31.6, 30.0, 29.9, 28.9, 26.5, 22.5, 14.0. HRMS (ES+): $C_{30}H_{37}N_4S_3Br_2$ requires 707.0547, found 707.0555. IR (KBr, cm^{-1}): 2921.9, 2852.2, 1586.8, 1501.8, 1353.0, 1296.8, 1240.5, 1072.1, 950.3, 794.3, 477.7.

Synthesis of compound **6**: Compound **6** was synthesized from *o*-nitroaniline according to the modified literature procedure reported by Zhu *et al*.[81] In 30 mL of glacial acetic acid was dissolved *o*-nitroaniline (10.00 g; 72.4 mmol) in two necked round bottom flask and the solution was kept under stirring at 50 °C. To this stirred solution, *N*-bromosuccinamide (12.90 g; 72.4 mmol) was added portion-wise over a period of 15 min. Resulting mixture was stirred for 3 h and then poured into 250 mL of ice-water. Orange yellow precipitates were filtered off and washed thoroughly with water. The precipitates were again dissolved in water and were re-precipitated by addition of water, which were collected by filtration. The crude product (compound **5**) thus obtained was dried under air flow and was used directly for the next step without any purification. In the next step, stannous chloride dihydrate (31.2 g; 138.2 mmol) was dissolved in 55 mL of concentrated hydrochloric acid in a 100 mL two necked round bottom flask and kept stirring at 60 °C. To this stirred solution, crude compound **5** (10.00 g; 46.0 mmol) was added and the reaction mixture was allowed to stir at the same temperature for 1 h. After completion of the reaction, the reaction mixture was allowed to cool at room temperature. To the cooled reaction mixture, 50% aqueous sodium hydroxide solution was added slowly, maintaining the temperature below 25 °C using ice-water bath. The precipitated whitish product was collected by filtration and the precipitates were re-dissolved in dichloromethane, washed with water and brine. The organic layer was dried over anhydrous sodium sulphate and evaporated to

dryness. The pure product was obtained by re-crystallization of the crude material from petroleum ether-dichloromethane, yielding pinkish white flakes.

Compound **6**[81]: Pinkish white solid (6.41 g, 75%); ^{1}H NMR (400 MHz, $CDCl_3$) δ: 6.84 (d, J = 2.4 Hz; 1H), 6.81−6.83 (dd, J_1 = 8.0 Hz, J_2 = 2.0 Hz, 1H), 6.57−6.59 (d, J = 8.0 Hz, 1H), 3.44 (s, 2H), 3.38 (s, 2H). ^{13}C NMR (100 MHz, $CDCl_3$): 136.4, 133.7, 122.6, 119.0, 117.9, 111.9.

Synthesis of **INQx-M3**: **INQx-M3** was synthesized according to the modified literature procedure reported by Dong *et al.*[82] 5-bromoisatin (0.309 g, 1.36 mmol), compound **6** (0.27 g; 1.43 mmol) and glacial acetic acid were heated at 130 ^{o}C under nitrogen atmosphere for 24 h. After cooling to the room temperature, reaction mixture was quenched by adding water and resulting precipitates were collected by filtration. The crude product was dried under vacuum at 50 ^{o}C to yield yellow solid which was re-dissolved in 30 mL of DMF. To this solution was added, K_2CO_3 (0.30 g; 2.2 mmol), *n*-dodecyl bromide (0.45 mL; 1.89 mmol) and reaction mixture was allowed to stir at 110 ^{o}C for 20 h. After completion of reaction, reaction mass was poured into 300 mL of water and extracted using ethyl acetate. The combined organic phase was washed with water, brine and dried over anhydrous sodium sulphate. The solvent was evaporated under the reduced pressure and the residue was subjected to column chromatography over silica gel, the first intense yellow band was eluted from the column using 10% ethyl acetate-petroleum ether mobile phase, which gave mixture of **INQx-M3** and **7** in 1:1 ratio. Extensive column chromatography of the mixture of **INQx-M3** and **7** using 5% ethyl acetate-petroleum ether yielded slow moving **INQx-M3** from the later fractions of column as relatively pure product. **INQx-M3** was further purified by re-crystallization from ethanol-chloroform solution, furnishing yellow needles.

INQx-M3: Yellow needles (0.199 g, 29%); ^{1}H NMR (400 MHz, $CDCl_3$) δ: 8.60 (d, J = 2.0 Hz, 1H), 8.46 (d, J = 2.4 Hz, 1H), 8.00−8.02 (d, J = 8.8 Hz, 1H), 7.83−7.86 (dd, J_1 = 8.8 Hz, J_2 = 2.0 Hz, 1H), 7.80−7.83 (dd, J_1 = 8.4 Hz, J_2 = 2.0 Hz, 1H), 7.39−7.41 (d, J = 8.8 Hz, 1H) 4.45−4.49 (t, J = 7.2 Hz, 2H), 1.90−1.96 (m, 2H), 1.24−1.39 (m, 18H), 0.87−0.90 (t, J = 7.2 Hz, 3H). ^{13}C NMR (100 MHz, $CDCl_3$): 145.5, 143.2, 140.0, 139.7, 139.3, 133.9, 132.4, 131.6, 129.2, 125.7, 120.9, 119.4, 113.8, 111.1, 41.7, 31.9, 29.7, 29.6, 29.5, 29.4, 29.3, 29.2, 28.4, 27.0, 22.7, 14.0. HRMS (ES+): $C_{26}H_{32}N_3Br_2$ requires

544.0963, found 544.0962. IR (KBr, cm^{-1}): 2921.4, 2850.2, 1627.0, 1602.2, 1574.7, 1456.1, 1270.6, 1121.1, 1053.2, 799.0, 448.7.

Synthesis of compound **8**: Compound **8** was synthesized according to the modified literature procedure reported by Li *et al.*[64] 5-bromoisatin (2.26 g; 10.00 mmol) and K_2CO_3 (6.20 g; 45.00 mmol) were added to the 20 mL anhydrous DMF under nitrogen atmosphere and were stirred at 60 ^oC for 5 min. To this stirred solution, *n*-dodecyl bromide (4.25 mL; 17.50 mmol) was added dropwise and the temperature was increased to 80 ^oC. The reaction mixture was allowed to stir for 2 h, after which the reaction mass was poured into 200 mL of water and extracted with ethyl acetate. Combined organic phase was washed with water, brine and evaporated to dryness under reduced pressure. The residual oily substance was subjected to column chromatography over silica gel and pure product was eluted using 10% ethyl acetate-petroleum ether mobile phase.

Compound **8**: Red solid (3.62 g, 92%); ^1H NMR (400 MHz, $CDCl_3$) δ: 7.72 (d, J = 1.2 Hz, 1H), 7.70−7.72 (d, J = 7.6 Hz, 1H), 6.82−6.84 (dd, J_1 = 7.6 Hz, J_2 = 1.2 Hz, 1H), 3.70−3.74 (t, J = 7.2 Hz, 2H), 1.65−1.73 (m, 2H), 1.26−1.34 (m, 18H), 0.87−0.91 (t, J = 7.2 Hz, 3H). ^{13}C NMR (100 MHz, $CDCl_3$): 181.2, 157.4, 149.8, 140.5, 128.2, 118.7, 116.4, 111.9, 40.4, 31.9, 29.6, 29.5, 29.4, 29.3, 29.2, 27.2, 26.9, 22.7, 14.1.

Synthesis of compound **9**: Compound **9** was synthesized according to the modified literature procedure reported by Bura *et al.*[83] Compound **8** (1.01 g; 2.56 mmol) and hydrazine hydrate, 99% (6.5 mL; 128.17 mmol) were taken in single neck round bottom flask and heated at 140 ^oC for 2 h under nitrogen atmosphere. After completion of the reaction, reaction mixture was dissolved in ethyl acetate, washed with water (3 X 30 mL) and dried over anhydrous sodium sulphate and concentrated under reduced pressure. To the resulting crude, 20 mL 6 N aqueous hydrochloric acid solution was added and heated at 60 ^oC overnight. The reaction mixture was poured into 200 mL of water and extracted with ethyl acetate. Combined organic phase was washed with water, brine, dried over anhydrous sodium sulphate and evaporated under reduced pressure. The crude product thus obtained, was subjected to the column chromatography over silica gel. The pure product was eluted using dichloromethane as mobile phase.

Compound **9**: Yellowish orange liquid (0.85 g, 88%); ^{1}H NMR (400 MHz, $CDCl_3$) δ: 7.39−7.41 (d, J = 8.0 Hz, 1H), 7.38 (s, 1H), 6.70−6.72 (d, J = 8.0 Hz, 1H), 3.66−3.70 (t, J = 7.6 Hz, 2H), 3.53 (s, 2H), 1.61−1.66 (m, 2H), 1.26−1.32 (m, 18H), 0.87−0.91 (t, J = 7.2 Hz, 3H). ^{13}C NMR (100 MHz, $CDCl_3$): 174.2, 143.7, 130.6, 127.6, 126.7, 114.7, 109.7, 40.2, 35.6, 31.9, 29.6, 29.5, 29.5, 29.4, 29.3, 27.3, 26.9, 22.7, 14.2.

Synthesis of **BIIG-M4**: **BIIG-M4** was synthesized according to the literature procedure reported by Li *et al.*[64] In 15 mL of absolute ethanol were added compound **9** (0.30 g; 0.79 mmol) and terphthalaldehyde (0.05 g; 0.39 mmol) under nitrogen atmosphere. To this stirred solution, piperidine (0.39 mL; 3.15 mmol) was added dropwise and reaction mixture was allowed to reflux for 24 h. After that, reaction mass was cooled to room temperature and the precipitated product was collected by filtration. Filtered product was washed with copious amount of absolute ethanol and dried at room temperature. The pure product was obtained by re-crystallization from petroleum ether-chloroform solution.

BIIG-M4: Reddish orange needles (0.23 g, 68%); ^{1}H NMR (400 MHz, $CDCl_3$) δ: 8.42 (s, 2H), 7.68−7.69 (d, J = 2.0 Hz, 1H), 7.53 (s, 1H), 7.40−7.42 (dd, J_1 = 8.4 Hz, J_2 = 1.6 Hz, 1H), 6.72−6.74 (d, J = 8.4 Hz, 1H), 3.74−3.78 (t, J = 7.6 Hz, 2H), 1.66−1.71 (m, 2H), 1.26−1.35 (m, 18H), 0.87−0.90 (t, J = 6.8 Hz, 3H). ^{13}C NMR (100 MHz, $CDCl_3$): 165.4, 141.0, 137.2, 135.6, 132.2, 131.6, 126.3, 126.2, 122.4, 114.4, 109.6, 40.1, 31.9, 29.6, 29.6, 29.5, 29.4, 27.6, 27.1, 22.7, 14.2. HRMS (ES+): $C_{48}H_{63}N_2O_2Br_2$ requires 857.3256, found 857.3280. IR (KBr, cm^{-1}): 3429.4, 2920.7, 2850.3, 1691.8, 1614.5, 1598.7, 1476.8, 1435.5, 1338.4, 1109.2, 802.6, 773.3, 444.6.

Synthesis of compound **10**: Compound **10** was synthesized according to the modified literature procedure reported by Li *et al.*[84] A two necked round bottom flask was charged with 2,1,3-benzothiadiazole (5.00 g; 36.76 mmol), paraformaldehyde (3.86 g; 128.67 mmol) and tetra-*n*-butylammonium bromide (2.37 g; 7.35 mmol). To this was added, 100 mL aqueous 48% hydrobromic acid, 60 mL glacial acetic acid and reaction mixture was purged with nitrogen gas for 10-15 min. Reaction mixture was refluxed for 8 h after which, the reaction was poured into the 400 mL ice-water and resulting precipitates were collected by filtration as a pale white solids.

Compound **10**[84]: White pale solid (7.46 g, 63%); ^{1}H NMR (400 MHz, $CDCl_3$) δ: 7.65 (s, 1H), 4.99 (s, 2H).

Synthesis of compound **11**: Compound **11** was synthesized according to the procedure given below. Compound **10** (1.00 g; 3.10 mmol) and *N*-bromosuccinamide (1.13 g; 6.36 mmol) were taken in 10 mL of monochlorobenzene. To this was added, azo-bis(isobutyro)nitrile (AIBN) (0.10 g; 0.62 mmol) and reaction mixture was heated at 80 ^{o}C for 8 h. Upon heating, reaction mixture became clear. The reaction mixture was poured into 200 mL of water and was extracted using dichloromethane, combined organic phase was washed thoroughly with water, brine, dried over anhydrous sodium sulphate and evaporated to dryness. The residues were subjected to the column chromatography over silica gel and pure product was eluted using 10% ethyl acetate-petroleum ether.

Compound **11**[84]: Yellowish white granular solid (0.80 g, 54%); ^{1}H NMR (400 MHz, $CDCl_3$) δ: 8.16 (s, 2H), 7.46 (s, 2H).

Synthesis of compound **12**: Compound **12** was synthesized according to the literature procedure reported by Li *et al*.[84] Compound **11** (1.00 g; 2.08 mmol) was dissolved in the refluxing 50 mL ethanol, to which was added solution of $AgNO_3$ (2.48 g; 14.58 mmol) in 6 mL of water. The reaction mixture was refluxed for 30 min, cooled to room temperature and evaporated to dryness under reduced pressure. The residues were subjected to column chromatography over silica gel, eluting the pure compound using 30% ethyl acetate-petroleum ether.

Compound **12**[84]: Beige yellow solid (0.14 g, 35%); ^{1}H NMR (400 MHz, $CDCl_3$) δ: 10.92 (s, 1H), 8.40 (s, 1H).

Synthesis of compound **13**: Compound **13** was synthesized according to the modified literature procedure reported by Sriramoju *et al*.[85] In a single neck round bottom flask, compound **6** (0.22 g; 1.17 mmol), compound **12** (0.10 g; 0.52 mmol) and 30 mL of DMF was taken. To this stirred solution, OXONE (1.28 g; 4.16 mmol) was added and reaction mixture was allowed to stir at 50 ^{o}C for 4 h. After completion of reaction, reaction mixture was poured into 300 mL of water and extracted using ethyl acetate. Combined organic extracts were washed with water, brine, dried over anhydrous sodium sulphate and evaporated under reduced pressure to dryness. Reddish brown crude product thus obtained was directly carried forward to the next step (*N*-alkylation) without further purification due to very low solubility and highly polar nature of the compound.

Synthesis of **BTD-IMD-M5**: To a solution of crude compound **13** (0.27 g; 0.52 mmol) obtained from previous step, in 10 mL of anhydrous DMF was added sodium hydride (60% suspension in mineral oil) (0.073 g; 1.82 mmol). Resulting mixture was stirred at room temperature for 30 min until gas evolution ceased. Then, *n*-octylbromide (0.36 mL; 2.08 mmol) was added dropwise and the reaction mixture was allowed to stir at 60 ^{o}C for 6 d. After completion of reaction, the mixture was poured in the brine solution and extracted with ethyl acetate. Combined organic phase was washed with water, dried over anhydrous sodium sulphate and evaporated to dryness under reduced pressure. The residue was subjected to the column chromatography over silica gel and pure compound was eluted from column using 40% ethyl acetate-petroleum ether as a mobile phase.

BTD-IMD-M5: Beige yellow solid (0.17 g, 45%); ^{1}H NMR (400 MHz, $CDCl_3$) δ: 8.13 (s, 1H), 8.04−8.05 (d, J = 1.6 Hz, 1H), 7.51−7.53 (dd, J_1 = 8.8 Hz, J_2 = 1.6 Hz, 1H), 7.41−7.43 (d, J = 8.4 Hz, 1H), 4.21−4.25 (t, J = 7.6 Hz, 2H), 1.69−1.76 (m, 2H), 1.13−1.23 (m, 10H), 0.82−0.86 (t, J = 7.2 Hz, 3H). ^{13}C NMR (100 MHz, $CDCl_3$): 153.1, 150.3, 144.6, 134.5, 131.7, 126.6, 125.8, 123.3, 115.7, 111.8, 45.6, 31.6, 30.9, 29.7, 29.0, 26.7, 22.6, 14.1. HRMS (ES+): $C_{36}H_{43}N_6SBr_2$ requires 749.1637, found 749.1659. IR (NaCl plate, cm^{-1}): 3684.0, 3020.4, 2959.6, 2929.9, 2857.6, 2400.7, 1584.6, 1523.5, 1469.5, 1427.8, 1215.6, 928.0, 772.1, 669.5, 438.0.

General procedure for synthesis of DTPBT-based polymers TP-TP-IMD, TP-INQx and TP-BIIG

To an oven dried two necked round bottom flask, monomer **TP-M2** (0.125 mmol; 0.5 eq.) and **BTD-IMD-M5** (0.125 mmol; 0.5 eq.) or **INQx-M3** (0.25 mmol; 1 eq.) or **BIIG-M4** (0.25 mmol; 1 eq.) was added. To this was added $Pd(PPh_3)_4$ (62.5 µmol; 0.25 eq.), 10 mL of anhydrous toluene and 4 mL of anhydrous DMF under nitrogen atmosphere and resulting solution was degassed by purging nitrogen gas for 15 min. To this stirred solution was added, solution of **TP-M1** (0.26 mmol; 1.05 eq.) in 5 mL of anhydrous toluene, dropwise. The reaction mass was heated at 120 ^{o}C for 48 h under nitrogen atmosphere. After completion, reaction mixture was allowed to cool at room temperature, poured into 150 mL of methanol and allowed to stir at the same temperature for 30 min. Resulting precipitates were filtered and washed with copious amounts of methanol. Obtained crude polymer was subjected to soxhlet extraction

using methanol, acetone, petroleum ether and pure polymer fraction was eluted using chloroform. The polymer was obtained by evaporation of chloroform under reduced pressure and further dried under vacuum at 50 ^{o}C to yield dark brown-black solids.

Block co-polymer TP-TP-IMD: Blackish brown solid (0.15 g; 62%); ^{1}H NMR (400 MHz, $CDCl_3$) δ: 8.12 (br s, 1H), 8.04 (br s, 1H), 7.75 (br, 4H), 7.40−7.49 (br, 6H), 7.15 (br, 2H), 4.28−4.45 (br, 16H), 1.73−1.85 (br, 20H), 1.19−1.26 (br, 70H), 0.83−0.93 (br, 30H). IR (KBr, cm^{-1}): 3079.5, 2954.6, 2923.2, 2852.1, 1658.7, 1639.8, 1553.7, 1462.7, 1349.0, 1294.2, 1148.8, 1093.7, 1051.6, 774.8.

Co-polymer TP-INQx: Brown solid (0.13 g; 49%); ^{1}H NMR (400 MHz, $CDCl_3$) δ: 8.06 (br, 3H), 7.29−7.75 (br, 5H), 4.20−4.57 (br, 6H), 2.30 (br, 6H), 1.00−1.49 (br, 40H), 0.88 (br, 9H). IR (KBr, cm^{-1}): 3418.3, 2921.4, 2850.9, 1631.7, 1609.3, 1566.0, 1466.8, 1352.7, 1279.9, 1126.4, 805.7, 790.2, 525.7.

Co-polymer TP-BIIG: Reddish brown solid (0.22 g; 70%); ^{1}H NMR (400 MHz, $CDCl_3$) δ: 7.88−8.00 (br, 2H), 7.74−7.79 (br, 2H), 7.35−7.65 (br, 8H), 6.92−7.02 (br, 2H), 4.53 (br s, 4H), 3.82 (br s, 4H), 1.70−1.88 (br, 8H), 1.00−1.49 (br, 56H), 0.89 (br, 12H). IR (KBr, cm^{-1}): 3398.3, 2922.8, 2851.1, 1706.4, 1606.3, 1480.9, 1462.2, 1351.1, 1294.0, 1174.7, 1112.5, 808.9, 563.1.

Spectral data

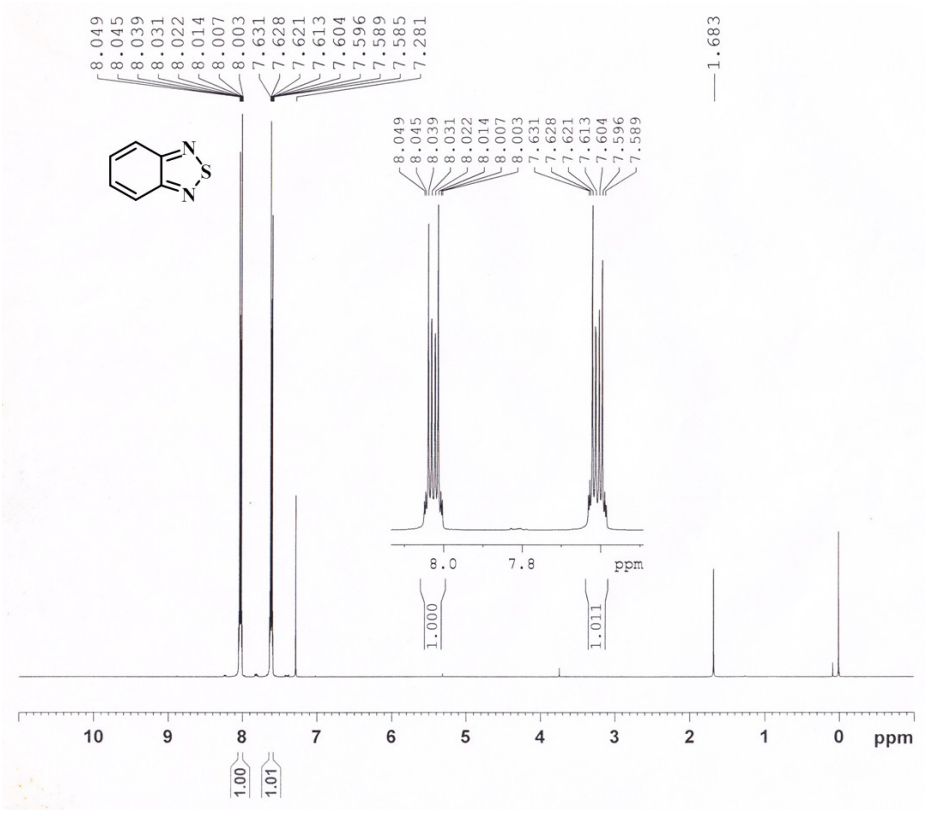

Figure 4.17 ^{1}H NMR spectrum of compound **1**

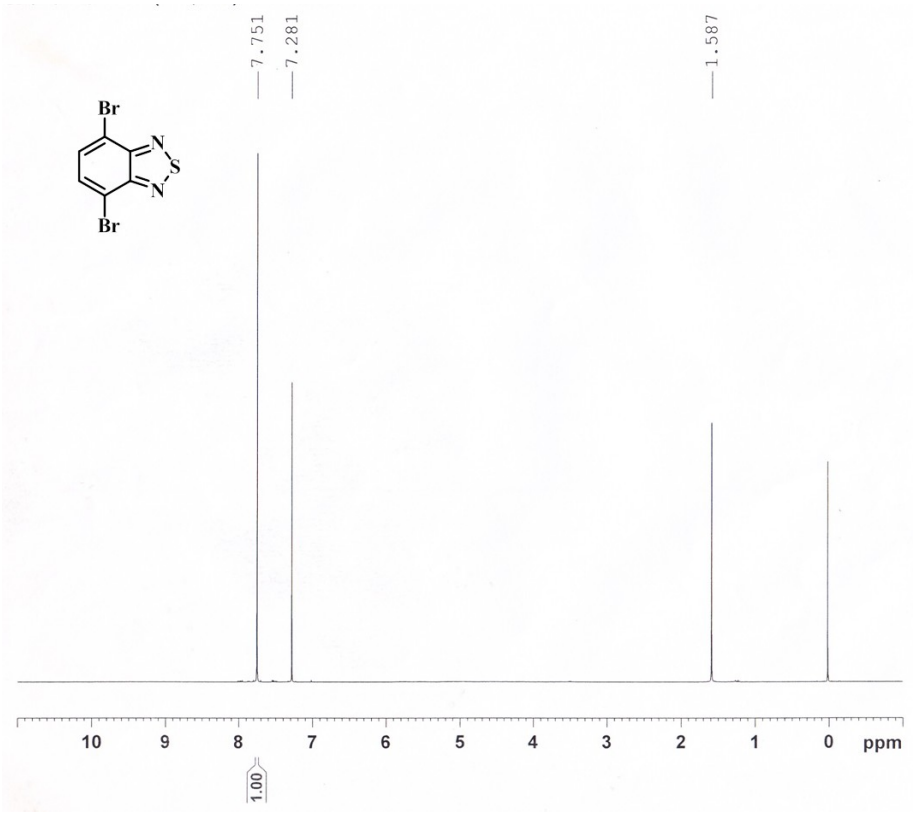

Figure 4.18 ^{1}H NMR spectrum of compound **2**

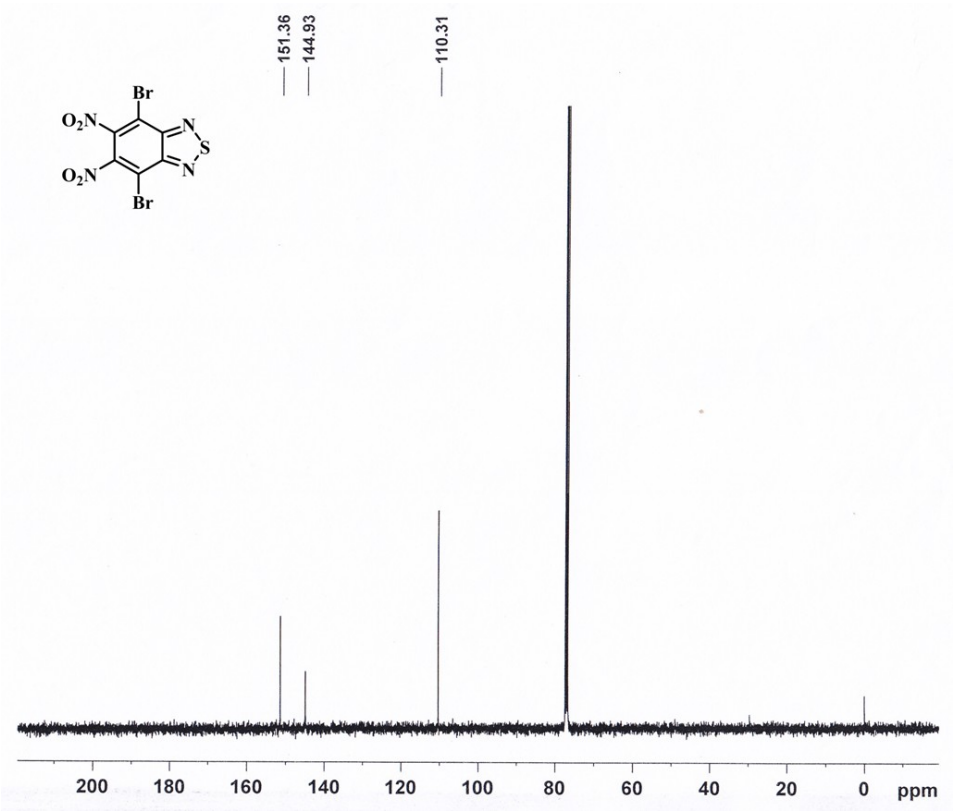

Figure 4.19 ^{13}C NMR spectrum of compound **3**

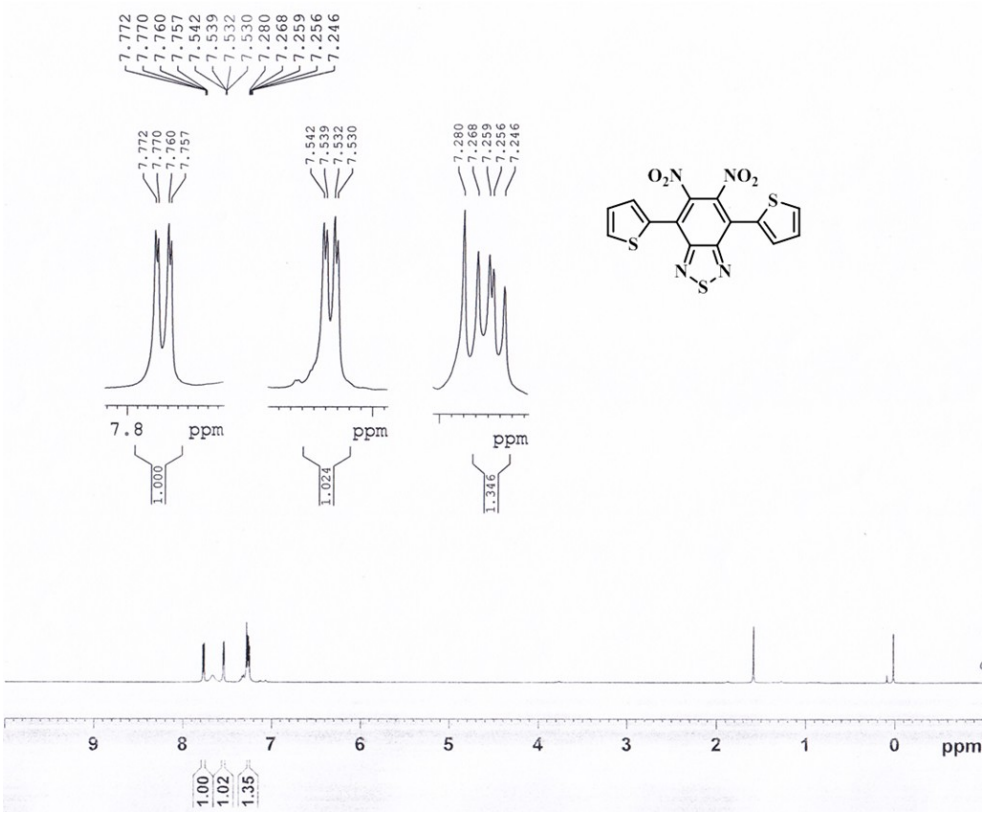

Figure 4.20 ^{1}H NMR spectrum of compound **4**

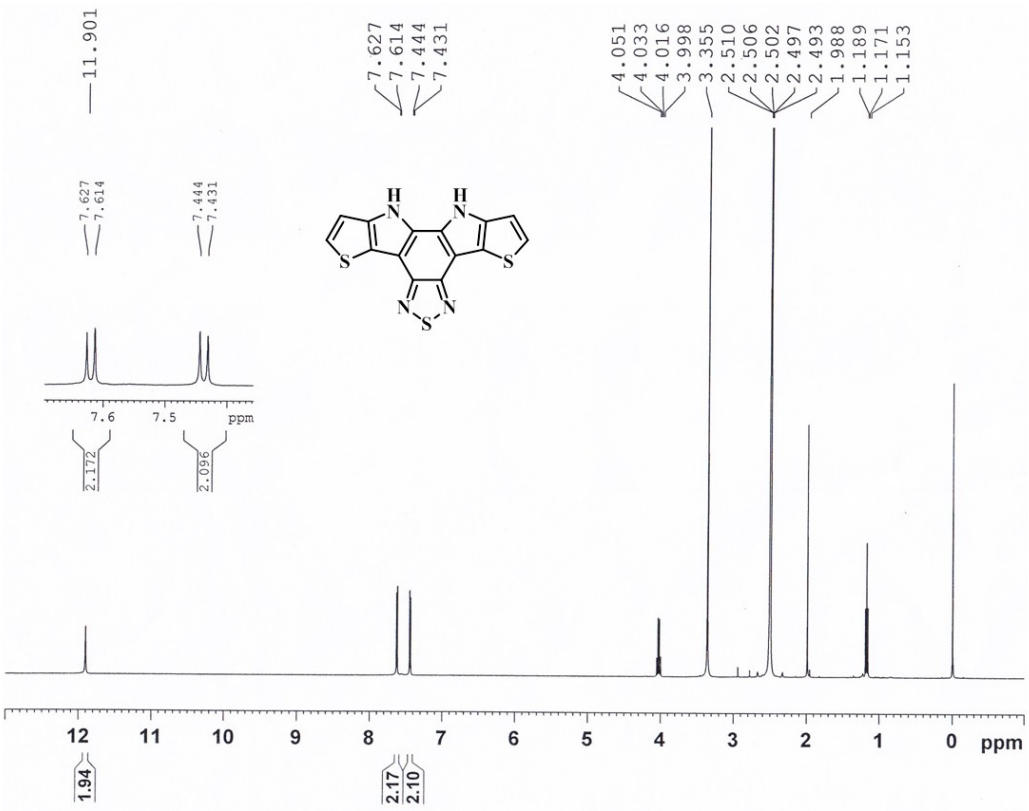

Figure 4.21 ^{1}H NMR spectrum of **DTPBT**

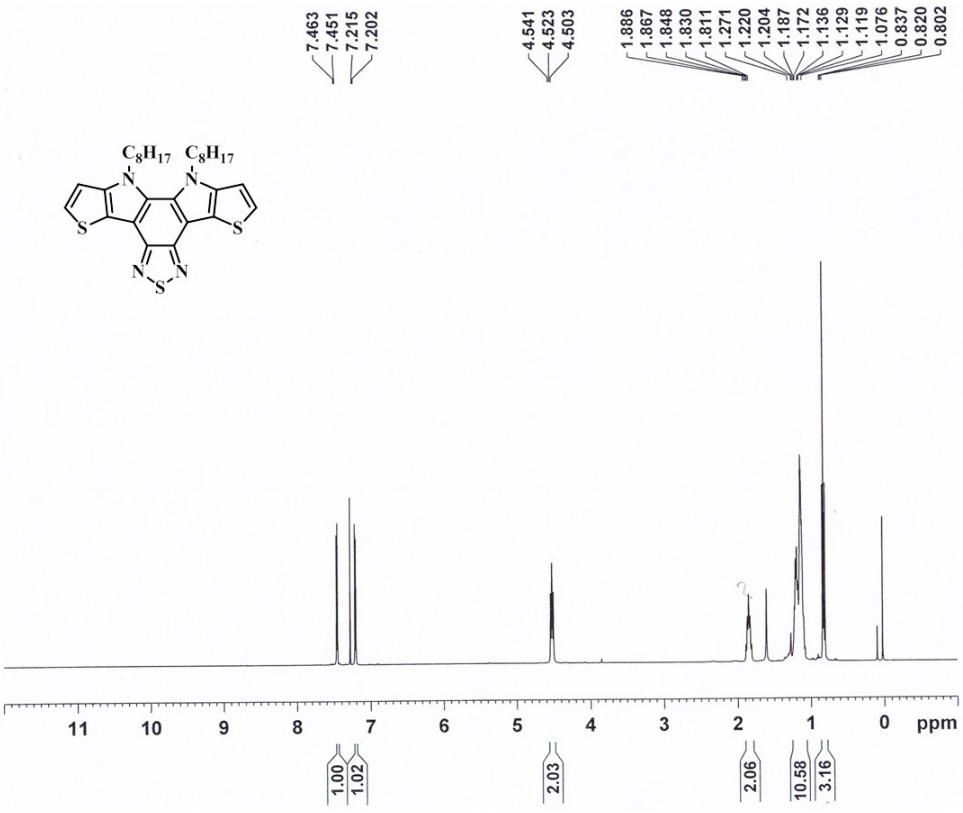

Figure 4.22 ^{1}H NMR spectrum of **DTPBT-C8**

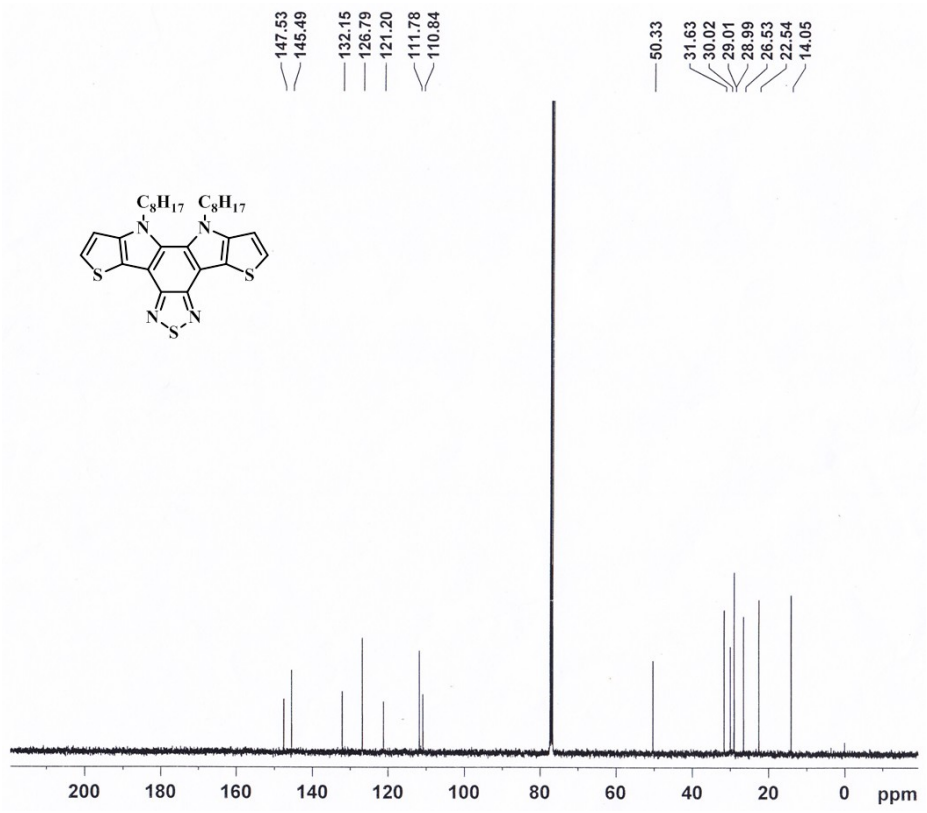

Figure 4.23 ^{13}C NMR spectrum of **DTPBT-C8**

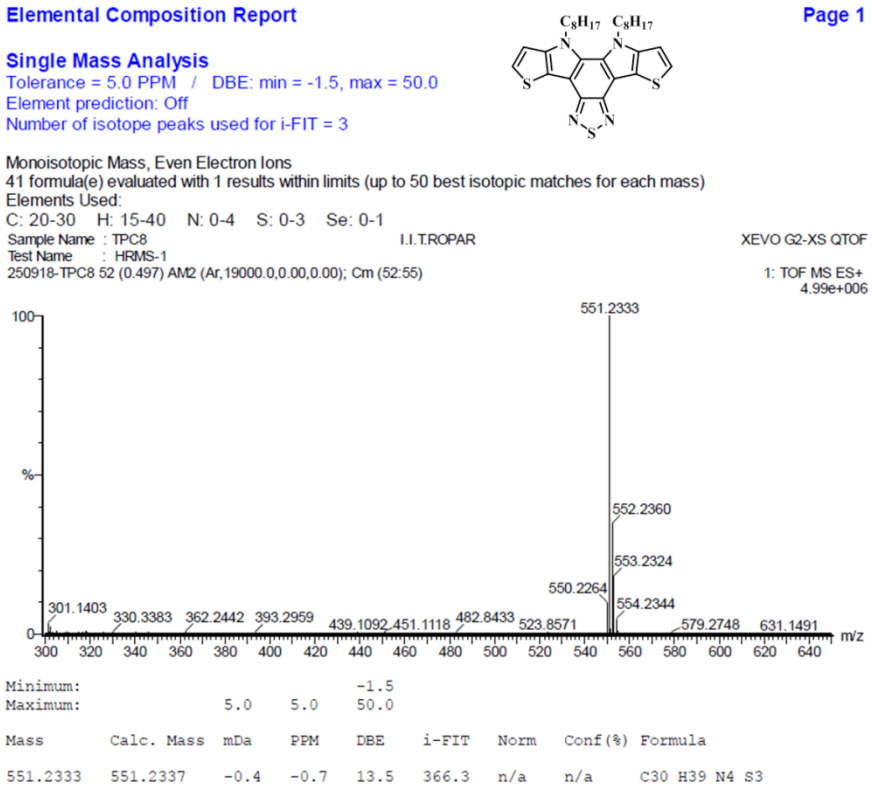

Figure 4.24 HRMS spectrum of **DTPBT-C8**

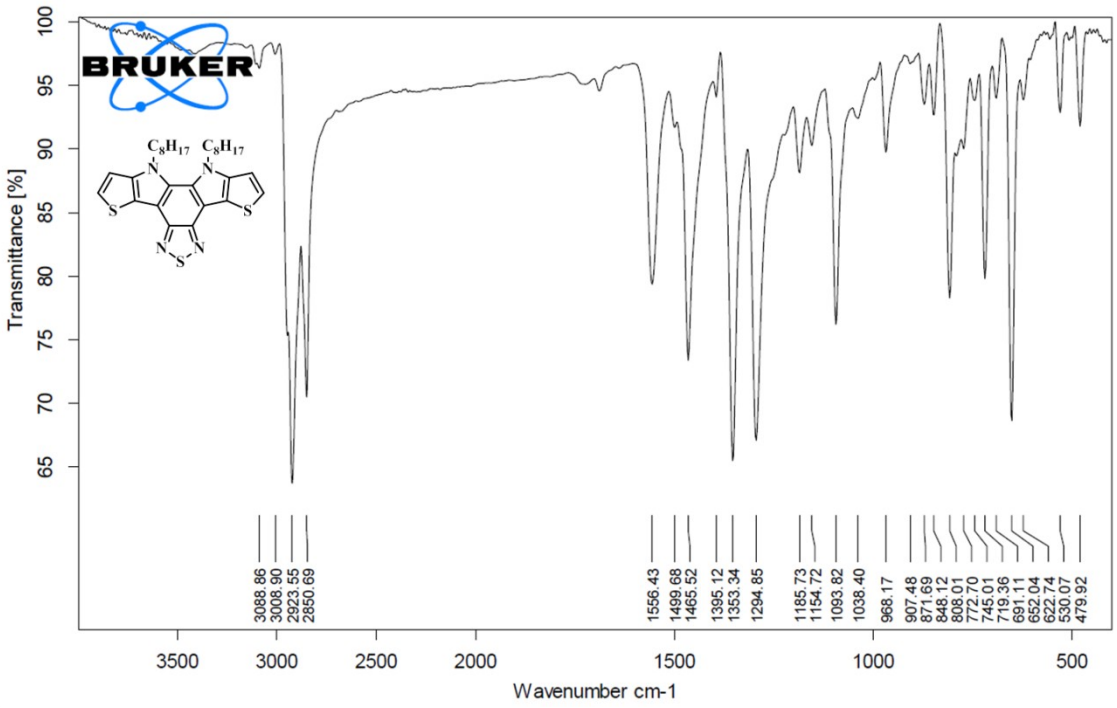

Figure 4.25 IR spectrum (KBr pellet) of **DTPBT-C8**

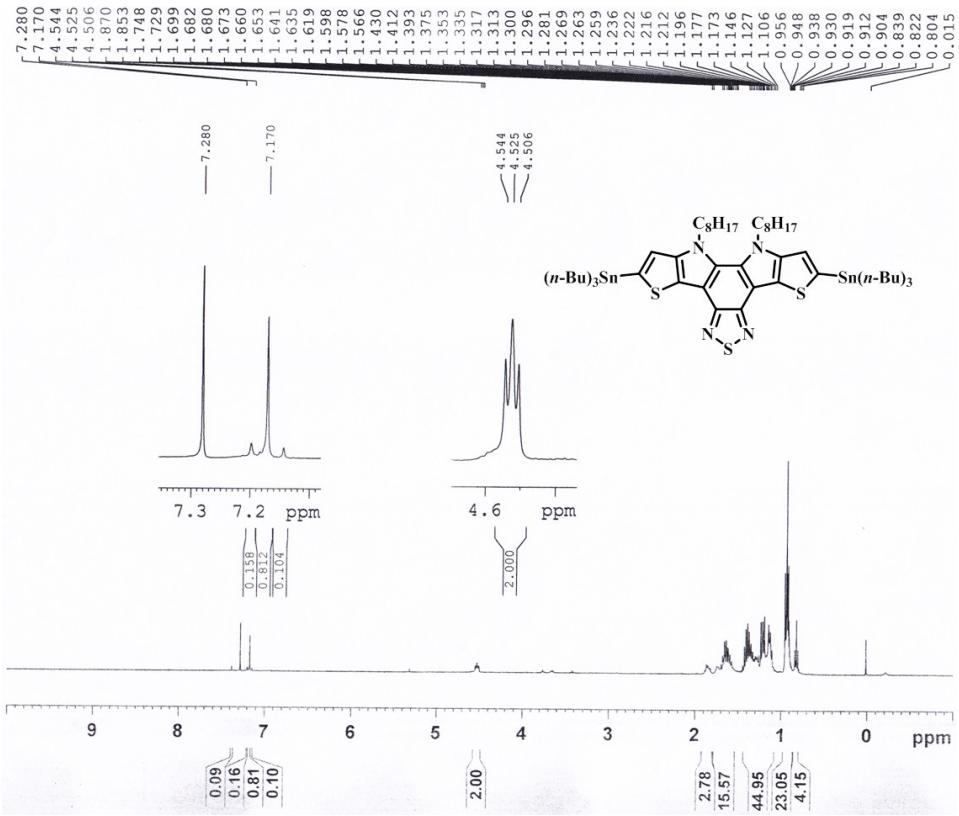

Figure 4.26 ^{1}H NMR spectrum of **TP-M1**

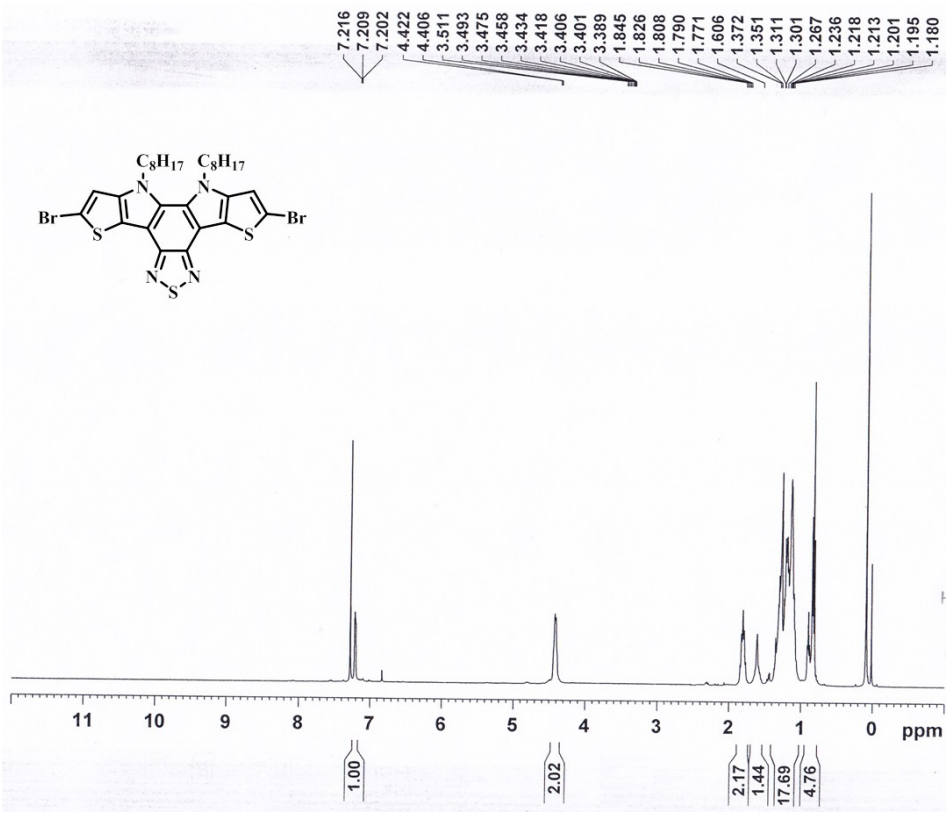

Figure 4.27 ^{1}H NMR spectrum of **TP-M2**

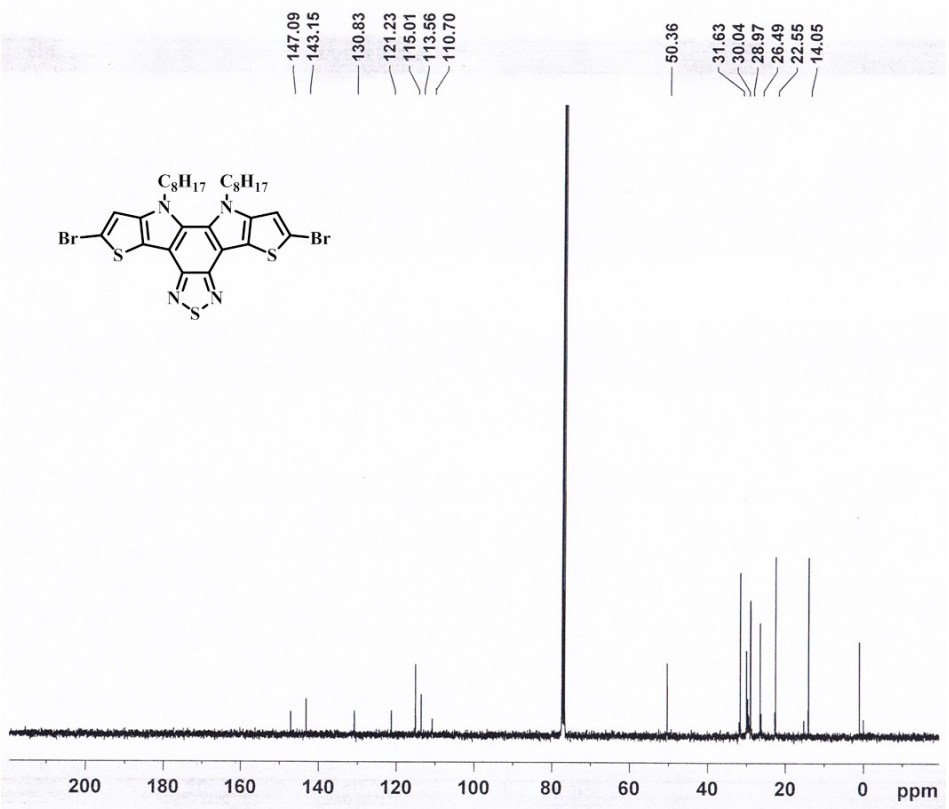

Figure 4.28 ^{13}C NMR spectrum of **TP-M2**

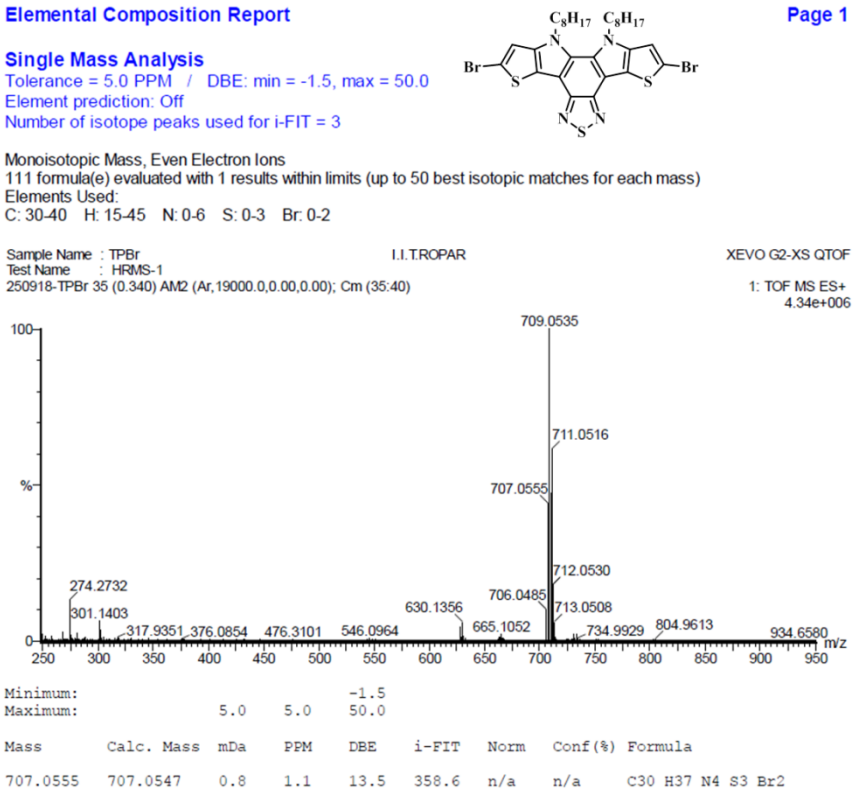

Figure 4.29 HRMS spectrum of **TP-M2**

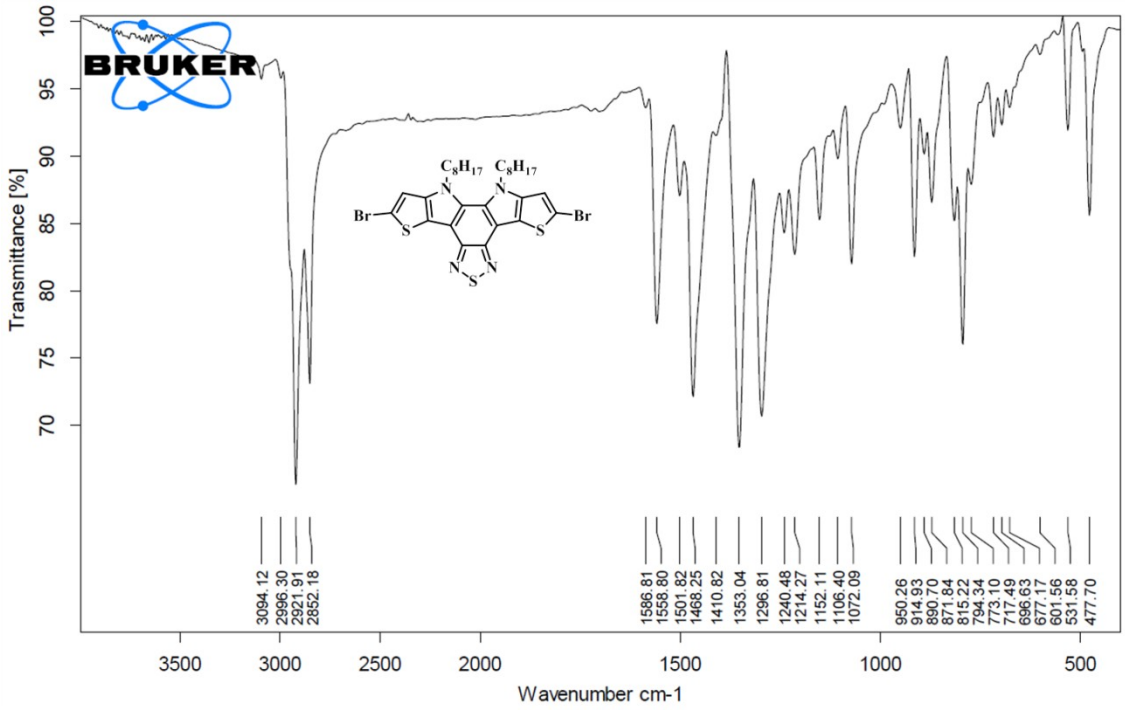

Figure 4.30 IR spectrum (KBr pellet) of **TP-M2**

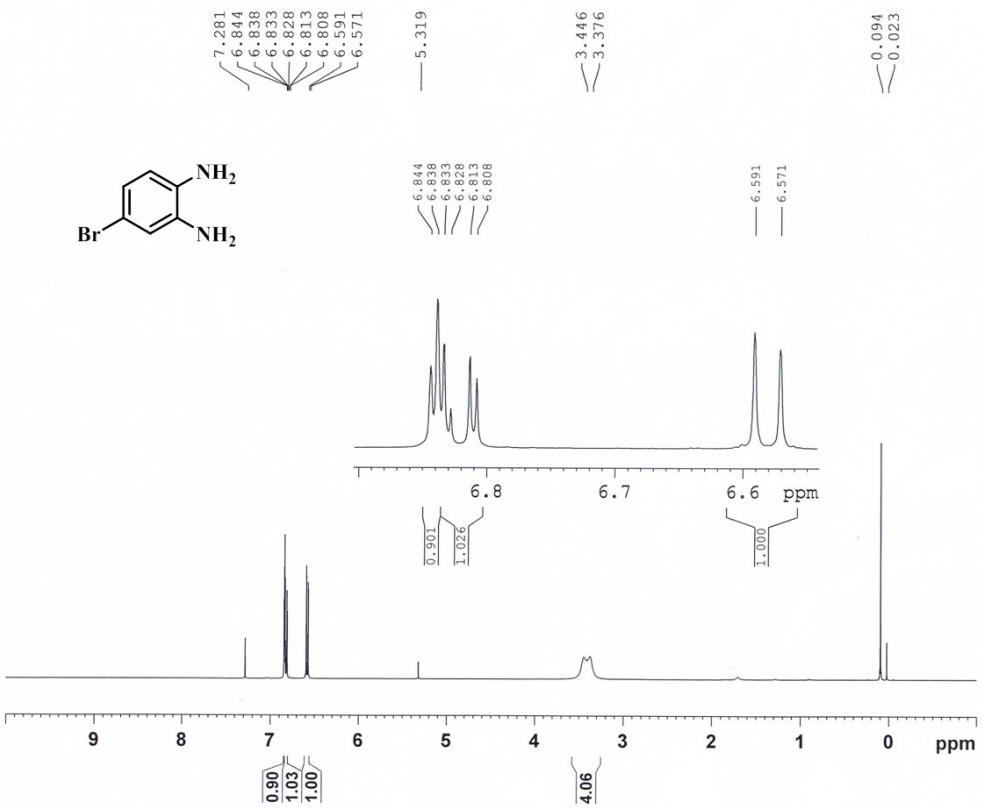

Figure 4.31 ^{1}H NMR spectrum of compound **6**

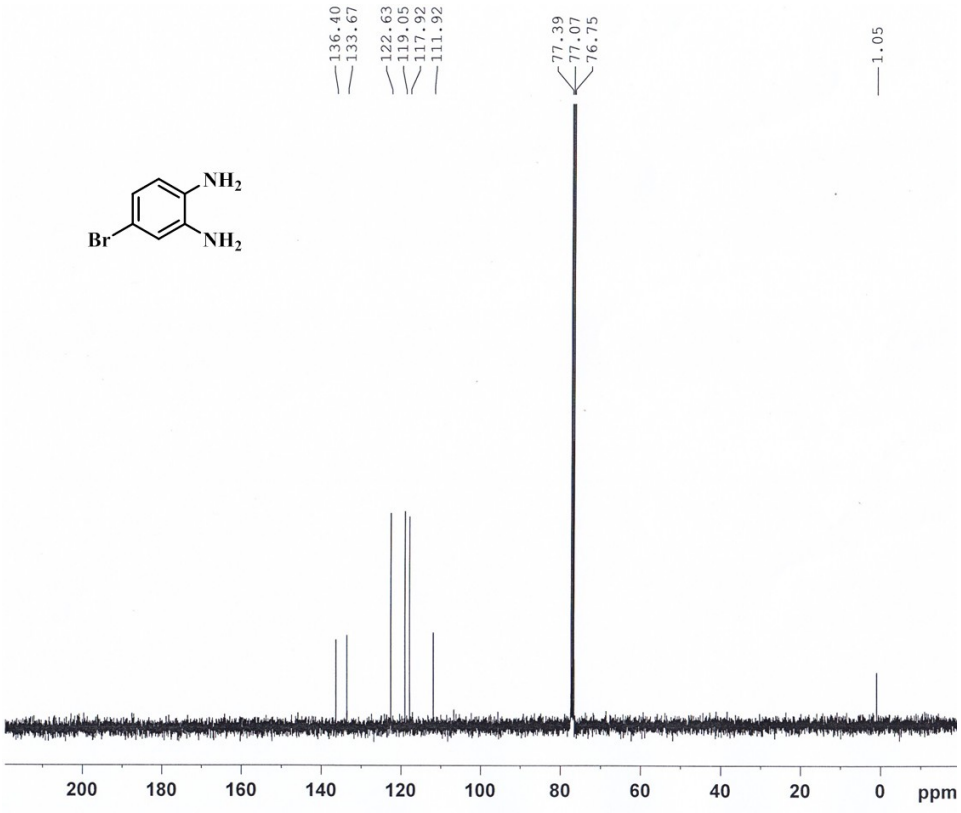

Figure 4.32 ^{13}C NMR spectrum of compound **6**

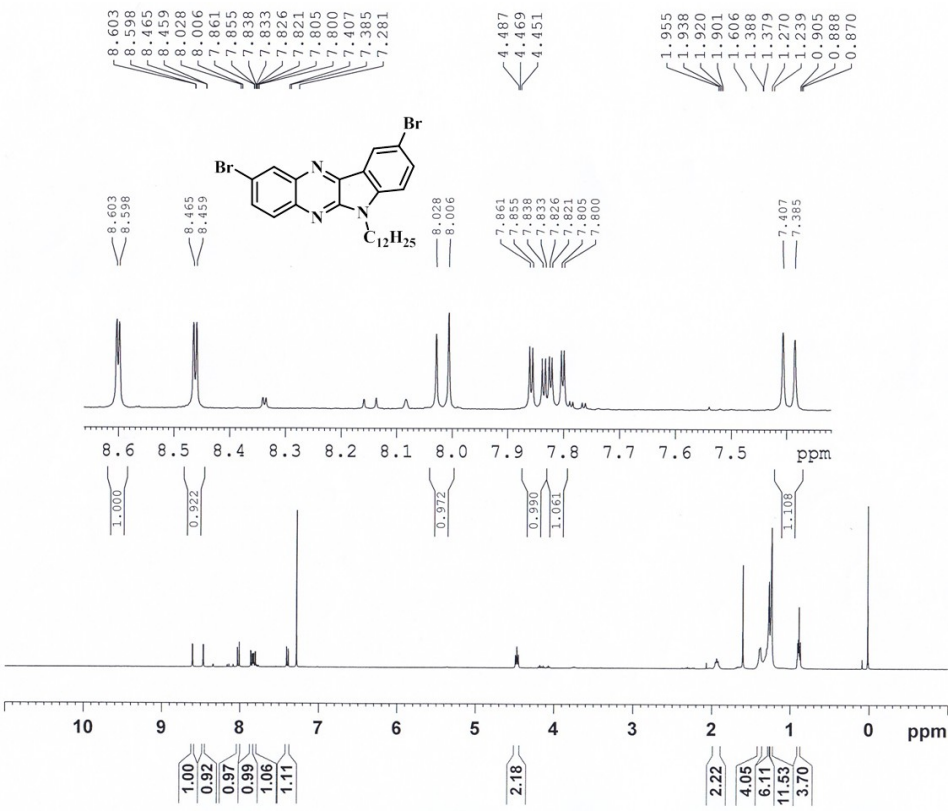

Figure 4.33 ^{1}H NMR spectrum of **INQx-M3**

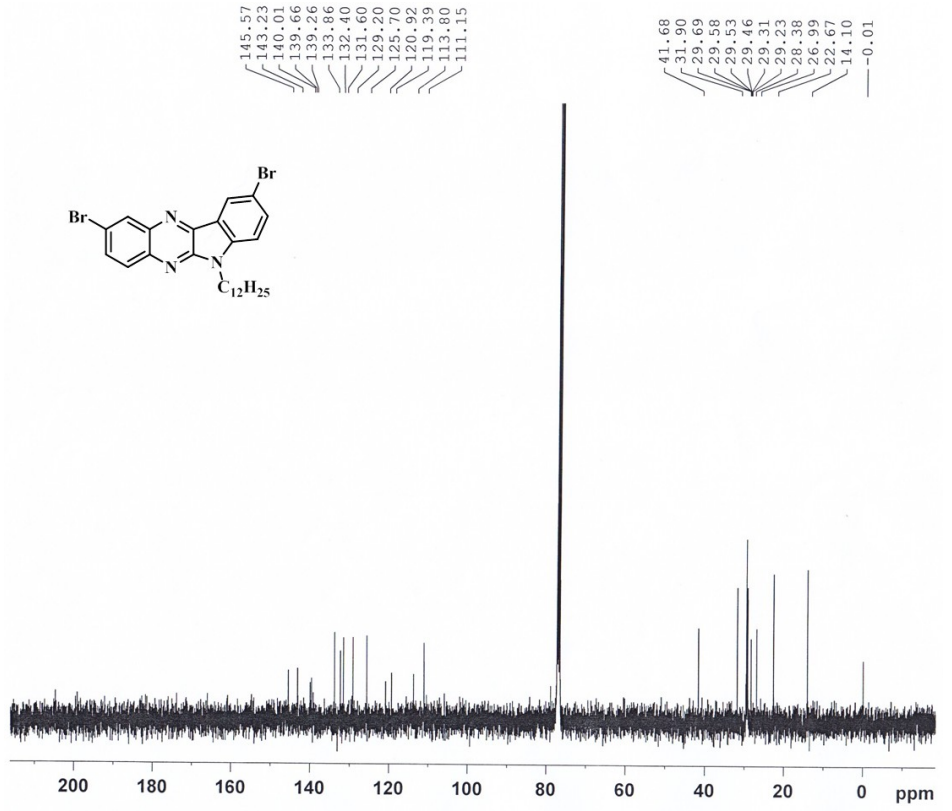

Figure 4.34 ^{13}C NMR spectrum of **INQx-M3**

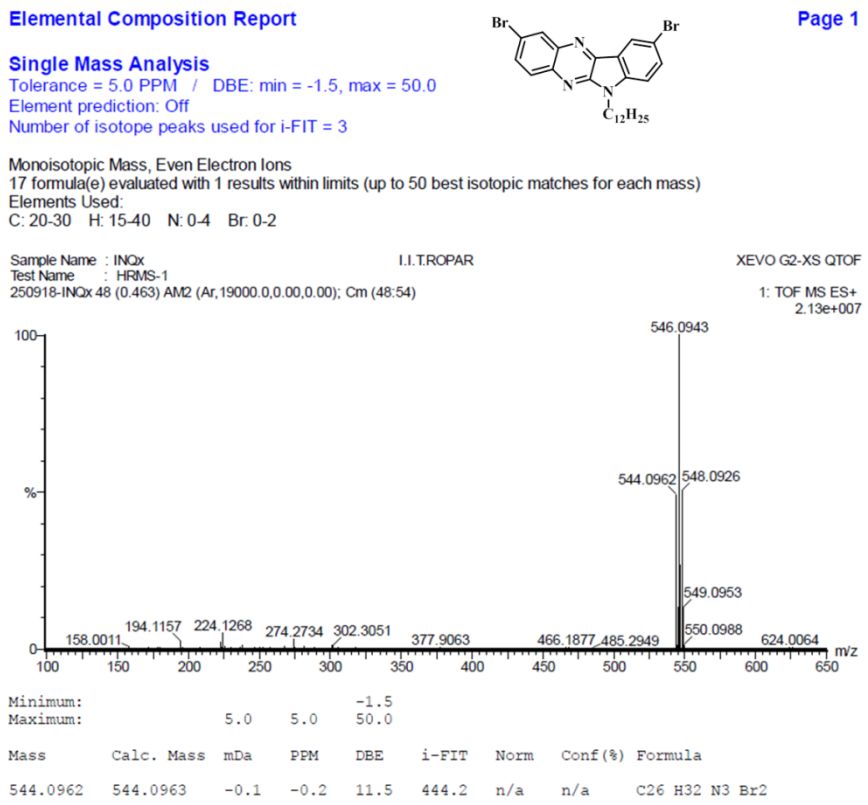

Figure 4.35 HRMS spectrum of **INQx-M3**

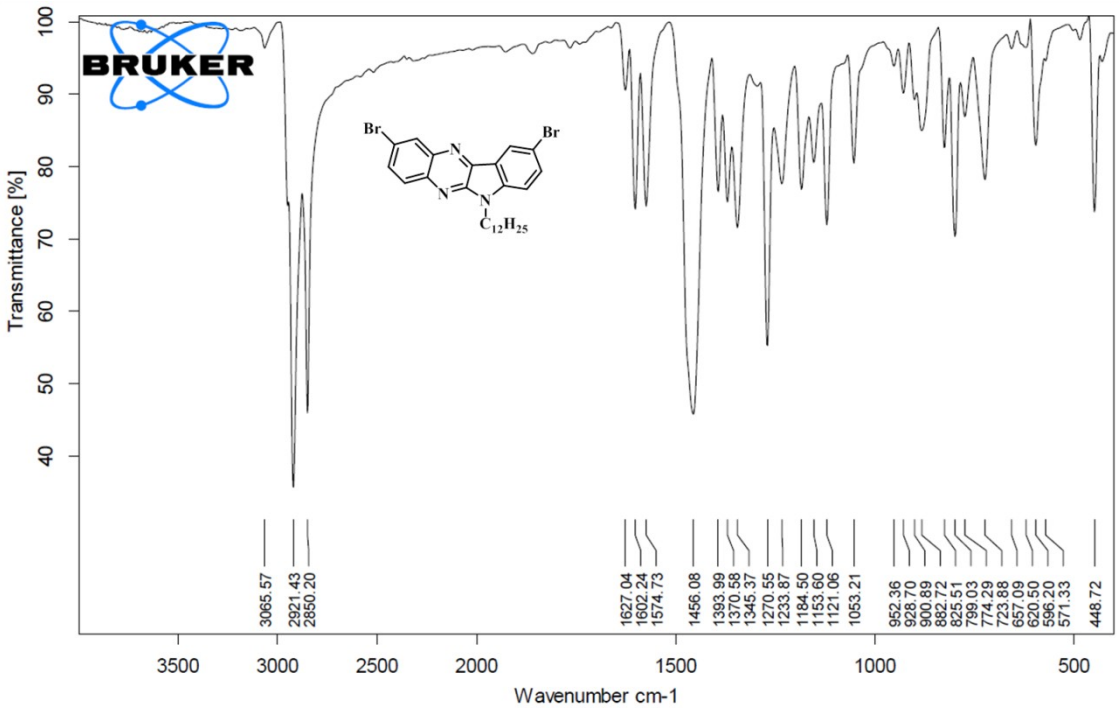

Figure 4.36 IR spectrum (KBr pellet) of **INQx-M3**

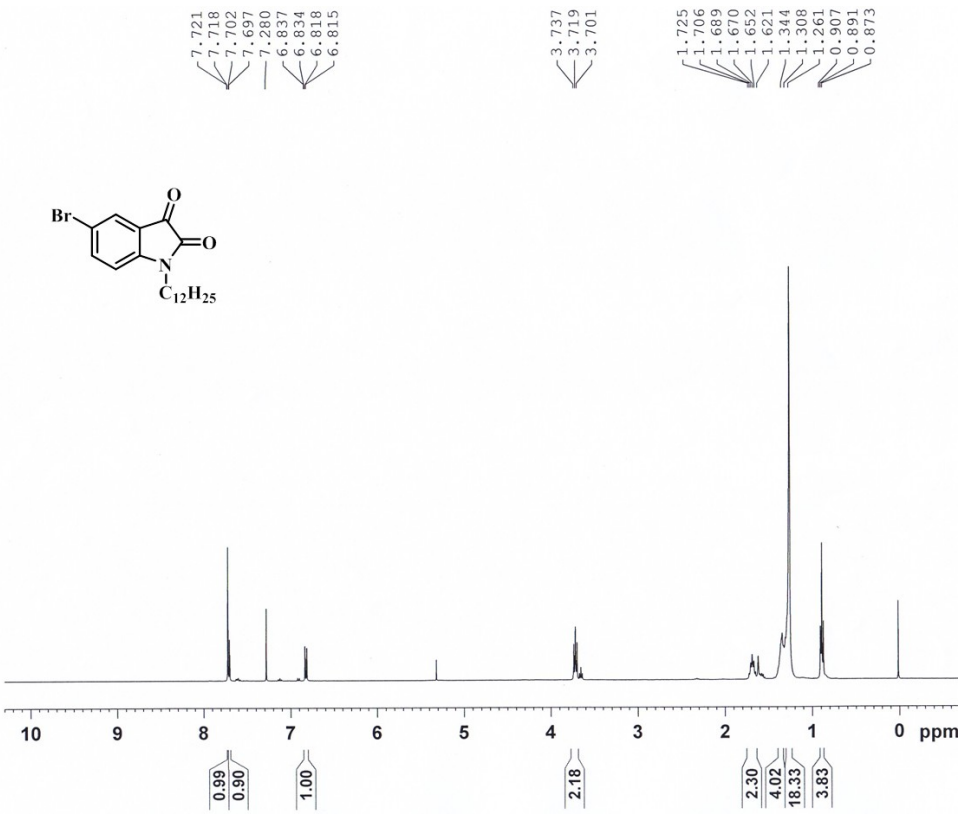

Figure 4.37 ^{1}H NMR spectrum of compound **8**

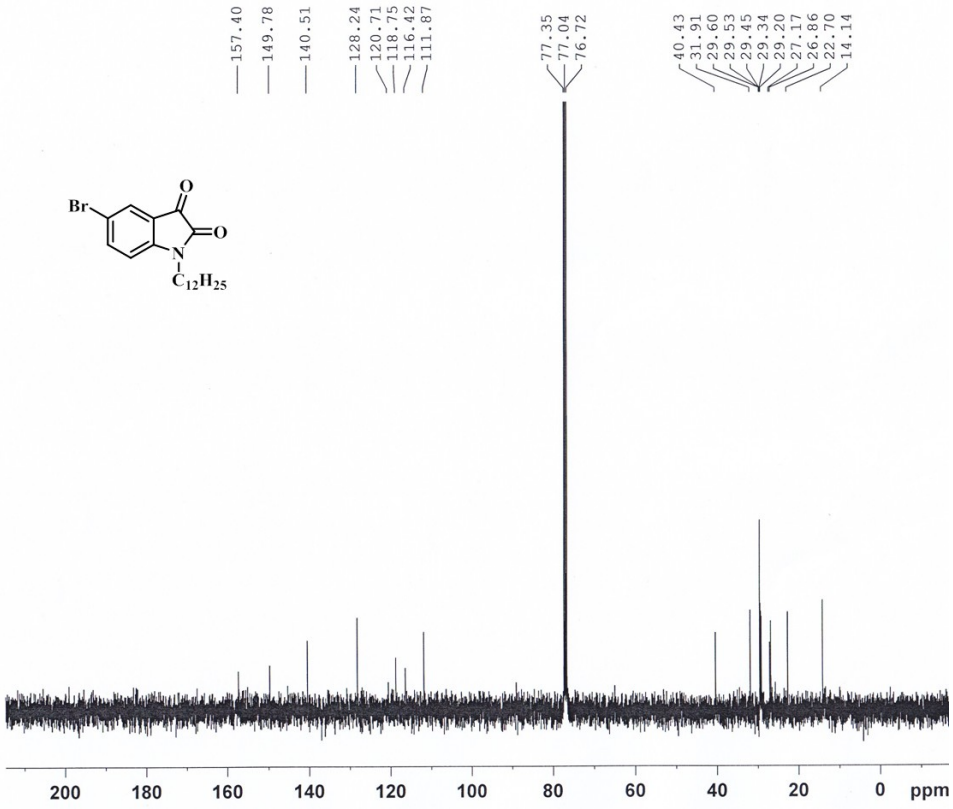

Figure 4.38 ^{13}C NMR spectrum of compound **8**

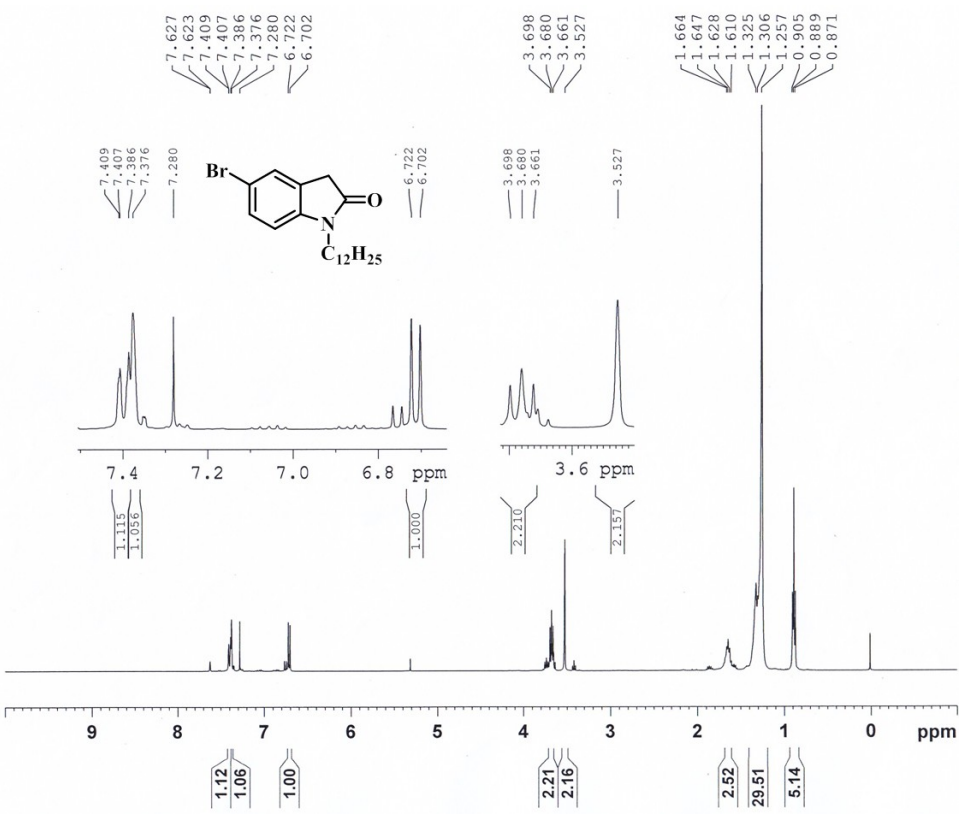

Figure 4.39 ^{1}H NMR spectrum of compound **9**

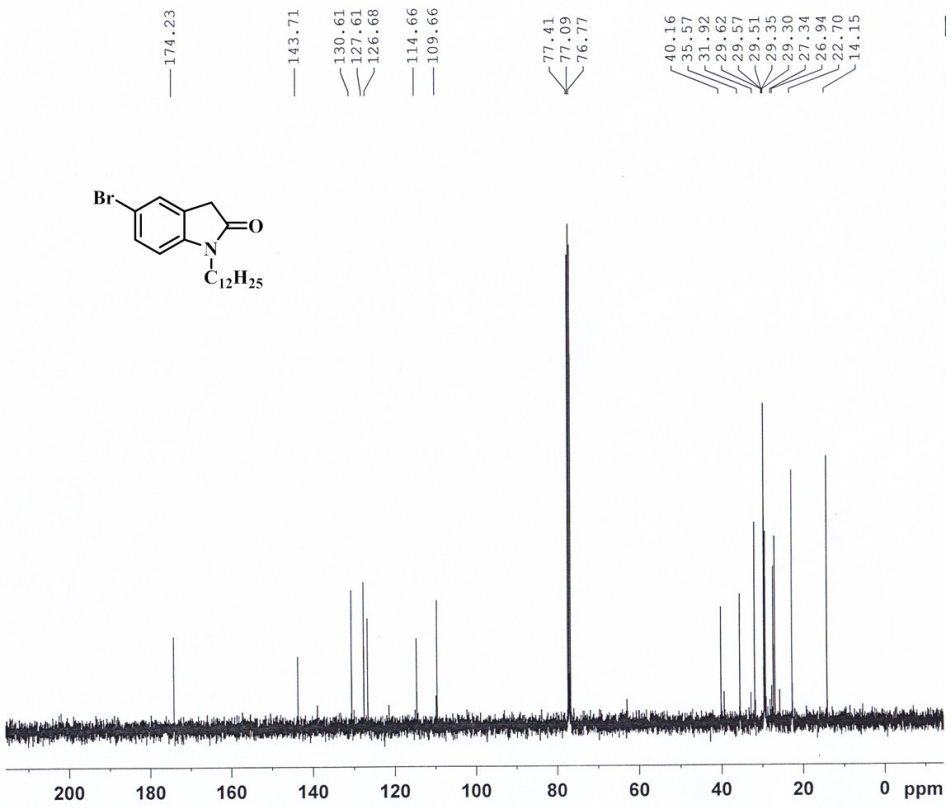

Figure 4.40 ^{13}C NMR spectrum of compound **9**

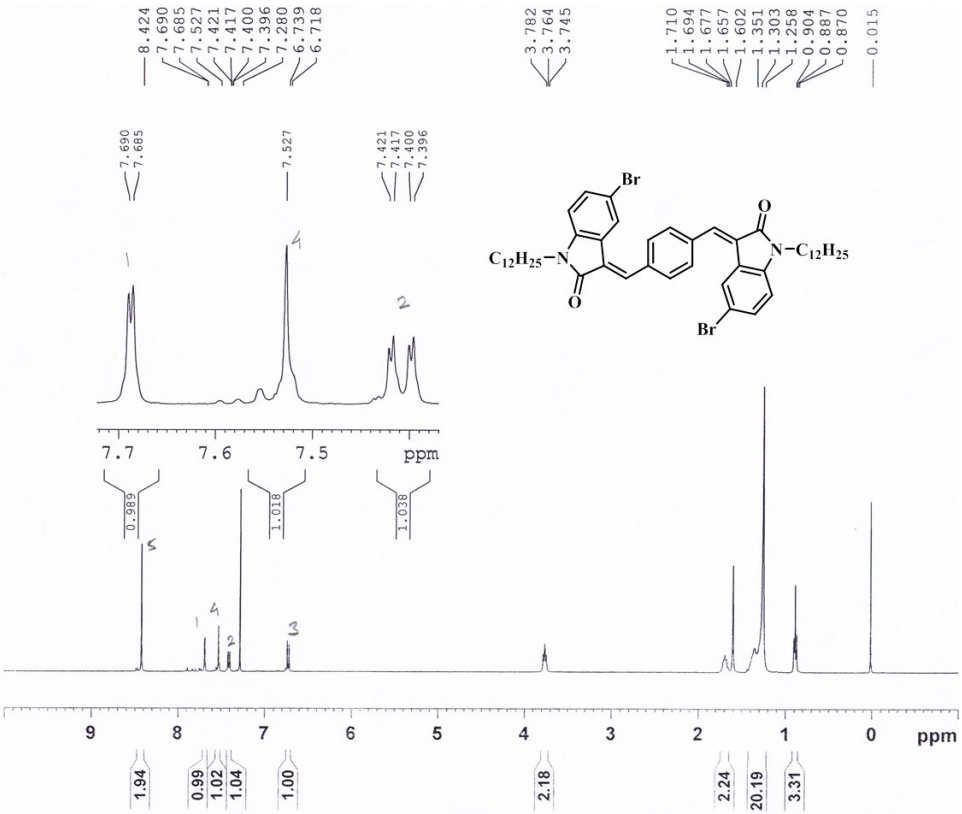

Figure 4.41 ^{1}H NMR spectrum of **BIIG-M4**

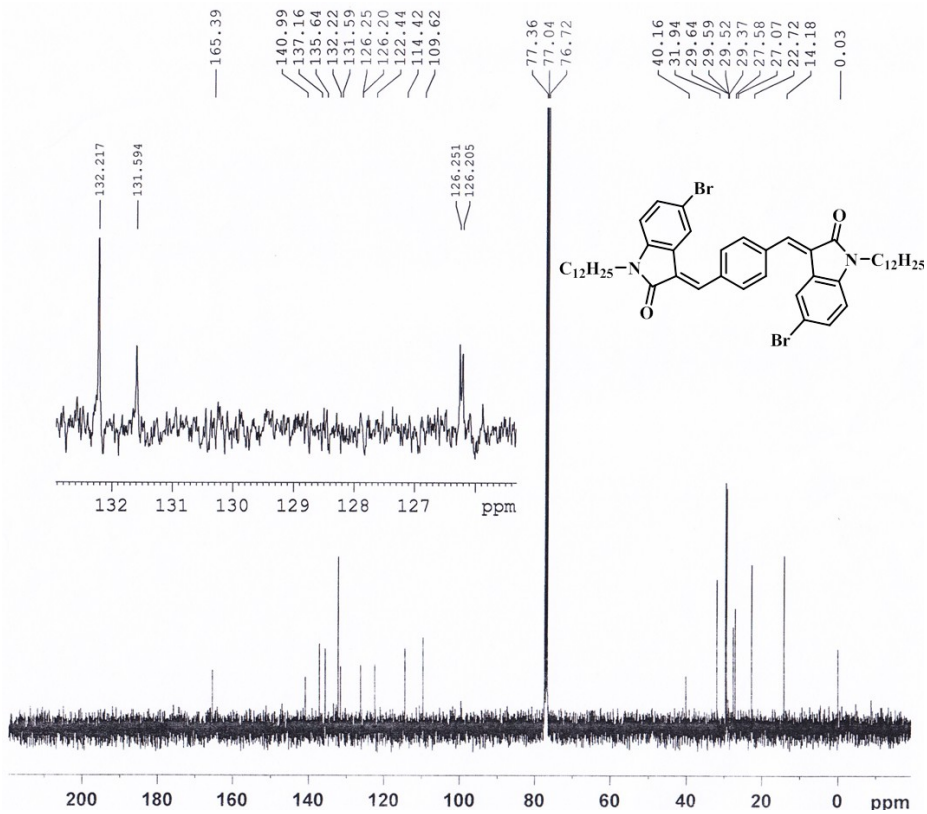

Figure 4.42 ^{13}C NMR spectrum of **BIIG-M4**

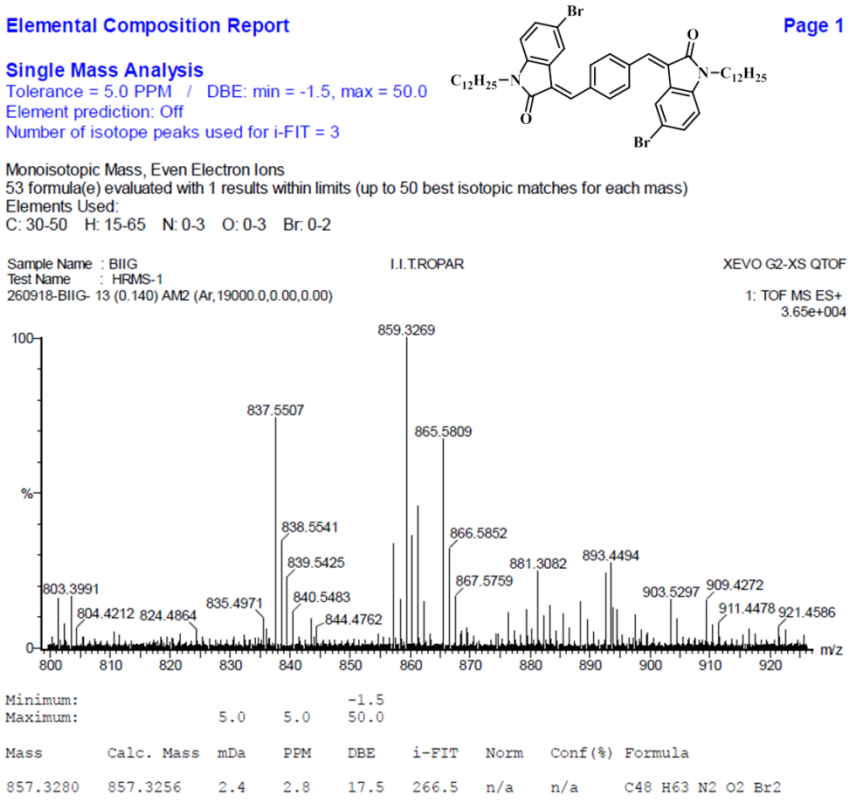

Figure 4.43 HRMS spectrum of **BIIG-M4**

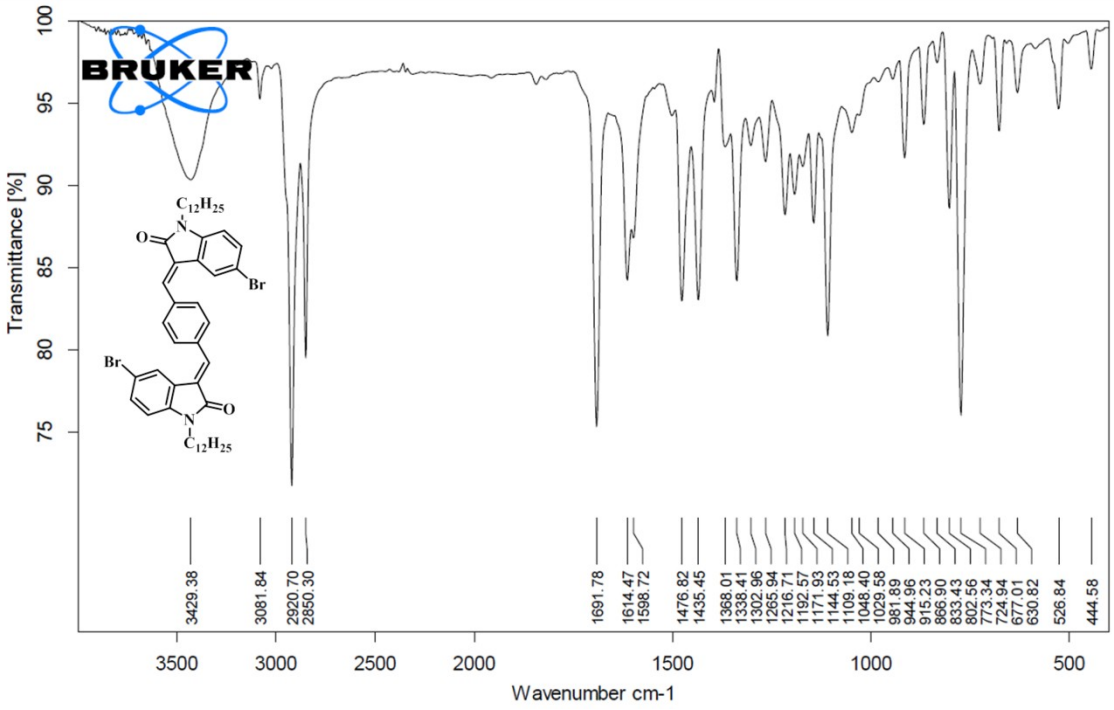

Figure 4.44 IR spectrum (KBr pellet) of **BIIG-M4**

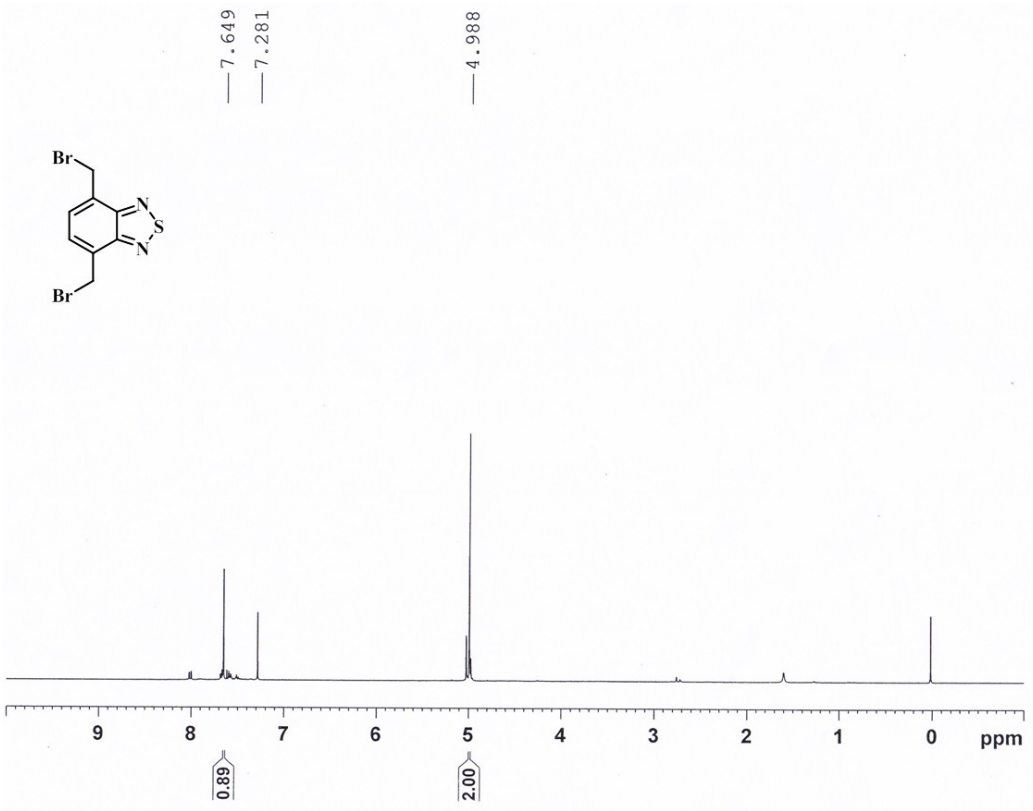

Figure 4.45 ^{1}H NMR spectrum of compound **10**

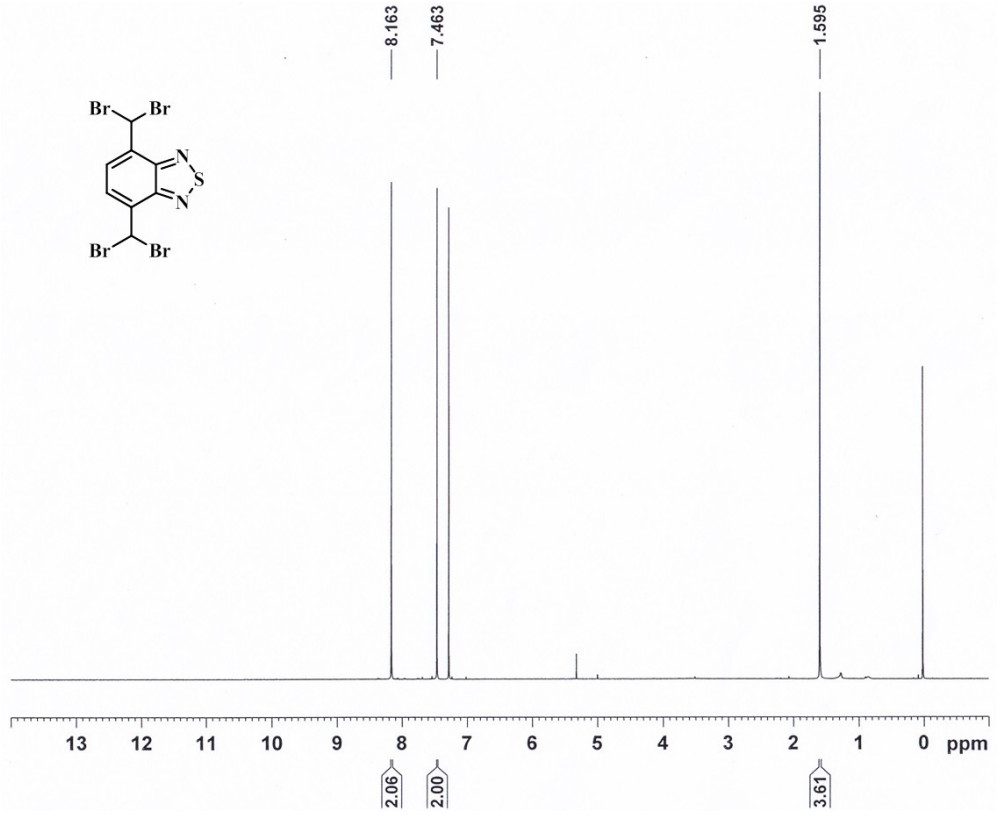

Figure 4.46 ^{1}H NMR spectrum of compound **11**

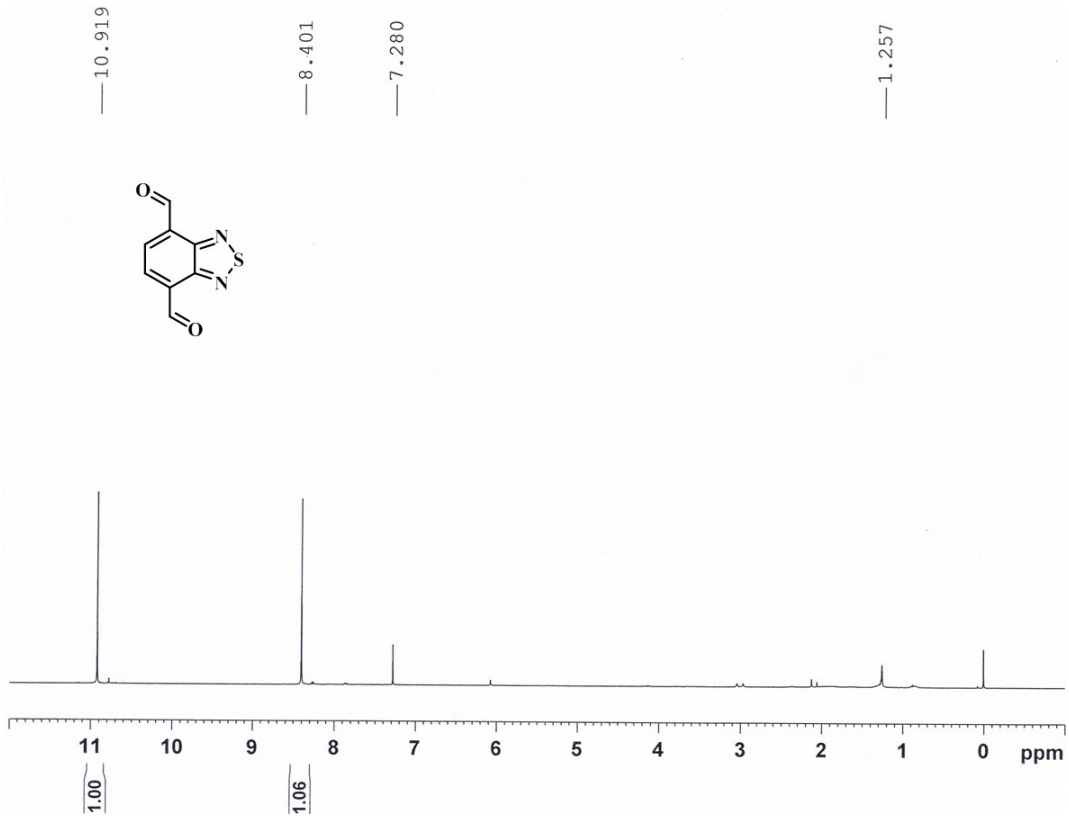

Figure 4.47 ^{1}H NMR spectrum of compound **12**

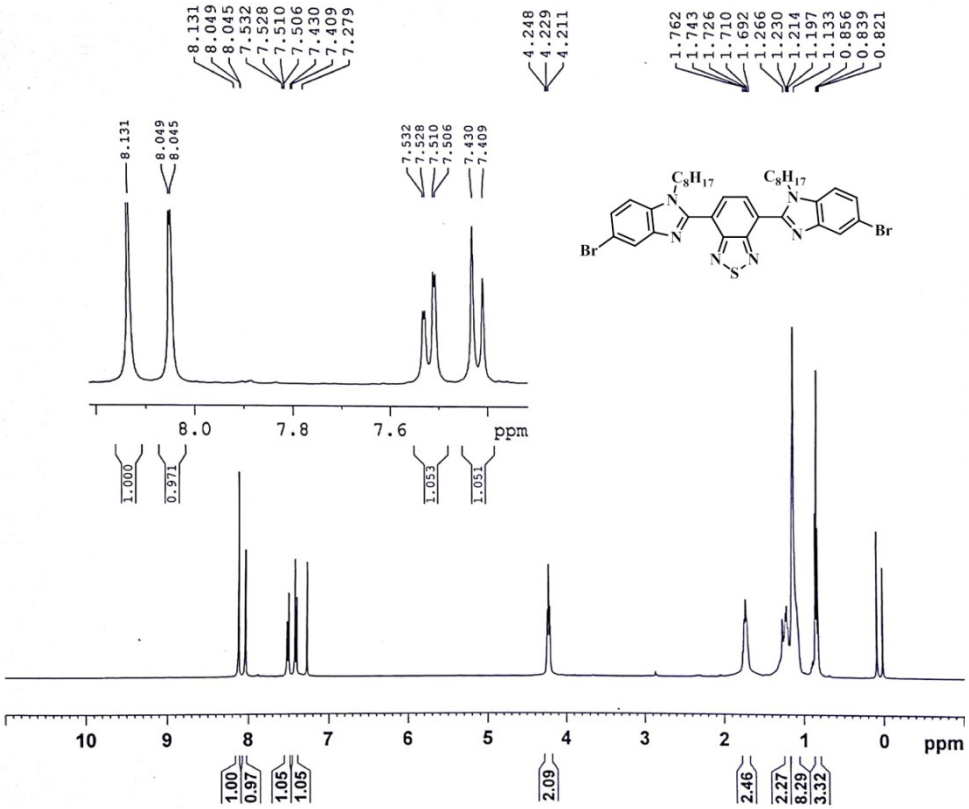

Figure 4.48 ^{1}H NMR spectrum of **BTD-IMD-M5**

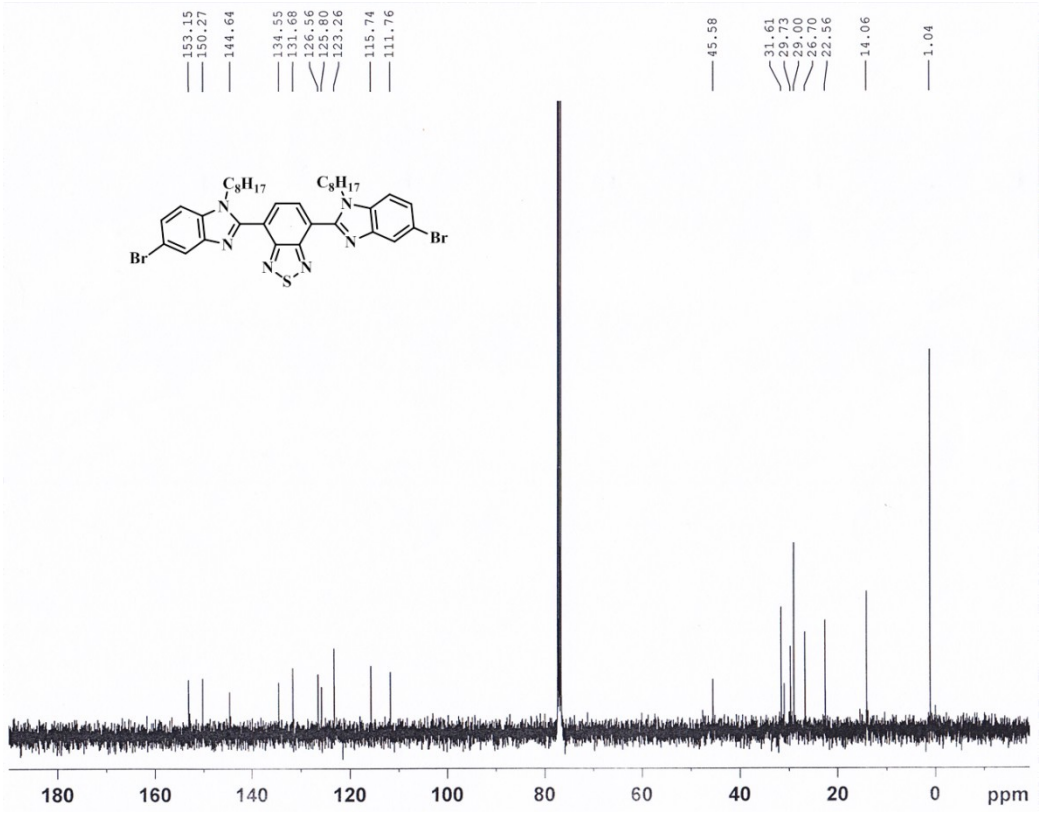

Figure 4.49 ^{13}C NMR spectrum of **BTD-IMD-M5**

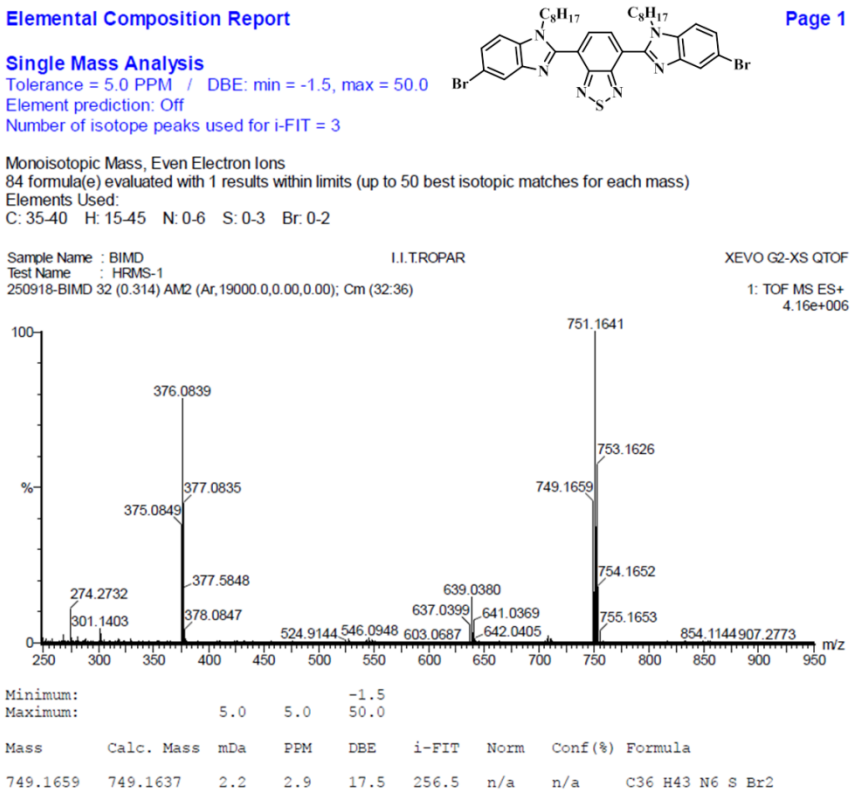

Figure 4.50 HRMS spectrum of **BTD-IMD-M5**

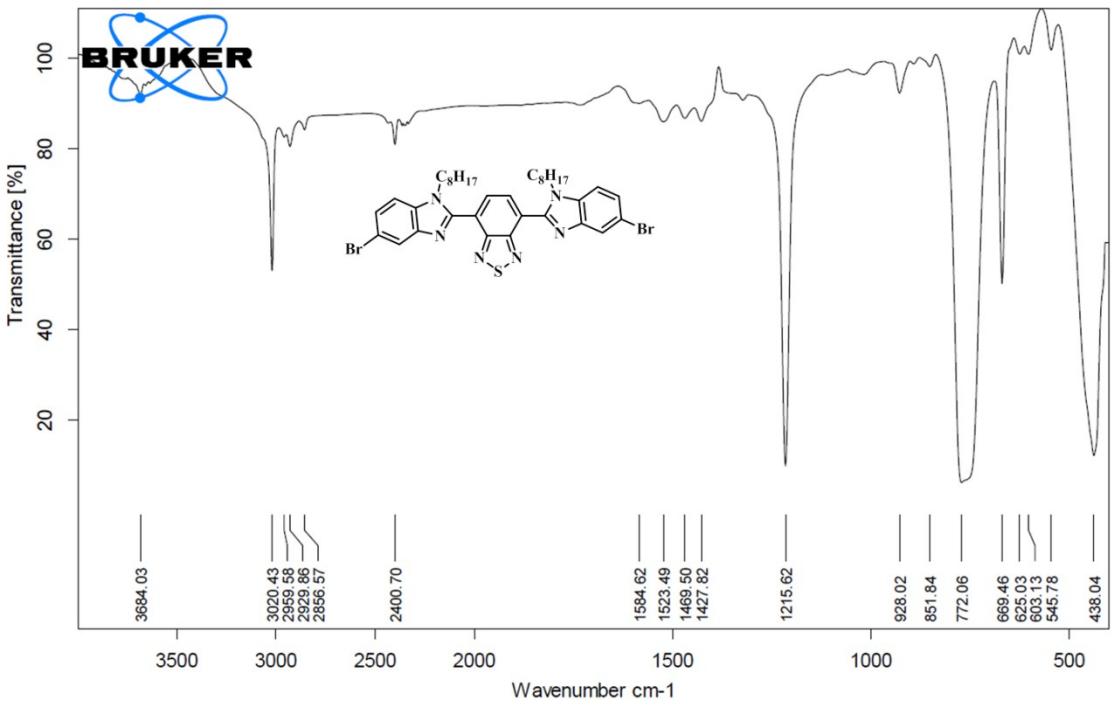

Figure 4.51 IR spectrum (NaCl plate) of **BTD-IMD-M5**

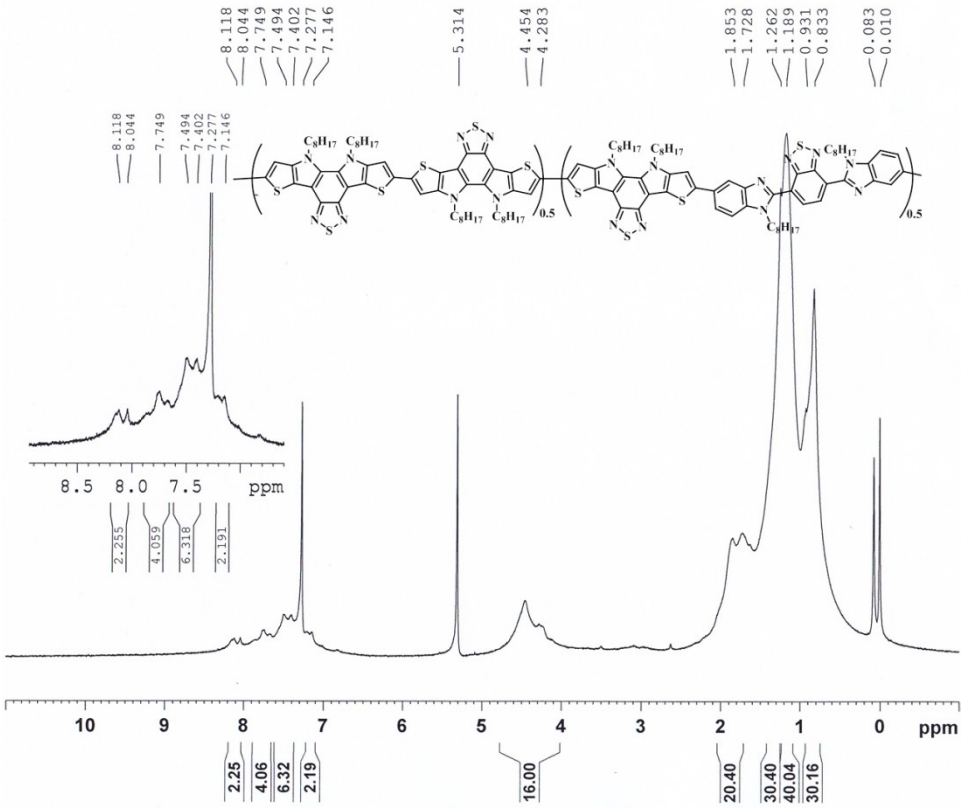

Figure 4.52 ^{1}H NMR spectrum of DTPBT-based polymer **TP-TP-IMD**

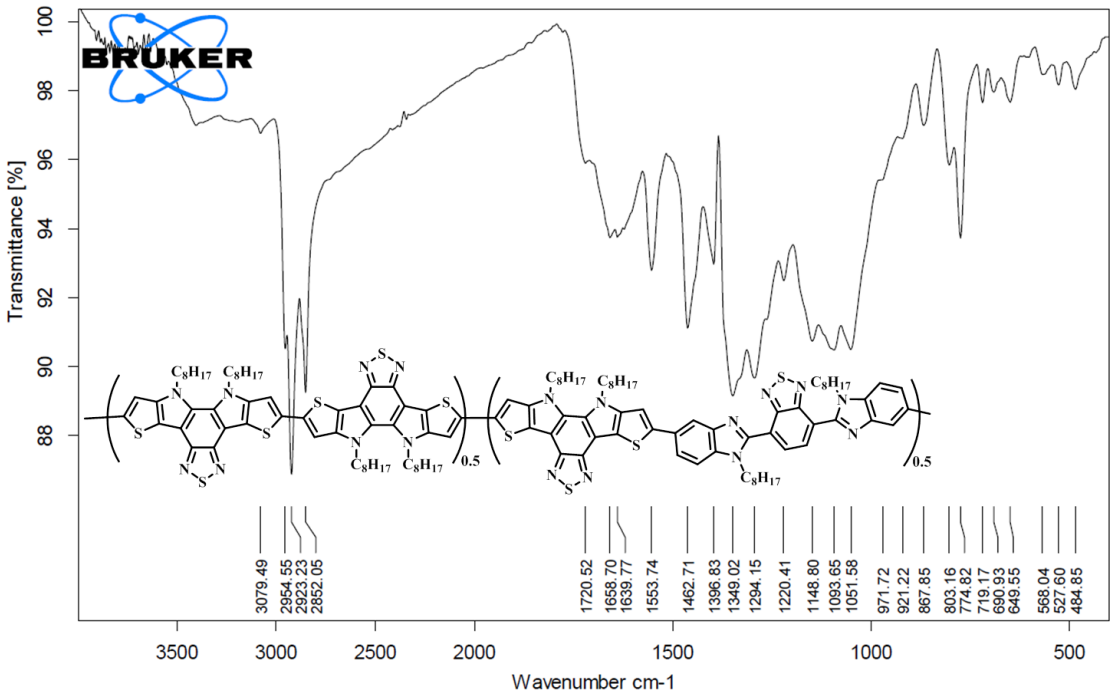

Figure 4.53 IR spectrum (KBr pellet) of **TP-TP-IMD**

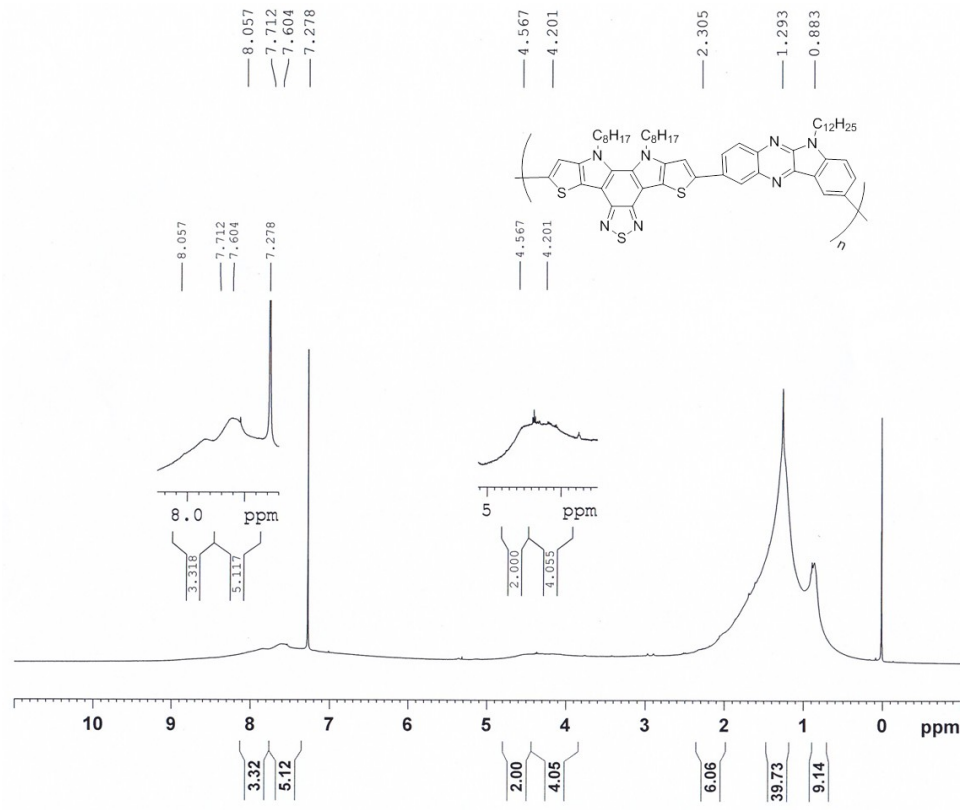

Figure 4.54 ^{1}H NMR spectrum of DTPBT-based polymer **TP-INQx**

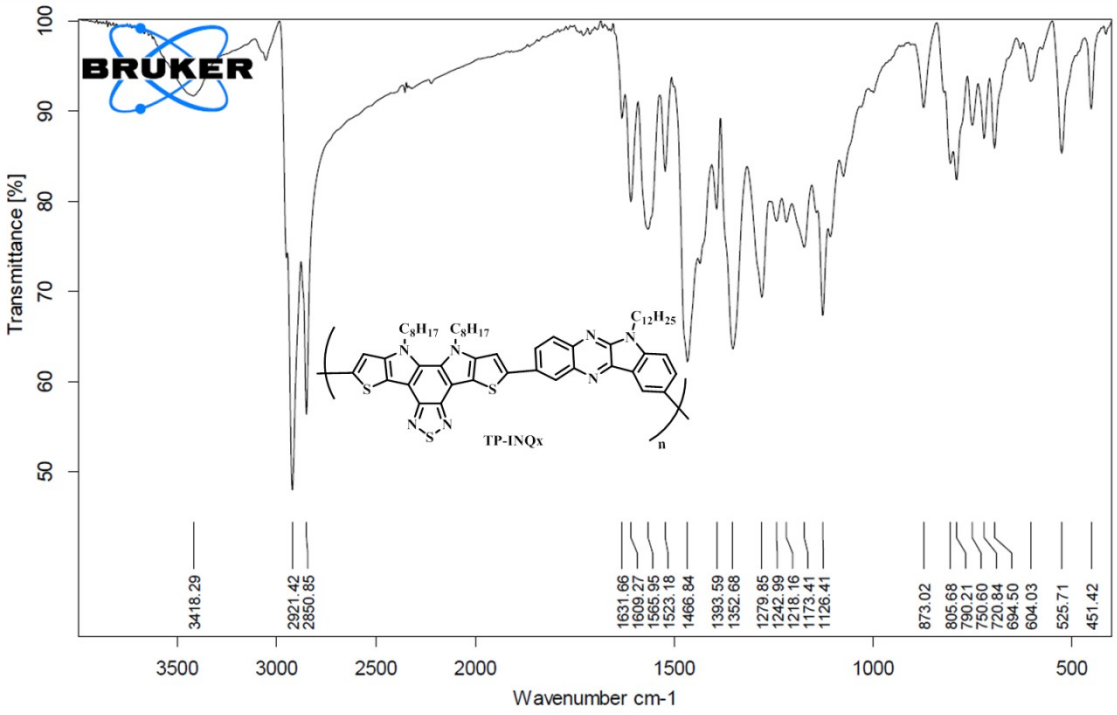

Figure 4.55 IR spectrum (KBr pellet) of **TP-INQx**

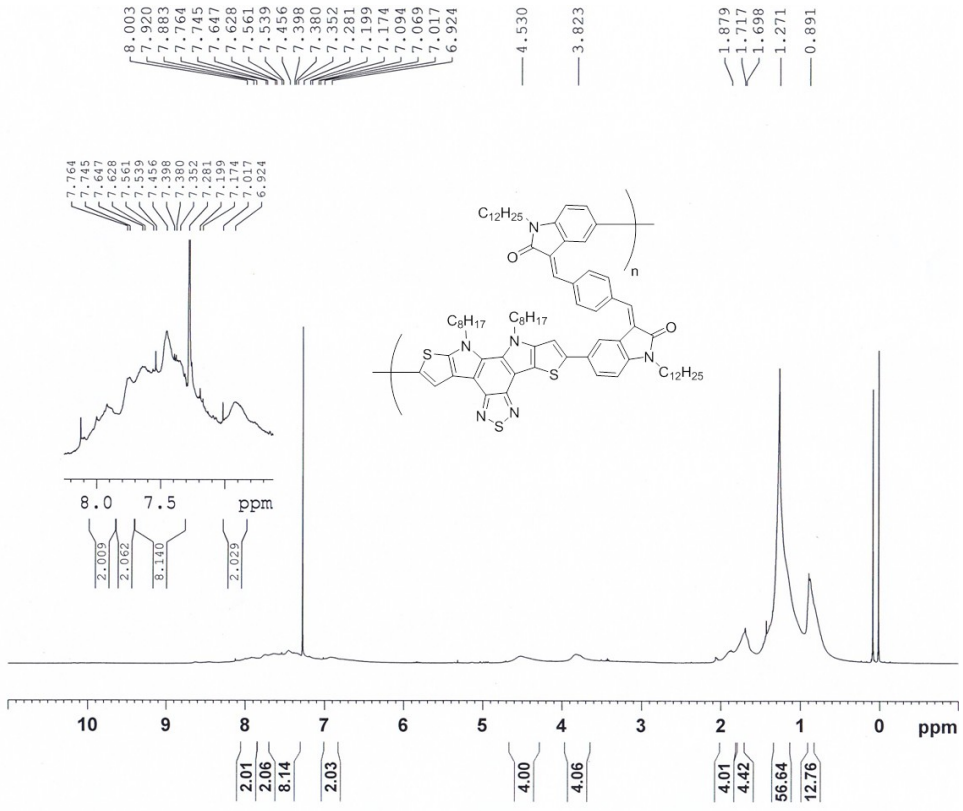

Figure 4.56 ^{1}H NMR spectrum of DTPBT-based polymer **TP-BIIG**

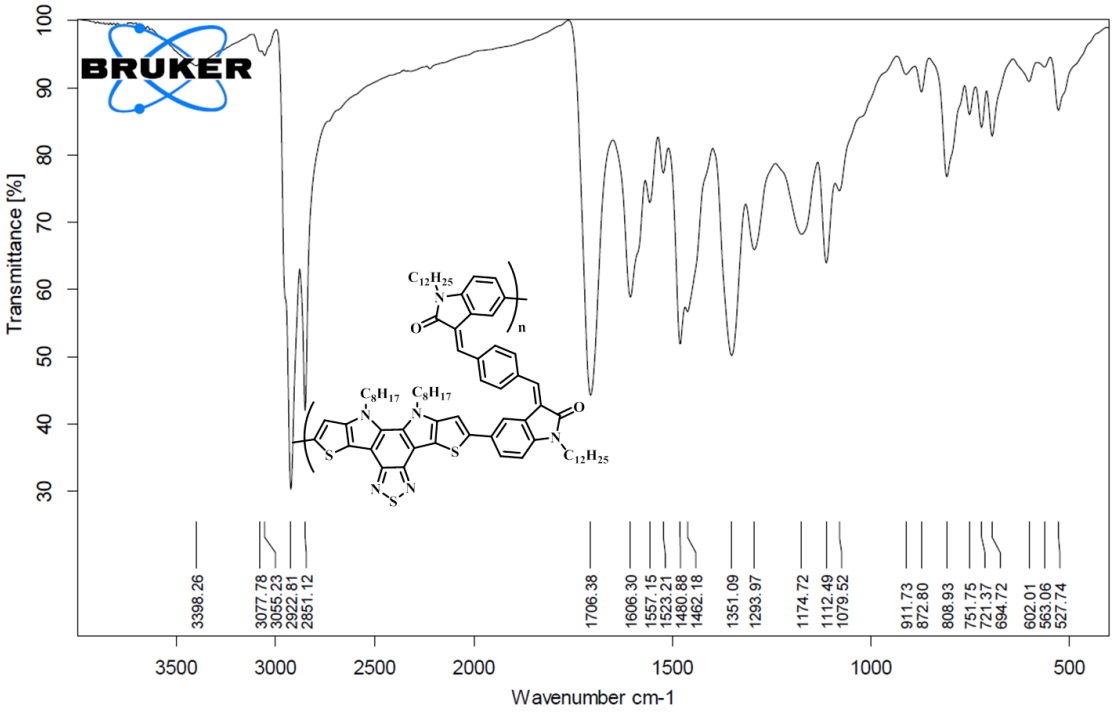

Figure 4.57 IR spectrum (KBr pellet) of **TP-BIIG**

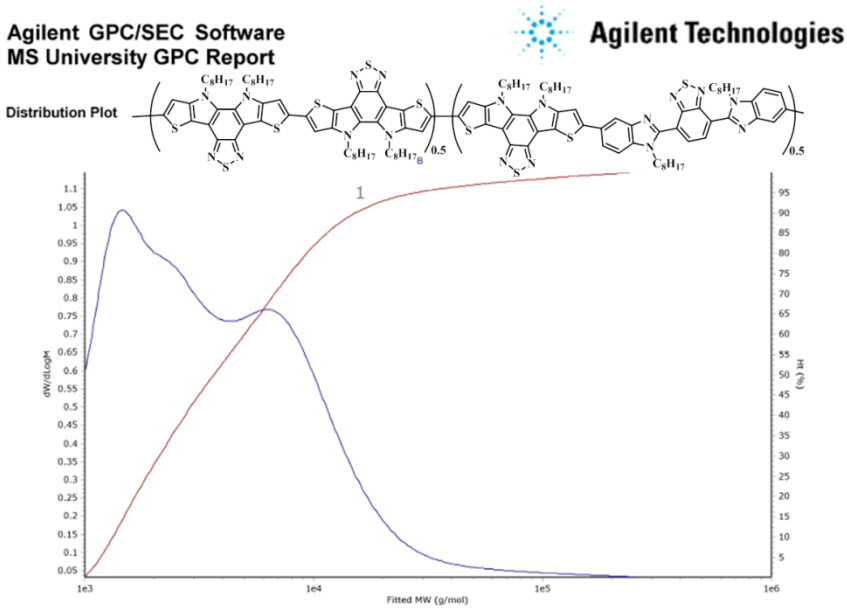

Results

Analysed by

Comments

Applied Chem at 13:51:44 on 06 July 2018

Molecular Weight Averages

Peak	Mp (g/mol)	Mn (g/mol)	Mw (g/mol)	Mz (g/mol)	Mz+1 (g/mol)	Mv (g/mol)	PD
Peak 1	1488	2885	9352	65041	152499	52482	3.242

Figure 4.58 GPC analysis report of DTPBT-based polymer **TP-TP-IMD**

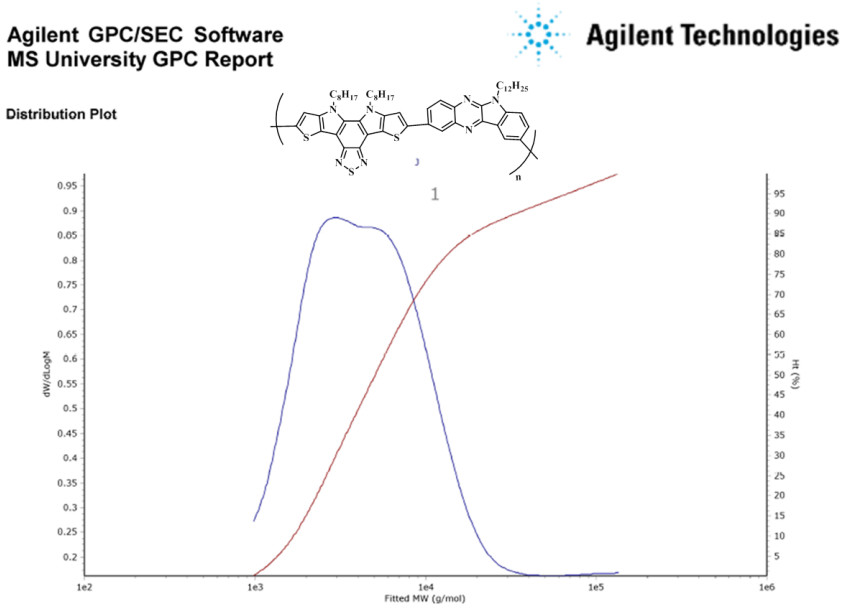

Results

Analysed by: Applied Chem at 17:18:50 on 05 June 2018

Comments

Molecular Weight Averages

Peak	Mp (g/mol)	Mn (g/mol)	Mw (g/mol)	Mz (g/mol)	Mz+1 (g/mol)	Mv (g/mol)	PD
Peak 1	5348	3787	13186	52508	87263	46429	3.482

Figure 4.59 GPC analysis report of DTPBT-based polymer **TP-INQx**

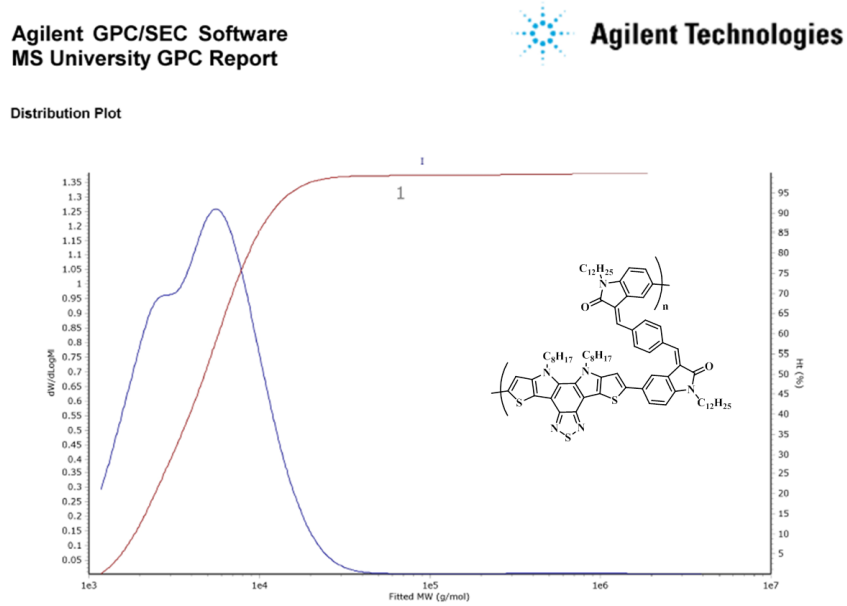

Results

Analysed by: Applied Chem at 17:14:56 on 05 June 2018

Comments

Molecular Weight Averages

Peak	Mp (g/mol)	Mn (g/mol)	Mw (g/mol)	Mz (g/mol)	Mz+1 (g/mol)	Mv (g/mol)	PD
Peak 1	5693	3769	12227	947131	2483851	688258	3.244

Figure 4.60 GPC analysis report of DTPBT-based polymer **TP-BIIG**

References

1 Y. Liu, F. Wu, B. Zhao and P. Shen, *Eur. Polym. J.*, 2016, **74**, 180–189.

2 S. I. Kato, T. Furuya, A. Kobayashi, M. Nitani, Y. Ie, Y. Aso, T. Yoshihara, S. Tobita and Y. Nakamura, *J. Org. Chem.*, 2012, **77**, 7595–7606.

3 S. Ghosh, S. Das, N. R. Kumar, A. R. Agrawal and S. S. Zade, *New J. Chem.*, 2017, **41**, 11568–11575.

4 Y. Cheng, C. Chen, Y. Ho, S. Chang, H. A. Witek and C. Hsu, *Org. Lett.*, 2011, **13**, 5484–5487.

5 Z. H. Zhou, T. Maruyama, T. Kanbara, T. Ikeda, K. Ichimura, T. Yamamoto and K. Tokuda, *J. Chem. Soc. Chem. Commun.*, 1991, **1460**, 1210–1212.

6 E. E. Havinga, W. ten Hoeve and H. Wynberg, *Synth. Met.*, 1993, **55**, 299–306.

7 Y. Wang and T. Michinobu, *J. Mater. Chem. C*, 2016, **4**, 6200–6214.

8 U. Scherf and K. Müllen, *Die Makromol. Chemie, Rapid Commun.*, 1991, **12**, 489–497.

9 U. Scherf, A. Bohnen and K. Müllen, *Die Makromol. Chemie*, 1992, **193**, 1127–1133.

10 A. Fukazawa and S. Yamaguchi, *Chem. – An Asian J.*, 2009, **4**, 1386–1400.

11 A.-D. Schlüter, *Adv. Mater.*, 1991, **3**, 282–291.

12 M. Forster, K. O. Annan and U. Scherf, *Macromolecules*, 1999, **32**, 3159–3162.

13 U. Scherf, *J. Mater. Chem.*, 1999, **9**, 1853–1864.

14 M. Bendikov, F. Wudl and D. F. Perepichka, *Chem. Rev.*, 2004, **104**, 4891–4946.

15 S. Yamaguchi, C. Xu and T. Okamoto, *Pure Appl. Chem.*, 2006, **78**, 721–730.

16 K. Takimiya, S. Shinamura, I. Osaka and E. Miyazaki, *Adv. Mater.*, 2011, **23**, 4347–4370.

17 A. C. Grimsdale and K. Müllen, in *Emissive Materials Nanomaterials*, Springer Berlin Heidelberg, Berlin, Heidelberg, 2006, pp. 1–82.

18 A. C. Grimsdale and K. Müllen, in *Polyfluorenes*, eds. U. Scherf and D. Neher, Springer Berlin Heidelberg, Berlin, Heidelberg, 2008, pp. 1–48.

19 J. L. Bredas, J. P. Calbert, D. A. da S. Filho and J. Cornil, *Proc. Natl. Acad. Sci. U. S. A.*, 2002, **99**, 5804–5809.

20 D. H. Kim, A. L. Ayzner, A. L. Appleton, K. Schmidt, J. Mei, M. F. Toney and Z. Bao, *Chem. Mater.*, 2013, **25**, 431–440.

21 Z. Zhang, S. Zhang, J. Min, C. Cui, H. Geng, Z. Shuai and Y. Li,

Macromolecules, 2012, **45**, 2312–2320.

22 Q. Shi, H. Fan, Y. Liu, J. Chen, L. Ma, W. Hu, Z. Shuai, Y. Li and X. Zhan, *Macromolecules*, 2011, **44**, 4230–4240.

23 R. Mondal, S. Ko, E. Verploegen, H. A. Becerril, M. F. Toney and Z. Bao, *J. Mater. Chem.*, 2011, **21**, 1537–1543.

24 J. S. Wu, S. W. Cheng, Y. J. Cheng and C. S. Hsu, *Chem. Soc. Rev.*, 2015, **44**, 1113–1154.

25 S. Cai, L. Chen, D. Zha and Y. Chen, *J. Polym. Sci. Part A Polym. Chem.*, 2013, **51**, 624–634.

26 Y. Cheng, Y. Ho, C. Chen, W. Kao, C. Wu, S. Hsu and C. Hsu, *Macromolecules*, 2012, **45**, 2690–2698.

27 B. Carsten, J. M. Szarko, L. Lu, H. J. Son, F. He, Y. Y. Botros, L. X. Chen and L. Yu, *Macromolecules*, 2012, **45**, 6390–6395.

28 S. Beaupré and M. Leclerc, *J. Mater. Chem. A*, 2013, **1**, 11097–11105.

29 J. Peet, J. Y. Kim, N. E. Coates, W. L. Ma, D. Moses, A. J. Heeger and G. C. Bazan, *Nat. Mater.*, 2007, **6**, 497.

30 C. B. Nielsen, R. S. Ashraf, N. D. Treat, B. C. Schroeder, J. E. Donaghey, A. J. P. White, N. Stingelin and I. McCulloch, *Adv. Mater.*, 2014, **27**, 948–953.

31 H. Zhou, L. Yang, A. C. Stuart, S. C. Price, S. Liu and W. You, *Angew. Chemie Int. Ed.*, 2011, **50**, 2995–2998.

32 S. H. Park, A. Roy, S. Beaupré, S. Cho, N. Coates, J. S. Moon, D. Moses, M. Leclerc, K. Lee and A. J. Heeger, *Nat. Photonics*, 2009, **3**, 297–302.

33 L. Biniek, C. L. Chochos, N. Leclerc, G. Hadziioannou, J. K. Kallitsis, R. Bechara, P. Lévêque and T. Heiser, *J. Mater. Chem.*, 2009, **19**, 4946–4951.

34 B. Qu, H. Yang, D. Tian, H. Liu, Z. Cong, C. Gao, Z. Chen, L. Xiao, Z. Gao, W. Wei and Q. Gong, *Synth. Met.*, 2012, **162**, 2020–2026.

35 Y. Xia, Z. He, J. Tong, B. Li, C. Wang, Y. Cao, H. Wu, H. Y. Woo and D. Fan, *Macromol. Chem. Phys.*, 2011, **212**, 1193–1201.

36 M. S. Almeataq, H. Yi, S. Al-Faifi, A. A. B. Alghamdi, A. Iraqi, N. W. Scarratt, T. Wang and D. G. Lidzey, *Chem. Commun.*, 2013, **49**, 2252–2254.

37 X. Wang, S. Chen, Y. Sun, M. Zhang, Y. Li, X. Li and H. Wang, *Polym. Chem.*, 2011, **2**, 2872–2877.

38 Y. Cao, T. Lei, J. Yuan, J.-Y. Wang and J. Pei, *Polym. Chem.*, 2013, **4**, 5228–5236.

39 H. Zhou, L. Yang, S. C. Price, K. J. Knight and W. You, *Angew. Chemie Int. Ed.*, 2010, **49**, 7992–7995.

40 L. Ye, S. Zhang, W. Zhao, H. Yao and J. Hou, *Chem. Mater.*, 2014, **26**, 3603–3605.

41 B. C. Schroeder, R. S. Ashraf, S. Thomas, A. J. P. White, L. Biniek, C. B. Nielsen, W. Zhang, Z. Huang, P. S. Tuladhar, S. E. Watkins, T. D. Anthopoulos, J. R. Durrant and I. McCulloch, *Chem. Commun.*, 2012, **48**, 7699–7701.

42 H. Bronstein, J. M. Frost, A. Hadipour, Y. Kim, C. B. Nielsen, R. S. Ashraf, B. P. Rand, S. Watkins and I. McCulloch, *Chem. Mater.*, 2013, **25**, 277–285.

43 J. A. Love, I. Nagao, Y. Huang, M. Kuik, V. Gupta, C. J. Takacs, J. E. Coughlin, L. Qi, T. S. van der Poll, E. J. Kramer, A. J. Heeger, T.-Q. Nguyen and G. C. Bazan, *J. Am. Chem. Soc.*, 2014, **136**, 3597–3606.

44 T. Qin, W. Zajaczkowski, W. Pisula, M. Baumgarten, M. Chen, M. Gao, G. Wilson, C. D. Easton, K. Müllen and S. E. Watkins, *J. Am. Chem. Soc.*, 2014, **136**, 6049–6055.

45 V. Tamilavan, M. Song, R. Agneeswari, S. Kim and M. H. Hyun, *Bull. Korean Chem. Soc.*, 2014, **35**, 1098–1104.

46 E. Wang, L. Hou, Z. Wang, S. Hellström, F. Zhang, O. Inganäs and M. R. Andersson, *Adv. Mater.*, 2010, **22**, 5240–5244.

47 E. Wang, L. Hou, Z. Wang, Z. Ma, S. Hellström, W. Zhuang, F. Zhang, O. Inganäs and M. R. Andersson, *Macromolecules*, 2011, **44**, 2067–2073.

48 H.-C. Chen, Y.-H. Chen, C.-C. Liu, Y.-C. Chien, S.-W. Chou and P.-T. Chou, *Chem. Mater.*, 2012, **24**, 4766–4772.

49 D. W. Chang, H. J. Lee, J. H. Kim, S. Y. Park, S.-M. Park, L. Dai and J.-B. Baek, *Org. Lett.*, 2011, **13**, 3880–3883.

50 X. Lu, Q. Feng, T. Lan, G. Zhou and Z.-S. Wang, *Chem. Mater.*, 2012, **24**, 3179–3187.

51 H. Hayashi, A. S. Touchy, Y. Kinjo, K. Kurotobi, Y. Toude, S. Ito, H. Saarenpää, N. V Tkachenko, H. Lemmetyinen and H. Imahori, *ChemSusChem*, 2013, **6**, 508–517.

52 K. Pei, Y. Wu, A. Islam, Q. Zhang, L. Han, H. Tian and W. Zhu, *ACS Appl. Mater. Interfaces*, 2013, **5**, 4986–4995.

53 X. Qian, H. Gao, Y. Zhu, L. Lu and J. Zheng, *J. Power Sources*, 2015, **280**, 573–580.

54 K. R. J. Thomas and P. Tyagi, *J. Org. Chem.*, 2010, **75**, 8100–8111.

55 P. Tyagi, A. Venkateswararao and K. R. J. Thomas, *J. Org. Chem.*, 2011, **76**, 4571–4581.

56 X. Qian, X. Wang, L. Shao, H. Li, R. Yan and L. Hou, *J. Power Sources*, 2016, **326**, 129–136.

57 A. Payne and G. C. Welch, *Org. Biomol. Chem.*, 2017, **15**, 3310–3319.

58 D. Dong, D. Fang, H. Li, C. Zhu, X. Zhao, J. Li, L. Jin, L. Xie, L. Chen, J. Zhao, H. Zhang and W. Huang, *Chem. – An Asian J.*, 2017, **12**, 920–926.

59 C. Dou, X. Long, Z. Ding, Z. Xie, J. Liu and L. Wang, *Angew. Chemie - Int. Ed.*, 2016, **55**, 1436–1440.

60 X. Long, Z. Ding, C. Dou, J. Zhang, J. Liu and L. Wang, *Adv. Mater.*, 2016, **28**, 6504–6508.

61 W. Li, W. S. C. Roelofs, M. M. Wienk and R. A. J. Janssen, *J. Am. Chem. Soc.*, 2012, **134**, 13787–13795.

62 T. Lei, J.-Y. Wang and J. Pei, *Acc. Chem. Res.*, 2014, **47**, 1117–1126.

63 R. S. Ashraf, A. J. Kronemeijer, D. I. James, H. Sirringhaus and I. McCulloch, *Chem. Commun.*, 2012, **48**, 3939–3941.

64 J.-L. Li, Y.-F. Chai, W. V. Wang, Z.-F. Shi, Z.-G. Xu and H.-L. Zhang, *Chem. Commun.*, 2017, **53**, 5882–5885.

65 G. Kim, S.-J. Kang, G. K. Dutta, Y.-K. Han, T. J. Shin, Y.-Y. Noh and C. Yang, *J. Am. Chem. Soc.*, 2014, **136**, 9477–9483.

66 T. Lei, Y. Cao, Y. Fan, C.-J. Liu, S.-C. Yuan and J. Pei, *J. Am. Chem. Soc.*, 2011, **133**, 6099–6101.

67 T. Lei, J.-H. Dou, Z.-J. Ma, C.-H. Yao, C.-J. Liu, J.-Y. Wang and J. Pei, *J. Am. Chem. Soc.*, 2012, **134**, 20025–20028.

68 S.-F. Liao, C.-T. Chen and C.-Y. Chao, *ACS Macro Lett.*, 2017, **6**, 969–974.

69 C. Lu, H.-C. Chen, W.-T. Chuang, Y.-H. Hsu, W.-C. Chen and P.-T. Chou, *Chem. Mater.*, 2015, **27**, 6837–6847.

70 S. I. Kato, T. Furuya, A. Kobayashi, M. Nitani, Y. Ie, Y. Aso, T. Yoshihara, S. Tobita and Y. Nakamura, *J. Org. Chem.*, 2012, **77**, 7595–7606.

71 B. Carsten, J. M. Szarko, L. Lu, H. J. Son, F. He, Y. Y. Botros, L. X. Chen and L. Yu, *Macromolecules*, 2012, **45**, 6390–6395.

72 O. V Dolomanov, L. J. Bourhis, R. J. Gildea, J. A. K. Howard and H. Puschmann, *J. Appl. Crystallogr.*, 2009, 42, 339–341.

73 G. M. Sheldrick, *Acta Crystallogr. Sect. A*, 2008, 64, 112–122.

74 G. M. Sheldrick, *Acta Crystallogr. Sect. C, Struct. Chem.*, 2015, 71, 3–8.

75 L. Palatinus and G. Chapius, *J. Appl. Cryst.*, 2007, **40**, 786–790.

76 L. Palatinus and A. van der Lee, *J. Appl. Crystallogr.*, 2008, **41**, 975–984.

77 L. Palatinus, S. J. Prathapa and S. van Smaalen, *J. Appl. Crystallogr.*, 2012, **45**, 575–580.

78 B. A. D. Neto, A. S. Lopes, G. Ebeling, R. S. Goncalves, V. E. U. Costa, F. H. Quina and J. Dupont, *Tetrahedron*, 2005, **61**, 10975–10982.

79 E. Wang, L. Hou, Z. Wang, S. Hellström, W. Mammo, F. Zhang, O. Inganäs and M. R. Andersson, *Org. Lett.*, 2010, **12**, 4470–4473.

80 C. Kitamura, S. Tanaka and Y. Yamashita, *Chem. Mater.*, 1996, **8**, 570–578.

81 H. Zhu, H. Tong, Y. Gong, S. Shao, C. Deng, W. Zhang and Y. Zhang, *J. Polym. Sci. Part A Polym. Chem.*, 2012, **50**, 2172–2181.

82 D. Dong, D. Fang, H. Li, C. Zhu, X. Zhao, J. Li and L. Jin, *Chem. - An Asian J.*, 2017, **12**, 920–926.

83 T. Bura, N. Leclerc, R. Bechara, P. Lévêque, T. Heiser and R. Ziessel, *Adv. Energy Mater.*, 2013, **3**, 1118–1124.

84 M. Li, H. Zhang, Y. Zhang, B. Hou, C. Li, X. Wang, J. Zhang, L. Xiao, Z. Cui and Y. Ao, *J. Mater. Chem. C*, 2016, **4**, 9094–9102.

85 V. Sriramoju, S. Kurva and S. Madabhushi, *New J. Chem.*, 2018, **42**, 3188–3191.